

Department of Chemical Engineering

Bed Agglomeration During Biomass Fast Pyrolysis in a Fluidized-bed Reactor

Alan Hamilton Burton

**This thesis is presented for the Degree of
Doctor of Philosophy
of
Curtin University**

March 2016

DECLARATION

To the best of my knowledge and belief this thesis contains no material previously published by any other person except where due acknowledgement has been made.

This thesis contains no material, which has been accepted for the award of any other degree or diploma in any university.

Signature:.....

Date:.....

To my beloved family

ABSTRACT

This thesis reports some significant research outcomes on the previously unreported phenomenon of bed agglomeration during the pyrolysis of mallee biomass in a fluidized-bed reactor (pyrolyser) under various conditions.

Firstly, under thermally thin conditions (biomass particle size: 355–500 μm ; bed sand materials: 125–250 μm ; Biot Number <0.1), bed agglomeration takes place due to the formation of char-char and/or char-sand agglomerates connected by carbon-enriched necks. There are two types of bed agglomeration: one formed due to solvent-soluble organic matter and dissembled upon solvent washing and the other due to solvent-insoluble organic matter produced from biomass pyrolysis. The total yield of bed agglomeration (Y_{AP}) decreases with increasing pyrolysis temperature. At low temperatures (e.g., 300 $^{\circ}\text{C}$), bed agglomeration is dominantly contributed by those formed by solvent-insoluble organic matter. As pyrolysis temperature increases, bed agglomeration due to solvent-soluble organic matter becomes increasingly important and reaches a maximum at 500 $^{\circ}\text{C}$. At pyrolysis temperatures above 600 $^{\circ}\text{C}$, there is a drastic reduction in the bed agglomeration formed by solvent-soluble organic matter due to thermal cracking so that solvent-insoluble organic matter again dominates bed agglomeration. Overall, bed agglomeration during biomass pyrolysis in a fluidized-bed reactor is due to the production of sticky agents, which are organic matter (both solvent-soluble and solvent-insoluble) produced from biomass pyrolysis reactions.

Secondly, a systematic set of experiments were also carried out to study the significant differences in bed agglomeration behaviour during the fast pyrolysis of various mallee biomass components (leaf, wood and bark) in the fluidized-bed reactor at 500 °C. The pyrolysis of mallee leaf and bark led to significant bed agglomeration yields of 12.0 wt. % and 13.4 wt. %, respectively, while the pyrolysis of the wood component results in bed agglomeration yield of <0.1 wt. %. Ethanol washing of the leaf and bark samples were carried out to prepare solvent-extracted leaf and bark samples (the solid residues after extraction) and the extract samples (obtained after evaporating the solvent from the extracted solvent solutions). Subsequent pyrolysis of the solvent-extracted leaf and bark samples showed drastically reduced bed agglomeration yields of 6.0 wt. % and 1.3 wt. %, respectively. Direct pyrolysis of the extract samples from leaf and bark resulted in substantial bed agglomeration yields of 24.4 wt. % and 34.1 wt. %, respectively, suggesting that the extractives within biomass play a critical role in the bed agglomeration during biomass fast pyrolysis. The experimental results indicate that if the biomass from the whole mallee tree is used as a feedstock for bio-oil production via fluidized-bed fast pyrolysis, then the leaf and bark components are expected to cause bed agglomeration, due to the substantial amount of extractives present in these biomass materials.

Thirdly, this study further proposes a new parameter (i.e., sand loading (S_L)), which is defined as the mass of sand sticking to the pyrolysing biomass particles in the bed to form bed agglomerates normalised to the total mass of biomass fed into the fluidized-bed reactor, for the diagnosis of bed agglomeration. It was found that S_L is a powerful diagnostic parameter for investigation into the interactions between the

pyrolysing biomass particles and the sand particles in the fluidized-bed. During continuous feeding of the biomass into the reactor, the sand in the bed and the pyrolysing biomass particles interact in a negative order reaction kinetic of 0.4. During holding upon the completion of biomass feeding, the sand and biomass particles interacted in a zero-order mechanism with respect to holding time, suggesting that the sand particles attach to the “active sites” (as part of the sticky agents) produced from biomass fast pyrolysis for the forming of bed agglomerates. It was also found that during continuous feeding, S_L decreases from 2.4 to 0.8 $g_{\text{sand}}/g_{\text{biomass (db)}}$. At a low feed fraction (<12 wt. % of the bed mass), the formed bed agglomerates are mainly sand-char bonded, but at higher feed fractions, char-char bonding becomes more important.

Fourthly, the new parameter sand loading has then applied to the diagnosis of bed agglomeration during biomass fast pyrolysis in the fluidized-bed reactor at 200–700 °C. Under all conditions, bed agglomeration can be modelled using S_L . The value of S_L during pyrolysis is greatly influenced by the ethanol-soluble extractive contained within the raw biomass. For the pyrolysis of the raw biomass, at temperatures <310 °C, S_L follows an endothermic reaction pathway ($E_a = 28$ kJ/mole, $A_k = 3.4E+02$) during which its values increase with increasing temperature. However, at higher temperatures >350 °C, S_L follows an exothermic reaction pathway ($E_a = -45$ kJ/mole, $A_k = 2.2 E-04$) during which its values decrease with increasing temperature.

Fifthly, S_L has also been applied to the diagnosis of biomass drying in the fluidized-bed reactor in air at 120–250 °C for 15 minutes. Surprisingly, bed agglomeration takes place even during drying. The bed agglomeration yield (Y_{AP}) increases from

5.2 wt. % at 120 °C to 17.3 wt. % at 250 °C. The interaction between biomass and sand bed particles during biomass drying can also be quantified using sand loading and found to follow the generic equation ($S_L = KR^{-0.5}$) as previously reported for biomass pyrolysis, where K is analogous to the Arrhenius equation and R is the biomass feed to sand ratio (i.e., the ratio between the total accumulated mass of biomass fed and the total mass of sand in the fluidized-bed). The activation energies (E_a) for bed agglomeration during biomass drying under air and argon atmosphere are estimated to be 19.7 and 29.3 kJ/mole, respectively.

Lastly, as the work in points 1–5 concerns biomass pyrolysis under thermally thin conditions, further investigation has been performed into the effect of biomass particle size on bed agglomeration. Sand loading (S_L), which is defined as the mass of sand sticking to the biomass particles normalised to the total mass of biomass fed, is used for quantifying the interaction between the pyrolysing biomass particle and sand in fluidized-bed to form bed agglomerates. At biomass particle sizes $\leq 500 \mu\text{m}$, sand loading increases with increasing biomass particle size. At biomass particle sizes $> 500 \mu\text{m}$, sand loading decreases with further increase in biomass particle size. The results further show that mass transfer of the sticky agent produced from biomass pyrolysis plays a key role in bed agglomeration. At small particle sizes ($\leq 500 \mu\text{m}$) sand loading is dominantly influenced by convective mass transfer of sticky agent from the particle, while at large particle sizes ($> 500 \mu\text{m}$) sand loading is mainly controlled by diffusive mass transfer of sticky agent within the pyrolysing biomass particle.

ACKNOWLEDGEMENTS

During any large undertaking there is more than one person involved. Many others helped and supported me along the way and I would like to thank these people.

First and foremost I would like to thank my Supervisor Professor Hongwei Wu for his guidance and encouragement throughout my time at Curtin University. Although it was not always a smooth ride, I greatly appreciated his input and advice along with lively discussions, which were always carried out in a friendly manner.

I would also like to thank:

- My wife, Sarah Mitchell, for her long-suffering support and help during my time at Curtin University. This thesis took much longer than was initially estimated but her resolve that I would finish this project never wavered. Sarah's support in editing the papers and this thesis was often provided during the late hours of what had already been a busy day. On the flip side, the extended length of study and associated reduced income provoked her to start another career and build a successful business. I guess it all worked out in the end.
- Lochlain Burton for his understanding from a young age about why Dad spent a lot of time in the shed by himself. If the only outcome of this research is that my son will value and respect the pursuit of education, then I'll be satisfied I've made an enduring contribution.
- Nigel Youngs of BP Kwinana Refinery along with Fred Gumbelton for their help in manufacturing specialised feeding tubes in their free time. These were used throughout the research project, and without them the research would not have been possible.

- BP Kwinana Management, in particular Laurie Costantin, Renee Hanemaaijer and Jason Cullen, for allowing me to work part time and odd hours during my time at University. I will always be extremely grateful to them for this opportunity. Without it, I would have been unable to support my family while completing this research.
- Brian Marsden and Simon Elwood who listened to my endless ramblings of how “things were going” and for the “encouragement” they gave me.
- Jeffrey Mayne for his advice and assistance to pursue this educational endeavour.
- One of the most underrated resources of any university is the Laboratory Technicians who help in setting up laboratory equipment and analysers. They have been a great help and, without them, I would not have been able to complete the research. I would like to thank Karen, Anne, Andrew, Jimmy, Jason and Arya for their time and efforts in assisting me throughout my research program.
- Wendy Wood took on the thankless task of reviewing the language, spelling, grammar, punctuation and formatting of this publication. Her expertise in subediting is matched only by her good nature in taking on an engineering research project. I’m forever grateful.

Finally, I would like to thank the Australian Government scholarship program.

Without this financial support of fees and subsidies, the research would not have been possible.

As I complete this body of work, I want to finish by reflecting on the qualities of knowledge and wisdom. It is my great hope this thesis increases the knowledge base of future conversion technologies in the renewable energy sector.

Knowledge is valuable in its own right. We are reminded, “There is gold and abundance of costly stones, but the lips of knowledge are a precious jewel”.^{Proverbs}

^{22:15} However, Albert Einstein counsels us, “Wisdom is not a product of schooling but of the lifelong attempt to acquire it.”

The combined value of knowledge and wisdom are evidenced by this passage, “For the protection of wisdom is like the protection of money, and the advantage of knowledge is that wisdom preserves the life of him who has it”. ^{Ecc1 7:12}.

LIST OF PUBLICATIONS

Journal papers

- [1] Burton, A; Wu, H, Mechanistic Investigation into Bed Agglomeration during Biomass Fast Pyrolysis in a Fluidized-Bed Reactor. *Energy Fuels* **2012**, 26, 6979-6987.
- [2] Burton, A.; Wu, H., Quantification of Interactions between Sand and Pyrolyzing Biomass Particles in Fluidized-Bed under Fast Pyrolysis Conditions Pertinent to Bio-Oil Production. *Ind Eng Chem Res* **2015**, 54, 7990-7997.
- [3] Burton, A; Wu, H, Differences in Bed Agglomeration Behavior during the Fast Pyrolysis of Mallee Bark, Leaf, and Wood in a Fluidized-Bed Reactor at 500 °C. *Energy Fuels* **2015**, 29, 3753-3759.
- [4] Burton, A.; Wu, H., Bed Agglomeration during the Drying of Mallee Leaf in Fluidized-bed. *Ind Eng Chem Res* **2016**, 55, 1796–1800
- [5] Burton, A.; Wu, H., Diagnosis of bed agglomeration in fluidized-bed under conditions for biomass pyrolysis at a wide range of temperatures. *Fuel* **2016**, 179, 103–107
- [6] Burton, A.; Wu, H., Influence of biomass particle size on bed agglomeration during biomass pyrolysis in fluidized-bed, submitted to *Proceedings of the Combustion Institute*, PROCI-D-15-00070, under review, submitted on 29 Nov 2015.

TABLE OF CONTENTS

DECLARATION.....I

ABSTRACT III

ACKNOWLEDGEMENTS..... VII

LIST OF PUBLICATIONS..... X

TABLE OF CONTENTS.....XI

LIST OF FIGURESXVI

LIST OF TABLESXXI

CHAPTER 1 INTRODUCTION 1

 1.1 Background and motive..... 1

 1.2 Scope and objectives 2

 1.3 Thesis outline..... 2

CHAPTER 2 LITERATURE REVIEW 5

 2.1 Introduction 5

 2.2 Importance of mallee biomass to Western Australia..... 6

 2.3 Mallee biomass structure 7

 2.3.1 Cellulose 8

 2.3.2 Hemi-cellulose 8

 2.3.3 Lignin..... 10

 2.3.4 Mallee extractives 10

 2.3.5 Influence of biomass structure on bed agglomeration 11

 2.4 Conventional biomass utilisation technologies - combustion and gasification 12

 2.4.1 Combustion..... 12

 2.4.2 Gasification 13

 2.4.3 Conventional combustors and gasifier reactors 13

2.4.4	Bed agglomeration in a fluidized-bed reactor	14
2.5	Fast pyrolysis a technology for producing bio-oil from biomass	17
2.5.1	Fast pyrolysis reactors	19
2.5.2	Mathematical modelling of pyrolysis	19
2.6	Research gaps	22
CHAPTER 3 METHODOLOGY AND EXPERIMENTAL TECHNIQUES		24
3.1	Introduction	24
3.2	Biomass sample collection and initial preparation	24
3.3	Ethanol leaching of biomass components	25
3.4	Fluidized-bed material	29
3.5	Characterisation of the fluidized-bed sand material	31
3.5.1	Free and packed bulk density and porosity	32
3.5.2	Surface area and particle size distribution of original screened bed material	33
3.5.3	Minimum fluidisation velocity of the selected sand bed material	33
3.6	Fluidized-bed pyrolyser reactor set up	35
3.7	Experimental procedures	38
3.7.1	Fast pyrolysis of biomass solids	38
3.7.2	Slow pyrolysis of biomass solids	40
3.7.3	Fast pyrolysis of biomass “extract”	42
3.7.4	Drying of biomass solids	44
3.7.5	Cleaning of the reactor	44
3.8	Analytical techniques	45
3.8.1	Determining particle size distribution	45
3.8.2	Determining the solvent-soluble and solvent-insoluble organic matter	45
3.8.3	Proximate analysis	46
3.8.4	Ultimate analysis	47
3.8.5	UV spectra	48
3.8.6	Analysis of inorganic species	48
3.8.7	Determining organic material in sand bed	50
3.8.8	Imaging	50

CHAPTER 4	MECHANISTIC INVESTIGATION INTO BED AGGLOMERATION DURING BIOMASS FAST PYROLYSIS IN A FLUIDIZED-BED REACTOR	52
4.1	Introduction	52
4.2	Experimental method.....	52
4.3	Results and discussion.....	53
4.3.1	Evidence of bed agglomeration during biomass fast pyrolysis in a fluidized-bed reactor	53
4.3.2	Dependence of bed agglomeration on pyrolysis temperature and holding time	57
4.3.3	Characteristics of bed agglomerates and correlations between bed agglomeration and organic matter in bed samples	59
4.3.4	Possible mechanisms responsible for bed agglomeration during biomass pyrolysis.....	64
4.4	Conclusions	69
CHAPTER 5	DIFFERENCES IN BED AGGLOMERATION BEHAVIOUR DURING THE FAST PYROLYSIS OF MALLEE BARK, LEAF AND WOOD IN A FLUIDIZED-BED REACTOR AT 500 ° C.....	71
5.1	Introduction	71
5.2	Experimental method.....	71
5.3	Results and discussion.....	71
5.3.1	Fast pyrolysis of raw mallee wood, leaf and bark	71
5.3.2	Fast pyrolysis of ethanol-washed mallee leaf and bark	74
5.3.3	Direct fast pyrolysis of extracts obtained from the ethanol-washing of mallee leaf and bark	78
5.3.4	Further discussion and practical implications.....	82
5.4	Conclusions	83
CHAPTER 6	QUANTIFICATION OF INTERACTIONS BETWEEN SAND AND PYROLYSING BIOMASS PARTICLES IN FLUIDIZED-BED UNDER FAST PYROLYSIS CONDITIONS PERTINENT TO BIO-OIL PRODUCTION	85
6.1	Introduction	85
6.2	Experimental method.....	85
6.3	Sand loading (S_L) as a key diagnosis parameter for bed agglomeration	86
6.4	Results and discussion.....	87

6.4.1	Distribution of char in bed agglomerates and non-agglomerate bed materials.....	87
6.4.2	Kinetics of bed agglomeration during continuous holding after the completion of feeding	91
6.4.3	Kinetics of bed agglomeration during biomass pyrolysis with continuous feeding.....	96
6.5	Conclusions	103
CHAPTER 7	DIAGNOSIS OF BED AGGLOMERATION DURING BIOMASS PYROLYSIS IN FLUIDIZED-BED AT A WIDE RANGE OF TEMPERATURES	104
7.1	Introduction	104
7.2	Experimental method.....	104
7.3	Results and discussion.....	105
7.3.1	Sand loading during biomass fast pyrolysis at a wide range of temperatures.....	105
7.3.2	Determination of activation energy (E_a) of the sand loading (S_L) during biomass fast pyrolysis	107
7.3.3	Overall equation of sand loading (SL) for bed agglomeration during biomass pyrolysis at a wide range of temperatures.....	113
7.4	Conclusions	116
CHAPTER 8	BED AGGLOMERATION DURING THE DRYING OF MALLEE LEAF IN FLUIDIZED-BED	117
8.1	Introduction	117
8.2	Experimental method.....	117
8.3	Results and discussion.....	118
8.3.1	Biomass recovery after drying in fluidized-bed and evidence of bed agglomeration	118
8.3.2	Nature of bed agglomerates during mallee leaf drying in fluidized-bed.....	120
8.3.3	Sand loading as a function of temperature during the drying of mallee leaf in fluidized-bed	122
8.4	Conclusions	126
CHAPTER 9	INFLUENCE OF BIOMASS PARTICLE SIZE ON BED AGGLOMERATION DURING BIOMASS PYROLYSIS IN FLUIDIZED-BED.....	127
9.1	Introduction	127
9.2	Experimental method.....	127

9.3	Results and discussion	128
9.3.1	Effect of biomass particle size on sand loading.....	128
9.3.2	Sand loading and mass transfer of sticky agent.....	130
9.3.3	Diffusive mass transfer of sticky agent	134
9.4	Conclusions	139
CHAPTER 10 CONCLUSIONS, IMPLICATIONS AND RECOMMENDATIONS FOR FUTURE TEST WORK		140
10.1	Conclusions from current test work.....	140
10.1.1	Agglomeration occurring in the pyrolyser.....	140
10.1.2	Differences in bed agglomeration behaviour of biomass components wood, leaf and bark	141
10.1.3	Determining whether the agglomeration is a random or a direct consequence of the pyrolysis process	141
10.1.4	How process conditions in the pyrolyser affect the interaction of the fluidized-bed sand material and the biomass particles	142
10.1.5	Effect of drying biomass.....	145
10.2	Practical implications of the current research.....	145
10.3	Recommendations and future work.....	147
REFERENCES		148
APPENDICES		163

LIST OF FIGURES

Figure 1.1	Thesis map	4
Figure 2.1	Structure of cellulose adapted from ⁶⁶	8
Figure 2.2	Chemical structure of galactoglucomannans in softwood adapted from ⁶⁸	8
Figure 2.3	Structure of arabinoglucuronoxylan in softwood adapted from ⁶⁹	9
Figure 2.4	Structure of glucuronoxylan found in hardwoods adapted from ^{1, 68}	9
Figure 2.5	Repeating chemical structure of Lignin adapted from ⁷⁰	10
Figure 2.6	Phase diagrams for sodium and potassium silicate eutectics adapted from ¹⁴³	17
Figure 3.1	Original sand material size distribution for the purchased thermal sand.....	29
Figure 3.2	Results for the bed column pressure drop vs. air flowrate for 125–250 µm sand bed material.....	34
Figure 3.3	Schematic diagram of fluidized-bed pyrolyser reactor used throughout the research experimentation.	36
Figure 3.4	Plot of furnace temperature vs. distance from top of furnace showing the isothermal zone (dashed lines) performed at furnace set temperatures of 700, 800 and 900 °C	37
Figure 3.5	Schematic diagram for feeding ethanol diluted extract during fast pyrolysis.....	43
Figure 4.1	Particle size distribution of total materials in the bed after biomass fast pyrolysis (pyrolysis temperature: 300–700 °C; feeding time: 4 minutes; holding time: 15 minutes; sand particle size: 125–355 µm; biomass particle size: 355–500 µm). A) before solvent washing; B) after solvent washing	54
Figure 4.2	SEM and optical images of bed agglomerates (pyrolysis temperature: 300, 500 and 700°C; holding time: 15 minutes); A, B and C: SEM images; D, E and F: optical images	56
Figure 4.3	Dependence of agglomeration yield on pyrolysis temperature (holding time: 15 minutes)	57
Figure 4.4	Dependence of agglomeration yield on holding time (pyrolysis temperature: 500 °C).....	59
Figure 4.5	Yield of total organic matter, solvent-soluble organic matter and solvent-insoluble organic matter as a function of pyrolysis temperature (holding time: 15 mins).....	61
Figure 4.6	Yield of total organic matter, solvent-soluble organic matter and solvent-insoluble organic matter as a function of holding time (pyrolysis temperature: 500 °C).....	62

Figure 4.7	Correlation between the yield of agglomeration (after the solvent washing of bed materials collected from biomass pyrolysis) and the yield of solvent-insoluble organic matter	63
Figure 4.8	Correlation between the reduction in the yield of agglomeration (due to the solvent washing of bed materials collected from biomass pyrolysis) and the yield of solvent-soluble organic matter	64
Figure 4.9	Distribution of bed agglomeration as a function of pyrolysis temperature (holding time: 15 mins)	65
Figure 4.10	UV fluorescence synchronous spectra of the solutions obtained from the solvent washing of bed materials collected from biomass pyrolysis at 400–700 °C (holding time: 15 minutes). The UV intensities are normalised to the amount of biomass fed into the pyrolysis reactor.	69
Figure 5.1	Particle size distributions (PSDs) of the bed materials collected from the fast pyrolysis of wood, bark and leaf in a fluidized-bed pyrolysis reactor at 500 °C and 15 minute holding time. Legends: 0 – bed material from wood pyrolysis, before the collected material being washed using solvent; 1 – bed material from bark pyrolysis, before the collected material being washed using solvent; 2 – bed material from leaf pyrolysis, before the collected material being washed using solvent; 3 – bed material from bark pyrolysis, after the collected material being washed using solvent; 4 – bed material from leaf pyrolysis, after the collected material being washed using solvent. The PSDs of sand (125–355 µm) and biomass (355–500 µm) fed to the reactor are omitted in the figure.....	72
Figure 5.2	Optical images of various samples. Legend: (A) bark particles (355–500 µm) before pyrolysis; (B) a typical bed agglomerate in the size fraction of 1.70–3.15 mm collected from bark pyrolysis; (C) leaf particles (355–500 µm) before pyrolysis; and (D) a typical bed agglomerate in the size fraction of 1.70–3.15 mm collected from leaf pyrolysis. The blue marks underneath the sample are the marks of millimetres.	74
Figure 5.3	Yield of extract (C% daf) from the washing of wood, bark and leaf using ethanol at room temperature for 4 hrs.	75
Figure 5.4	PSDs of the bed materials collected from the fast pyrolysis of ethanol-washed bark and leaf in a fluidized-bed pyrolysis reactor at 500 °C and 15 minute holding. Legends: 1 – bed material from ethanol-washed bark pyrolysis, before the collected material being washed using solvent; 2 – bed material from ethanol-washed leaf pyrolysis, before the collected material being washed using solvent; 3 – bed material from ethanol-washed bark pyrolysis, after the collected material being washed using solvent; 4 – bed material from ethanol-washed leaf pyrolysis, after the collected material being washed using solvent. The PSDs of sand (125–355 µm) and biomass (355–500 µm) fed to the reactor are omitted in the figure.....	76
Figure 5.5	Bed agglomeration yields during the fast pyrolysis of various feeding materials in a fluidized-bed reactor at 500 °C and 15 minute holding	

	time. The feeding materials include wood, bark, leaf, ethanol-washed bark (bark-EW), ethanol-washed leaf (leaf-EW), bark extract and leaf extract.....	77
Figure 5.6	PSDs of the bed materials collected from the fast pyrolysis of the extracts from bark and leaf in a fluidized-bed pyrolysis reactor at 500 °C and 15 minute holding. Legends: 1 – bed material from bark extract pyrolysis, before the collected material being washed using solvent; 2 – bed material from leaf extract pyrolysis, before the collected material being washed using solvent; 3 – bed material from bark extract pyrolysis, after the collected material being washed using solvent; 4 – bed material from leaf extract pyrolysis, after the collected material being washed using solvent. The PSDs of sand (125–355 µm) in the reactor has been omitted from the figure.	80
Figure 5.7	Optical images of typical bed agglomerates collected from the fast pyrolysis of leaf and bark extract sample in the fluidized-bed reactor at 500 °C and a holding time of 15 minutes. (A) agglomerated materials (>1.7 mm) resulting from the fast pyrolysis of leaf extract; (B) agglomerated materials (>1.7 mm) resulting from the fast pyrolysis of bark extract	82
Figure 6.1	Comparison in bed agglomeration yield Y_{AP} , which is the mass of bed agglomerates as percentage of the total mass of the bed sample, considering either particles with sizes >250 µm or particles with sizes >500 µm as bed agglomerates	88
Figure 6.2	Contribution of char in the bed materials below 500 µm to the total char recovered from the whole bed sample (i.e., M_C/M_C) during biomass fast pyrolysis in the fluidized-bed reactor at 500 °C. Panel (A): with continuous biomass feeding at various periods of time (1–17 minutes) then followed with a constant holding time of 15 minutes; Panel (B): with a fixed feeding time of 6 minutes then followed with various holding times (1–35 minutes).	89
Figure 6.3	Sand loading (S_L), expressed as g of sand in bed agglomerates per g biomass feed (db), as a function of holding time during biomass undergoing pyrolysis at 500 °C	91
Figure 6.4	Plot of biomass sand loading (S_L) vs char recovery (X_R) for biomass pyrolysis at 500 °C after the completion of 6 minutes feeding and varying holding time (1–35 mins)	93
Figure 6.5	Plots of (A) $\ln(X_R)$ vs holding time (t_h) and (B) Sand load (S_L) vs $\ln(X_R/X_{R0})$ for biomass pyrolysis at 500 °C after the completion of 6 minutes feeding and various holding time (1–15 minutes).....	95
Figure 6.6	Char recovery (X_R) as a function of biomass feed to sand ratio (R), due to continuous feeding of biomass into the fluidized-bed reactor (R is between 1.5 and 25 wt. %) during fast pyrolysis.....	97
Figure 6.7	Fraction of sand in bed agglomerate as a function of biomass feed to sand ratio R , due to continuous feeding of biomass into the fluidized-bed reactor (R is between 1.5 and 25 wt. %) during fast pyrolysis	98

Figure 6.8	Sand loading S_L as a function of biomass feed to sand ratio R , due to continuous feeding of biomass into the fluidized-bed reactor (R is between 1.5 and 25 wt. %) during fast pyrolysis.....	98
Figure 6.9	Bed agglomeration yield Y_{AP} as a function of biomass feed to sand ratio R , due to continuous feeding of biomass into the fluidized-bed reactor (R is between 1.5 and 25 Wt. %) during fast pyrolysis	99
Figure 6.10	Relationship between $\ln(S_L)$ and $\ln(R)$, due to continuous feeding of biomass into the fluidized-bed reactor (R is between 1.5 and 25 wt%) during fast pyrolysis.....	101
Figure 6.11	Back-calculated S_{L0} as a function of biomass feed to sand bed ratio R , due to continuous feeding of biomass into the fluidized-bed reactor (R is between 1.5 and 25 Wt%) during fast pyrolysis	102
Figure 7.1	Sand loading as function of temperature for bed agglomeration during the fast pyrolysis of the raw biomass, extract and ethanol-washed biomass samples at different temperatures (200–700 °C)	105
Figure 7.2	$\ln(S_L / R^{-0.5})$ as a function of $1/T$ for bed agglomeration during the fast pyrolysis of the raw biomass (A), extract (B) and the ethanol-washed biomass (C) samples at 200–700 °C	110
Figure 7.3	Mass of bed agglomeration per unit equivalent mass of biomass fed into the reactor during the fast pyrolysis of the raw biomass and extract samples at 170–275 °C during the build-up phase of the sand loading showing relative slopes	112
Figure 7.4	$\ln K_R$ or $\ln K_S$ as a function of $1/T$ for bed agglomeration during fast pyrolysis at 200–600 °C.....	114
Figure 7.5	Modelled sand loading for bed agglomeration during the fast pyrolysis of the raw biomass in a fluidized-bed reactor at different temperatures 200 – 700 °C	115
Figure 8.1	Biomass recovery (X_{Rb}) as a function of drying temperature (120–250 °C) in a fluidized-bed reactor in an air atmosphere	118
Figure 8.2	Particle size distribution results of bed samples collected after the drying of mallee leaf in a fluidized-bed reactor under air atmosphere at (1)120 °C, (2)170 °C, (3)190 °C and (4)250 °C	119
Figure 8.3	Bed agglomeration yield Y_{AP} (wt. %) as a function of drying temperature during the drying of mallee leaf in a fluidized-bed reactor at 120–250 °C in an air atmosphere.....	120
Figure 8.4	Typical optical microscope images of bed agglomerates in the bed samples collected after the drying of leaf in a fluidized-bed reactor at 170 °C under air atmosphere; panel A: bed agglomerate with sand-biomass binding of multiple particles in the size fraction of 500–710 μm ; panel B: bed agglomerate with both sand-particle and biomass-biomass binding of multiple particles in the size fraction of 500–710 μm ; panel C: bed agglomerate with both sand-biomass and biomass-biomass binding of multiple particles in the size fraction of 710–1000 μm ; panel D: bed agglomerate with both sand-biomass and biomass-	

	biomass binding of multiple particles in the size fraction of 1000–1700 μm	121
Figure 8.5	Modelled and measured sand loading values for raw leaf undergoing drying in an inert (argon) and air atmosphere in a fluidized-bed reactor at 120–250 °C. Legend: (Δ) measured values for biomass drying in inert atmosphere; (\square) measured values for leaf drying in air atmosphere; (dash curve) modelled values for biomass drying in inert atmosphere; and (solid curve) modelled values for biomass drying in air atmosphere.....	123
Figure 8.6	Plot of $\ln(S_L/R^{-0.5})$ as a function of $1/T$ during leaf drying in a fluidized-bed reactor at 120–250 °C under inert atmosphere (argon) and air atmosphere	124
Figure 9.1	Sand loading (S_L) as a function of biomass particle size (D_P) during the pyrolysis of leaf (panel A) and bark (panel B) in fluidized-bed at 500 °C under fast or slow heating conditions.....	129
Figure 9.2	$\ln(S_L)$ as a function of $\ln(D_P)$ during the pyrolysis of leaf and bark with various particles sizes (53–3000 μm) at 500 °C. Panel A: slow pyrolysis of leaf; panel B: fast pyrolysis of leaf; panel C: slow pyrolysis of bark; and panel D: fast pyrolysis of bark.....	133
Figure 9.3	Char recovery (X_R) as a function of particle size (D_P) during the pyrolysis of leaf (panel A) and bark (panel B) in fluidized-bed at 500 °C under fast or slow heating conditions.....	136
Figure 9.4	Differential particle size as a function of differential char recovery during the pyrolysis of leaf and bark with various sizes (430–3000 μm) at 500 °C. Panel A: fast pyrolysis of leaf; panel B: slow pyrolysis of leaf; panel C: fast pyrolysis of bark; panel D: slow pyrolysis of bark biomass.	138

LIST OF TABLES

Table 2.1	Summary of approximate mass concentrations of lignin, cellulose, hemi-cellulose and total extractives from mallee biomass components (wt. % dry basis)	11
Table 3.1	Summary of the ultimate and proximate results for biomass components washed with ethanol for 4 hrs. at ambient temperature.....	26
Table 3.2	Summary of ICP-AES AAEM results for various biomass components along with fraction of AAEM recovered in the extract biomass components used in the experiment.....	28
Table 3.3	Summary of ICP-AES analysis results for the sand bed material used throughout the experimental program, showing the chemical analysis for the major elements present.....	31
Table 3.4	Summary of the measured free and packed bulk densities and the calculated free and packed bulk porosities for the fluidized-bed sand material size fractions.	32
Table 3.5	Summary of the Malvern Mastersizer results for each of the original sand distributions analysed.	33
Table 4.1	Elemental analysis of chars collected at various pyrolysis temperatures and a holding time of 15 minutes.....	67
Table 7.1	Activation energies (E_a) and frequency factor (A_k) determined based on sand loading (S_L) for bed agglomeration during the fast pyrolysis of the raw biomass, ethanol-extracted biomass and extract samples at 200–700 °C	111
Table 8.1	Activation energies (E_a) and pre-exponential constants (A_k) for bed agglomeration during mallee leaf drying in fluidized-bed at 120–250 °C under air and argon atmosphere.....	124
Table 9.1	Values of N and K_M for sand loading during the pyrolysis of biomass particles	133
Table 9.2	Values of the average overall mass transfer coefficient K_D during the pyrolysis of biomass with various sizes at 500 °C and 15 minutes holding under either slow or fast heating conditions	137

CHAPTER 1 INTRODUCTION

1.1 Background and motive

Fast pyrolysis in a fluidized-bed reactor is one of the most promising technologies that can be used for the production of bio-oil. The bio-oil can not only be used as fuel source for combustion in furnaces, but with further upgrading and refining, it can be transformed into transport fuels¹⁻⁹ such as biodiesel. Bed agglomeration is a common phenomenon that has a detrimental influence on the durable operations of fluidized-bed reactors.¹⁰⁻¹⁶ Currently, most of the open literature is dedicated to agglomeration in fluidized-bed reactors when they are operating in either combustion or gasification modes. Very little has been performed on bed agglomeration occurring when they operate in pyrolysis mode.

Therefore, the research program designed and conducted in this thesis is geared towards at least three goals. The first goal is to evaluate if bed agglomeration does take place during fast pyrolysis of biomass in a fluidized-bed reactor. If so, what are the characteristics of bed agglomerates and the underlying fundamental mechanism governing such bed agglomeration. The second goal is to identify which components of the mallee wood, leaf or bark will dictate bed agglomeration if the whole biomass of mallee tree is processed in a fluidized-bed reactor. The third and last goal is to develop useful parameter(s) for diagnosing bed agglomeration during biomass fast pyrolysis in fluid bed under various conditions, including the effect of pyrolysis temperature, atmosphere, particle size, etc.

1.2 Scope and objectives

The scope of this thesis is to carry out a systematic investigation into bed agglomeration during biomass fast pyrolysis in a fluidized-bed reactor under various conditions.

The main objectives are to:

- Determine whether bed agglomeration does take place during biomass fast pyrolysis in fluidized-bed;
- Characterise bed agglomerates formed during biomass fast pyrolysis;
- Probe into the fundamental mechanism responsible for bed agglomeration;
- Identify the differences in bed agglomeration behaviour among the fast pyrolysis of various mallee biomass components (wood, leaf and bark) in fluid bed;
- Develop new parameter(s) for diagnosing bed agglomeration during biomass fast pyrolysis in fluidized-bed;
- Apply the new parameter(s) for diagnosing bed agglomeration during biomass fast pyrolysis under thermally-thin conditions at 300–700 °C;
- Apply the new parameter(s) for diagnosing bed agglomeration during biomass drying at 120–250 °C;
- Apply the new parameter(s) for diagnosing the effect of biomass particle size on bed agglomeration during biomass fast pyrolysis in fluidized-bed.

1.3 Thesis outline

This thesis has a total of 10 chapters and an appendix. The thesis structure is schematically illustrated in the thesis map (Figure 1.1), with the synopsis of each chapter given below:

Chapter 1 provides an overall introduction of this thesis, including background, motives, scope, objectives and thesis outlines;

Chapter 2 reviews the literature and identifies research gaps, which leads to the determination of specific objectives for the current research;

Chapter 3 presents the research methodologies employed in this study;

Chapter 4 presents the evidence to show that agglomeration during pyrolysis occurs;

Chapter 5 determines the differences in bed agglomeration from various biomass components during pyrolysis in fluidized-bed;

Chapter 6 introduces a new parameter, sand loading (S_L), for diagnosing the interaction between sand and pyrolysing biomass particles to form bed agglomerates;

Chapter 7 investigates bed agglomeration during biomass pyrolysis in fluidised bed at a wide range of temperatures using S_L ;

Chapter 8 investigates bed agglomeration during the drying of leaf biomass in a fluidized-bed dryer in an inert or air atmosphere using S_L ;

Chapter 9 investigates the influence of biomass particle size on bed agglomeration during biomass pyrolysis in fluidized-bed using S_L ;

Chapter 10 summarises the conclusions and outlines the practical implications of the current study along with recommendations for future research.

Appendix collates the permissions obtained for the use of the published papers in this thesis.

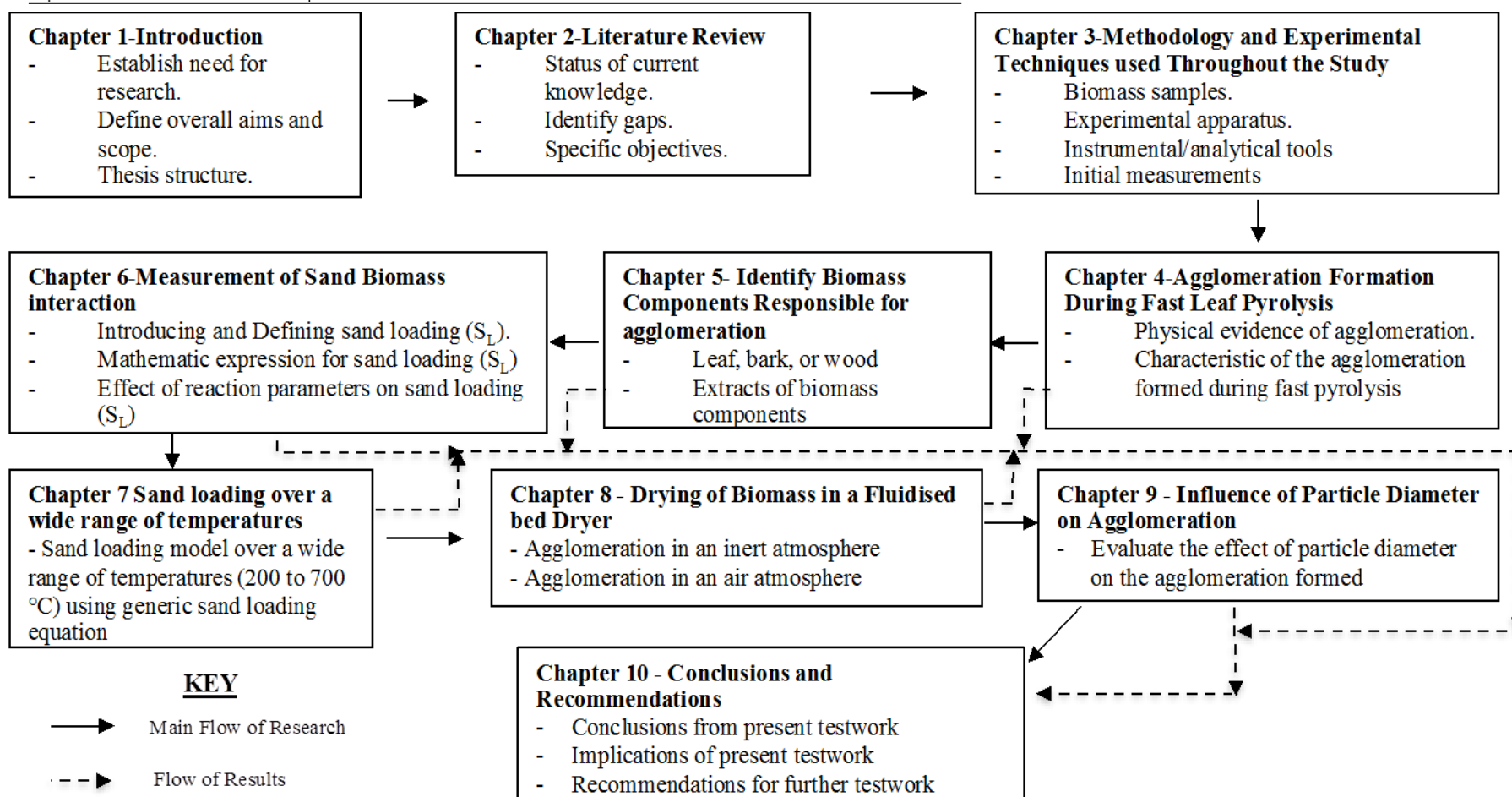


Figure 1.1 Thesis map

CHAPTER 2 LITERATURE REVIEW

2.1 Introduction

Low cost and plentiful energy in all its forms is generally the backbone of all modern economies and is essential for a well-ordered and functioning society.¹⁷ This is particularly true and important for Australia, whose citizens enjoy a post-modern lifestyle. Since energy is a vital part of any economy, most governments have now placed energy security as part of their policy and strategies.¹⁷⁻²¹ Australia is no different and has its own policies in place^{22, 23} as noted by the formation in 2001 of the think tank, Australian Strategic Policy Institute, by the Australian government. The Western Australia state government also has an energy security paper²⁴ which is used to direct research and the development of energy resources within the state.

Although energy may be the backbone of an economy, it is also arguably the cause of climate change,²⁵⁻³⁰ due to the subsequent release of carbon dioxide (CO₂) during its conversion (or combustion) to usable energy. Governments and industry around the world are actively looking at ways to slow the amount of CO₂ being placed into the atmosphere by supplementing energy requirements with renewable energy sources,²⁵⁻³⁹ such as solar, wind, geothermal, hydro and biomass, to name a few. Of particular importance to the West Australian government is the biomass component of the energy mix used for the control and abatement of salinity in the farming areas of Western Australia, particularly the Narrogin region.⁴⁰⁻⁴⁴

2.2 Importance of mallee biomass to Western Australia

The southwest of Western Australia is one of the largest agricultural farming areas in the state, producing grain and livestock for both the local and international markets. Dry land salinity in this region has caused approximately 7000 farms (~1.2 million hectares) to show significant signs of degradation,⁴¹ this currently represents 10–12 % of the farmland available within the region. On a business as usual scenario, it is expected that approximately 30% of West Australian farms and approximately 15%, on average, for all Australian farmland will show significant degradation due to salinity by the year 2050.^{44, 45}

Salinity of the soils has mainly been caused by land clearing or the removal of the natural vegetation. Most of the removed vegetation consisted of deep-rooted perennial plants in the form of trees, which have been replaced with the shallow-rooted annual crops. These crops consist mainly of wheat and various types of grain, along with postural grassland used to raise livestock.^{42, 46, 47}

The land clearing, along with current farming practises, produced overt problems in the hydrology within the region.⁴² The removal of the natural deep-rooted vegetation caused the water table level to rise in some areas. With this rise, the stable salts stored in the lower levels of the soil mobilised to the surface with the water table. This in turn, caused large tracts of land to either be waterlogged or too saline for crops and pasture growth, rendering the land unusable for farming.^{40, 41, 47}

Various authors performed research into reclamation and treatment of these areas.^{40-42, 44-54} The most cost-effective remedy for the treatment of the affected

areas is to plant mallee trees in alleys between annual crops. This solves two issues: firstly, it controls the level of the water table as normal rainfall washes the salts from the surface to lower levels in the soil, rendering the soil useable for farming again. Secondly, the mallee trees have also been identified as a secure and carbon neutral biomass resource, which can be used as the feed source to the fledgling bio-fuels and bio-energy industries^{46, 50, 55-59} within the state. Mallee trees have been calculated to have an energy ratio in the region of 20–41 compared to an annual crop residual, which has an energy ratio from 4–7.^{60, 61} Energy ratio is calculated as the total energy output divided by the total non-renewable energy input (both direct and indirect), making mallee biomass an ideal candidate for the fledgling agro-forestry industry in the area. These trees can not only be harvested for their energy content but also for the eucalyptus oils and chemicals contained within them; these can be used as a feed stock for the bio-refining industry⁵⁹ to produce transport fuels such as biodiesel.

2.3 Mallee biomass structure

Mallee trees consist of three major biomass components - wood, bark and leaf. The average overall mass composition of these components of the tree are 50% wood, 15% bark and twigs, with the remaining 35 % being leaves.⁵⁹ Each of these biomass components are essentially composed of three main organic polymerized chemical structures – cellulose, hemi-cellulose and lignin – in varying amounts depending on the plant species and component type (leaf, wood or bark).^{62, 63}

2.3.1 Cellulose

Figure 2.1 (below) is a schematic representation of the repeating structure of cellulose. Cellulose is composed of polymerized linear chains of D-Glucose linked by β -1,4 glycosidic bonds with carbon content from 1000 to 10000 units.^{1, 64-66}

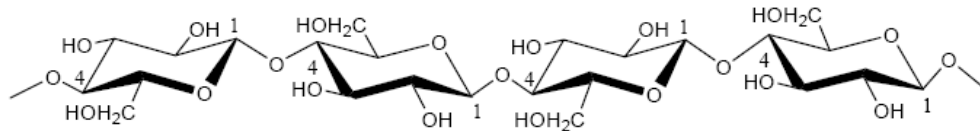


Figure 2.1 Structure of cellulose adapted from⁶⁶

2.3.2 Hemi-cellulose

The chemical composition of hemi-cellulose is varied depending on the hardness of the wood. In softwood the main components are galactoglucomannans (shown in Figure 2.2) and arabinoglucuronoxylan (shown in Figure 2.3).^{67, 68}

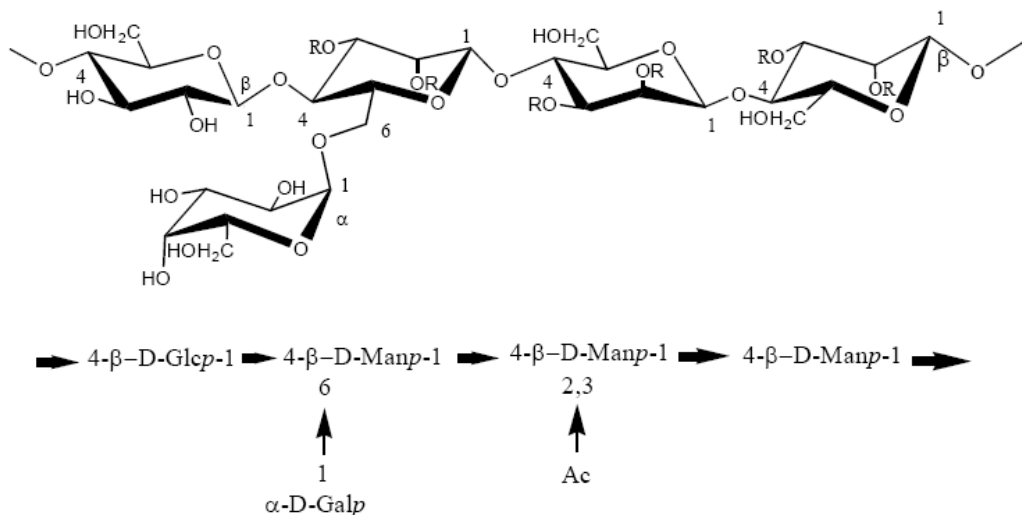


Figure 2.2 Chemical structure of galactoglucomannans in softwood adapted from⁶⁸

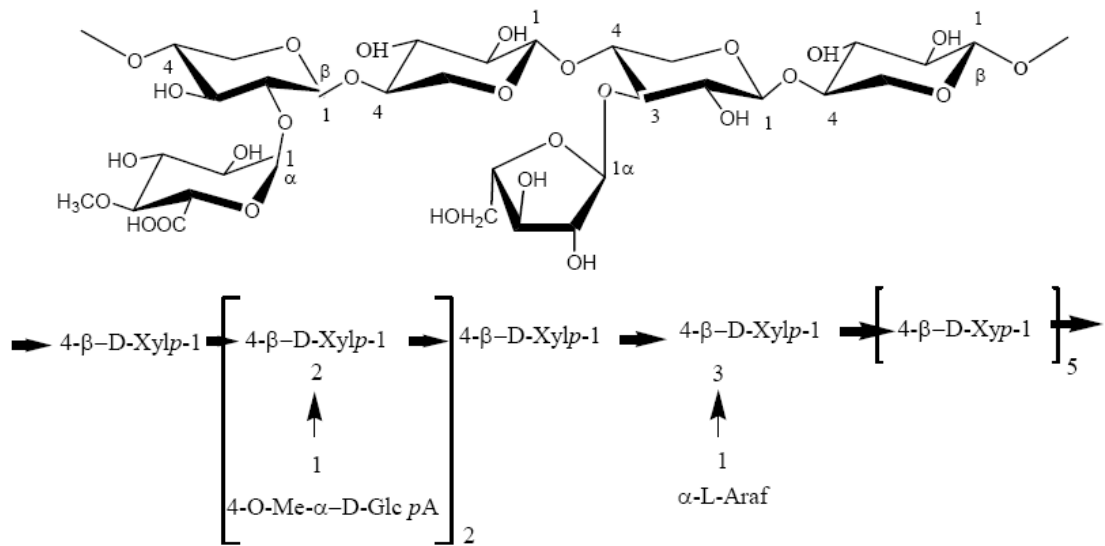


Figure 2.3 Structure of arabinoglucuronoxylan in softwood adapted from [Error! Hyperlink reference not valid.](#)

For hardwoods the main component is glucuronoxylan. Figure 2.4 (below) is an abbreviated chemical structure for the glucuronoxylan structure found in hardwoods.¹

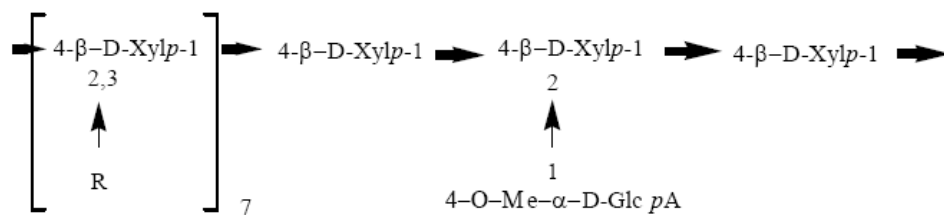


Figure 2.4 Structure of glucuronoxylan found in hardwoods adapted from^{1,68}

2.3.3 Lignin

Figure 2.5 is a chemical representation of the repeating chemical structure of lignin.⁷⁰ Lignin is generally accepted as a polymerised group of phenol compounds; these compounds are responsible for the rigidity of the cell wall.⁶⁴

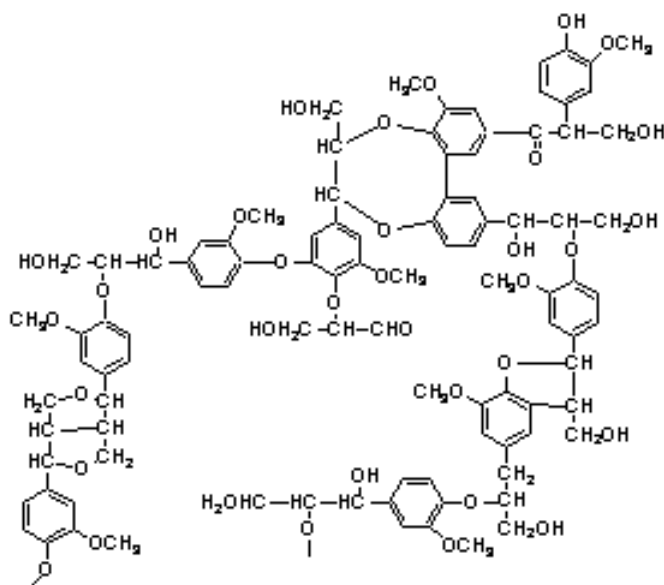


Figure 2.5 Repeating chemical structure of Lignin adapted from⁷⁰

2.3.4 Mallee extractives

Not only does the mallee biomass comprise of the three main organic polymerised chemical structures – cellulose, hemi-cellulose and lignin as discussed above – it also contains extractives. These are organic compounds that can be extracted by the use of polar and non-polar solvents, acid solvents and water^{62, 63, 71-74} and range from simple oils such as eucalyptus oil, to complex flavonoid compounds.

The contents for the cellulose, hemi-cellulose, lignin and extractives contained in the mallee leaf, bark and wood have been previously^{62, 63} reported by other authors and the results are summarised below in Table 2.1.

Table 2.1 Summary of approximate mass concentrations of lignin, cellulose, hemi-cellulose and total extractives from mallee biomass components (wt. % dry basis)

Compound	Leaf ⁶²	Bark ⁶³	Wood ⁶²
Lignin	25.9	14.4	24.9
Cellulose	14.6	30.9	22.2
Hemi-cellulose	14.8	19.5	40.7
Total Extractives *	44.7	35.2	12.2
* Calculated by difference			

2.3.5 Influence of biomass structure on bed agglomeration

To date there has been no definitive study into how each of the polymerised structures cellulose, hemi-cellulose, lignin and extractives affect the bed agglomeration during pyrolysis. There has however been a multitude of studies performed by various authors on the effect each of the structures on the pyrolysis gasification and combustion reactions. Section 2.5 below in part discusses the individual effect of the biomass structure on the pyrolysis reactions, which are pertinent to this study.

2.4 Conventional biomass utilisation technologies - combustion and gasification

Conventional biomass conversion technologies employ either combustion or gasification for the conversion of biomass to energy (in the case of combustion) or synthesis gas (in the case of gasification).

2.4.1 Combustion

Combustion of biomass, either as biomass only or co-combustion (mixed in with coal), involves the oxidation of the biomass with excess air (1.1 to 1.3 times stoichiometric requirement) to produce heat, CO and CO₂, along with small amounts of SO_x and NO_x.⁷⁵⁻⁸² Combustion is generally defined as a complex sequence of chemical reactions where a fuel and oxygen react at sufficiently high temperatures so heat and light evolve.⁸³

Combustion of biomass can be considered as a three- or four-step process^{75, 77, 78, 80, 84} depending on the drying and volatilisation steps being taken as one or two steps. The sequenced steps are listed below:

- Drying of the biomass particle;
- De-volatilisation of entrapped hydrocarbons;
- Pyrolysis of the particle to form char and volatiles;
- Combustion of the char and volatiles.

Modelling the combustion of biomass particles reaction is essentially based on the simultaneous numerical solution of heat and mass balance equations for each of the above mentioned process steps and is comparable to the combustion of coal.^{77, 78, 80}

2.4.2 Gasification

Gasification is the partial oxidation of the biomass by sub-stoichiometric (<0.8) amounts of air.⁸⁵⁻⁸⁸ This process produces organic vapours (low calorific value gas) and energy. The synthesis gas can either be fed directly into a boiler or gas turbine and combusted or can be further upgraded by Fischer-Tropsch reactions to form chemical building blocks for downstream chemical industries⁸⁹⁻⁹⁹ and transport fuels such as biodiesel.

2.4.3 Conventional combustors and gasifier reactors

The combustion of biomass, or the co-combustion of biomass and coal up to a maximum of 20 wt. % biomass in some cases,¹⁰⁰ can be performed in various types of combustors such as pile burners, stoke graters (both stationary and moving),¹⁰¹ bubbling fluidized-bed, circulating fluidized-bed^{76, 77, 101-103} and suspension burners, to name a few. Fluidized-bed or circulating fluidized-bed reactors are the most common commercially used reactors for both gasification and combustion. This is due to the good thermal efficiency, feed combustion / gasification completion and the flexibility of feed that can be fed to the combustor or gasifier.^{101, 103, 104} Although the fluidized-bed is the most popular type of combustor / gasifier used commercially for the conversion of biomass, one major factor plagues the operation of these reactors, that is agglomeration of the bed which usually occurs when trying to operate at high (>650 °C) reaction temperatures.¹⁰⁵⁻¹¹¹

2.4.4 Bed agglomeration in a fluidized-bed reactor

One of the major factors in the expansion of using fluidized-bed reactors in the conversion of biomass to energy either operating in gasification or combustion mode, is that the operation of a fluidized-bed at elevated temperatures ($>650\text{ }^{\circ}\text{C}$) is usually limited due to the tendency of the particles to form agglomerates.^{13, 112-114} Formation of these agglomerates, in turn, leads to the de-fluidising of the bed resulting in unplanned shut downs of the reactor while it is cleaned out. In the worst cases, the total fluidising bed is replaced. This results in a lower overall conversion efficiency for the process as the availability of the reactor is compromised during this period. The point of de-fluidisation may occur at temperatures well below the normal melting or softening point of the sand bed particles themselves.^{14, 114-118} This phenomenon is not only prevalent in the combustion or gasification of biomass, but also has been encountered in several other processes which include coal combustion and gasification, iron ore reduction and cement manufacture.^{14, 15, 113, 118-120}

Agglomeration is seen to be caused by the gathering of sintered particles^{112, 115, 121} (in the case of combustion it is seen as the ash particles) coming together and then combining with the fluidized-bed particles to form larger particles or agglomerates which de-fluidise from the bed. The de-fluidisation rate increases at elevated temperatures, causing more rapid and stronger bonding of the agglomeration of the particles^{118, 121-124} to occur.

A number of techniques have been developed over the years to prevent the agglomeration or, at the very least, to extend the time taken for agglomeration to occur. These include increased particle size, lower operating temperatures

(<650 °C), higher fluid velocities (leading to the development of the circulating bed combustors and gasifiers) and varied types of fluidized-bed material which is designed to absorb the sintering particles themselves.^{14, 16, 114-116, 118, 125-127}

Other researchers^{12, 128-134} have investigated the initial connections and continuing interaction of the particles forming agglomerates in a fluidized-bed and they have concluded that the production of the agglomeration is the continuous resultant of 2 inter-particle forces: the forces that allow agglomeration to occur and the forces that cause deterioration of the agglomeration formed. The adhesive forces, which allow agglomeration to form, include electrostatic, Vander Waals and liquid capillary action (can be caused by heating or chemical reaction products), this is also known as “bridge force”. The forces that seek to decrease the agglomeration include collision (effect of particle-particle interaction) along with elastic repulsive forces. The main culprits for strengthening agglomerates in the fluidized-bed reactors especially at high temperatures >650 °C have been identified as the contained silica and alkali earth metal species^{14,105,135-138} such as Na, Mg, Ca and K, to name a few. These metals are inherently present in all forms of biomass and to a certain extent in coal. Four main mechanisms^{118,121,125,137} have been identified for transport of material from sintered particles to form the bonds necessary for agglomeration with the sand bed material. These are surface diffusion, volume diffusion, viscous flow and vaporisation/condensation. Surface and volume diffusion involves the movement of atoms from a region of high density to the porous sections of the particle.¹¹⁵ Surface diffusion is only important during the initial stages of sintering as significant densification cannot occur by this mechanism.¹¹⁸ In some cases, the

surface diffusion is the starting mechanism causing the particles to adhere, after which volume diffusion occurs and causes densification.¹¹⁵

Viscous flow due to surface tension: surface tension varies with the curvature of the surface of the particle allowing flow from convex to concave regions within the particles.¹¹⁵ This phenomenon is also known as sintering in the presence of a “liquid phase”. Agglomerates formed by viscous flow sintering are usually more strongly bonded than agglomerates formed by diffusion.¹¹⁵ Transport of material by vapour is known as vaporisation and condensation. The rate at which the material is transported by the vapour is expressed as a function of the difference in equilibrium pressures of the surfaces. The vapour pressure above a concave surface is lower than that of a convex surface allowing condensation to occur.¹¹⁵ It is proposed^{105, 115} that initial sintering of the particles is caused by the interaction of the particles in the bed. Surface diffusion causes the initial sticking of the particle followed by the densification of that site by either volume diffusion or viscous flow. Many authors^{11, 137, 139-141} report viscous flow is the probable route for the densification of the initial contact site. This is due to the fact that both sodium and potassium form a liquid phase at normal reaction conditions (650 to 920 °C) with silica; Figure 2.6 (below) is an indication of this. Some authors^{11, 15, 138, 142} have also suggested the condensation and vaporisation of the alkali earth metals are also responsible for the densification of the initial contact site, although it may be to a lesser extent.

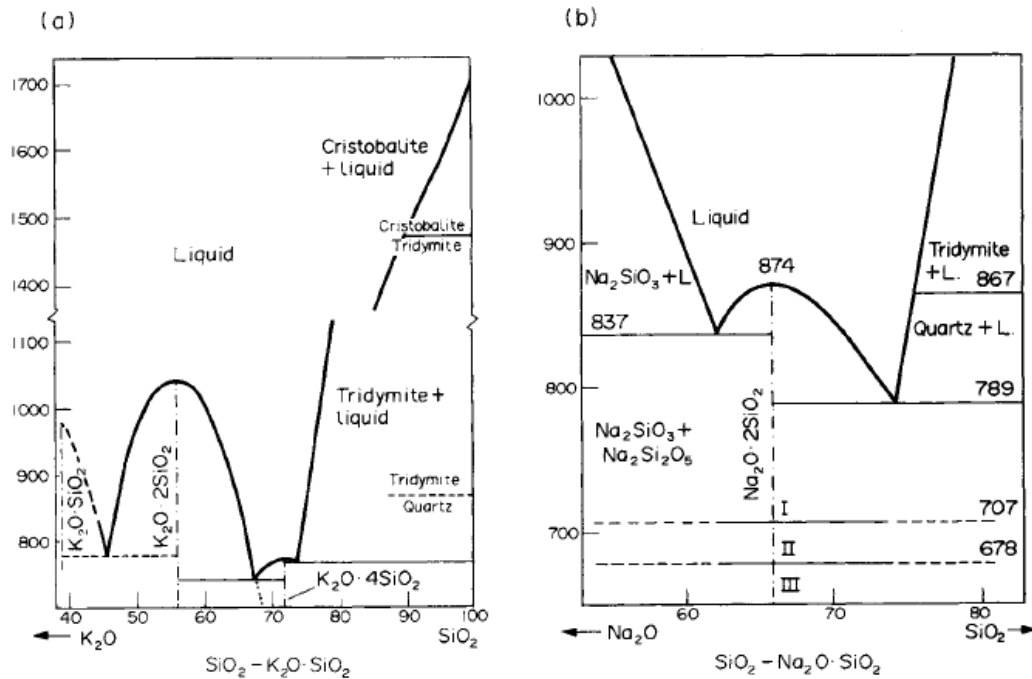


Figure 2.6 Phase diagrams for sodium and potassium silicate eutectics adapted from¹⁴³

The pressure drop across the bed increases as agglomeration is taking place. Once agglomeration is complete, the pressure drop across the bed is reduced to below the fluidisation pressure drop¹³¹ and the bulk temperature in the bed increases causing further agglomeration and, in the worst cases, total bed agglomeration.

Various methods to predict the agglomeration of a bed before it occurs have been investigated by a large number of authors. The methods used vary from extremely sensitive pressure and temperature measurements, to differential pressure analysis and conductivity measurements of the fluidized-bed itself.^{10, 109, 110, 117, 131}

2.5 Fast pyrolysis a technology for producing bio-oil from biomass

Pyrolysis is generally defined as the thermal breaking down of organic material in the absence of oxygen.¹⁴⁴ The products of pyrolysis are smaller gas compounds such

as methane, ethane, CO and CO₂, along with the production of bio-oils and bio-char.^{1, 144-147}

Two forms of pyrolysis exist, fast and slow. Each is totally dependent on the heat-rate selected for the pyrolysis reaction. In slow pyrolysis, the particle heating rate is generally <200 K/min. While for fast pyrolysis, the heating rate of the particle is >200 K/sec.^{1, 145, 147-154}

The products produced by each of the types of pyrolysis differ. Slow or conventional pyrolysis, where heating rates from 1×10^{-3} to 200 K/min are applied, produces high charcoal yields from the biomass.¹⁵³⁻¹⁵⁵ Fast or flash pyrolysis, where heating rates exceed 200 K/sec, results in low char yield dependent on the reactor temperature and gas residence times. For high gas yield, the residence times are around one second and temperature is above 920 K. For a high “liquid” or bio-oil yield, the reactor temperature ranges from 620 to 920 K and residence times are shorter than one second.^{1, 144, 154-156} Thus, fast or flash pyrolysis is the best pyrolysis reaction for the production of bio-oil from biomass.

The gasses generated from the pyrolysis reaction can be directly converted to energy by either being co-combusted with another fuel gas or by itself in an industrial boiler system, which could be making steam for heating or electrical power generation.^{79,}

¹⁵⁷ The “liquids” or bio-oil generated in the pyrolysis reaction are more valuable than the gases generated and can be collected from condensers that quench cool the exiting gas from the outlet of the reactor. The non-condensing gases are usually combusted directly in industrial furnaces, boilers and gas turbines.¹⁵⁸⁻¹⁶⁰ The bio-oils

are collected and can be further upgraded in value in a bio-oil refinery^{1, 161, 162} with further processing to produce transport fuels such as biodiesel and chemical building blocks for further chemical industry feed stocks such as phenols and alcohols.

2.5.1 Fast pyrolysis reactors

Pyrolysis can be performed in a variety of reactors such as fixed bed, fluidized-bed, circulating fluidized-bed ablative or rotary cone reactors.^{1, 144, 146, 148, 156, 163-169} Each of these reactors has advantages and disadvantages.^{1, 144, 156, 166} The most common type of reactor presently used in commercial plants is a fluidized-bed or a modified fluidized-bed, in the form of a circulating fluidized-bed reactor.^{1, 144, 148, 163, 166}

Argon and nitrogen are the most commonly used industrial gases to provide both the required inert atmosphere and the subsequent bed fluidisation gas^{1, 144, 166} for the reactors. These reactors provide a number of advantages over the other types listed above. Firstly, they are more thermally efficient.^{144, 155, 158, 170-172} Secondly, the pyrolysis products from the reactor can be manipulated by adjusting the gas residence time, reactor temperature profiles and feed rates.^{1, 144, 145, 154, 155, 166} This makes them a lot more flexible in operation and the ideal reactor for the manufacture of bio-oils from biomass directly.

2.5.2 Mathematical modelling of pyrolysis

Two main effective overall models for the reaction mechanisms have been developed to aid in the modelling of the reaction kinetics of the pyrolysis process. The first, a simple overall model of the biomass pyrolysis reaction mechanism was first developed by Pyle and Zaror.¹⁷³ This model assumes a constant ratio of char to

volatile yield for all reaction temperatures.¹⁷⁴ This, however, cannot be extended to general cases and is thus limited in its use, although still useful for overall general trends. The second model is more complex in nature; it was developed by Chan et al,^{150, 151} who proposed a two-stage, semi-global reaction mechanism model in which the reaction kinetics of pyrolysis includes both primary and secondary reactions. This model takes into account successive and parallel reactions taking place during the process of pyrolysis. Where the biomass is decomposing into gasses, char and tar, the tar further decomposes to form char and gasses.

In biomass, which is mainly composed of cellulose, hemi-cellulose and lignin as indicated above, each of these complex organic molecules undergoes pyrolysis separately.¹⁷⁴ Maximum pyrolysis rates are achieved at different temperatures for each of these compounds: cellulose (640 K), hemi-cellulose (565 K) and lignin (620 K). Lignin decomposes slower than both the cellulose and hemi-cellulose but over a wider temperature range¹⁷⁴ starting at about 384 K and finishing at 1173 K.¹⁷⁵ Pyrolysis reactions (fast or slow) have been found to follow Arrhenius's rate law.^{145, 173, 176, 177} The single reaction model is the most frequently used¹⁷⁸ model for both fast and slow pyrolysis. When the model is used for the overall global modelling of both the kinetics and pyrolysis process, the order of the reaction generally encompasses the thermal and transport effects experienced by the particle during the pyrolysis process, reaction order ranges from 0.83 to 1.81.¹⁷⁹ Most researchers use a first-order reaction rate to model the pyrolysis reaction^{144, 145, 148, 150, 151, 178} whether the reaction is due to fast or slow pyrolysis in either a fixed or fluidized-bed reactor.

For an accurate model for either fast or slow pyrolysis, the following processes need to be determined and modelled: ^{144, 146, 148, 176, 180}

- Heat transfer to the particle by radiation, convection and conduction;
- Diffusion of gaseous reactants to the particle through the gas film separating the particle from the bulk fluid;
- Heat transfer within the particle by conduction and radiation;
- Diffusion of gaseous reactants through the unconverted virgin solid;
- Chemical reaction of the convertible solid, forming the primary products of pyrolysis;
- Intra- and extra-particle, homogeneous and heterogeneous chemical reactions of the primary pyrolysis products;
- Diffusion of gaseous products through the converted solid product;
- Diffusion of gaseous products away from the particle through the gaseous boundary layer.

From the summarized process outlined above, there are large interactions between the internal and external transport processes, along with the actual reaction kinetics, which are dependent on these processes. Any model needs to account for them.

Various characteristic numbers ^{155,171} have been developed to measure the ratio or relative values of the internal and external effects of each of the transport processes listed above. This is done in order to determine which of the effects is controlling the overall process. One of the most important numbers developed is that of the Biot number (B_i). This number measures the relative magnitudes of the internal (particle) and external mass and heat transfer. ^{171, 180} When $B_i > 1$ then the internal heat transfer is smaller than the convective heat transfer and there is a tendency for large heat gradients to be formed in the particle. This regime is also known as the thermally

thick region where the reaction is controlled by internal heat and mass transfer effects. For $B_i \ll 1$ this is known as the thermally thin region which indicates that there is very little temperature gradient within the particle and as such that the pyrolysis reaction itself is controlling the overall process.¹⁵³ The thermally thin region for wood particles experimentally was found to be less than 20 mm.^{171, 180-183}

2.6 Research gaps

The use of a fluidized-bed reactor operating under fast pyrolysis conditions is the ideal type of reactor for the manufacture of bio-oils. This is due to the fact that the reaction conditions can be manipulated to maximise the bio-oil yield and the overall thermal efficiency. There is a large amount of research available on the modelling of the pyrolysis reaction both for fast and slow pyrolysis, either carried out in a fixed bed or fluidized-bed reactor. There also exists a good understanding of the agglomeration that occurs during combustion and gasification as to its initiation, cause and effect on the fluidized-bed. However, the agglomeration phenomenon as it pertains to the pyrolysis in a fluidized-bed reactor, or the actual interaction of the biomass particle undergoing pyrolysis and the fluidized-bed sand particle, has not previously been reported or researched in any depth in the open literature. The following research gaps have been identified and will be answered in this thesis:

- It is largely unknown if bed agglomeration takes place during biomass pyrolysis in fluidized-bed;
- The fundamental mechanism governing bed agglomeration during biomass fast pyrolysis in fluidized-bed is unclear;

- It is unknown if there are any differences in bed agglomeration behaviour among the pyrolysis of different biomass components (wood, leaf and bark);
- The effect of process conditions in the fluidized-bed reactor on bed agglomeration needs to be explored;
- It is unknown if bed agglomeration takes place in fluidized-bed dryer at low temperatures in air conditions;
- There is a strong need to develop parameter(s) which can be used to diagnose bed agglomeration during biomass fast pyrolysis in fluid bed.

CHAPTER 3 METHODOLOGY AND EXPERIMENTAL TECHNIQUES

3.1 Introduction

This chapter details the sample preparation, apparatus, methodologies and analytical techniques used throughout the experimental program. The chapter outlines:

- Sample collection and preparation of the biomass components;
- Ethanol leaching of the biomass components to produce the samples required for the experimentation program;
- Collection and preparation of the sand material;
- Characterisation of the sand bed material;
- Fluidized-bed reactor set-up;
- Outline of pyrolysis experimental procedures used;
- Analytical techniques encompassed.

3.2 Biomass sample collection and initial preparation

Green mallee trees were harvested from a field in Narrogin, Western Australia. The trees were manually separated into their respective biomass components (wood, leaf and bark). These components were allowed to air dry in the laboratory until the moisture content reached <10 wt. %. Once dry, the components were milled; each component was milled separately and the mill was cleaned before and after each component, to minimise the risk of contamination during the milling process. The resulting milled samples were then subjected to mechanical sieving into the following nine size fractions <106 μm , 106–125 μm , 125–355 μm , 355–500 μm ,

0.5–0.71 mm, 0.71–1.0 mm, 1.0–1.7 mm, 1.7–3.15 mm and >3.15 mm. The sieves were cleaned using a stiff nylon brush and finally immersed in a sonic bath before being used for the next biomass component. The sieves used were calibrated standard Tyler series sieves, which are commercially available for laboratory use. Once the samples were sieved, each size fraction was placed into an airtight container to reduce the risk of contamination, moisture ingress and sample degradation during storage.

3.3 Ethanol leaching of biomass components

Ethanol of 99.5 % purity was used to extract the solvent-soluble oils and compounds from the biomass components. A portion (10g) of the wood, leaf and bark components were subjected to an ethanol (200 ml) leach in which the biomass and ethanol were stirred continuously in a vessel for four hours at ambient temperature. The stirrer speed was adjusted to ensure intimate contact between the biomass and the ethanol was achieved. The ethanol was added in excess of the biomass to ensure the concentration gradient was sufficient to extract as much as possible from the biomass components.

Once the leaching was completed, the solids and ethanol were separated using filtration. After filtration the solids were washed with fresh ethanol to remove any residue from the surface of the biomass solids. The ethanol washings were combined with the leachate and subjected to evaporation of the ethanol from the leachate. Evaporation of the ethanol was carried out in a fume cupboard using a hotplate set at 45 °C. Once the ethanol was evaporated, the “extract” was collected and placed into airtight containers to prevent contamination during storage.

To differentiate the material being used in subsequent experiments, the material before ethanol leaching was given the prefix “raw”. The biomass solid material after leaching with ethanol was given the prefix “washed”. The material resulting from the evaporation of ethanol was given the suffix “extract”. Table 3.1 is a summary of the results for the approximate ultimate analysis of the “raw”, “washed” and “extract” material from each of the biomass components treated. Methods used for the proximate and ultimate analysis can be found in 3.8.3 and 3.8.4, respectively.

Table 3.1 Summary of the ultimate and proximate results for biomass components washed with ethanol for 4 hrs. at ambient temperature.

Ultimate Analysis wt. % daf						Proximate Analysis wt. % db			
Component	C	H	N	S	O ^a	Moisture	Ash	VM ^b	FC ^c
Raw Wood	45.95%	6.10%	0.16%	0.64%	47.14%	2.6%	0.6%	83.0%	13.8%
Washed Wood	46.12%	6.33%	0.22%	0.80%	46.52%	3.3%	0.5%	80.7%	15.5%
Wood Extract	48.72%	7.62%	0.42%	0.92%	42.32%	2.8%	1.8%	74.7%	20.7%
Raw Bark	46.80%	5.41%	0.36%	0.73%	46.72%	3.6%	5.4%	69.0%	22.%
Washed Bark	44.04%	6.06%	0.51%	0.76%	48.63%	2.4%	6.3%	72.0%	19.3%
Bark Extract	55.46%	6.11%	0.17%	0.87%	37.39%	9.1%	0.7%	54.2%	35.9%
Raw Leaf	52.19%	6.55%	1.35%	0.72%	39.19%	4.8%	3.7%	71.2%	20.4%
Washed Leaf	47.82%	6.12%	1.71%	0.79%	43.57%	2.1%	4.4%	72.8%	20.8%
Leaf Extract	57.32%	7.91%	0.31%	0.88%	33.58%	10.2%	1.6%	67.5%	20.7%

a Calculated by difference, b Volatile Material, c Fixed Carbon

The individual biomass components were analysed for the inorganic species using ICP-AES and the results have been summarised in Table 3.2. The methods used for the analysis can be found in 3.8.6.

The concentrations reported for each of the raw, washed and extracts of the various biomass components have been calculated as a wt. % daf of the individual sample

analysed. The second part of Table 3.2 indicates the overall mass % recovery of the individual inorganic species back calculated to the original raw biomass component on a daf basis. It represents the mass fraction of the inorganic species reported to the extract from the original raw biomass component. It can be seen in Table 3.2 relatively small amounts of Ca in the raw biomass components (wood (0.61 wt. %)), leaf (0.28 wt. %) and bark (0.11 wt. %)) was extracted by ethanol washing. This suggests the Ca is either bound in molecular structures or in compounds that are insoluble in ethanol. Mg in the leaf, however, was extracted in appreciable amounts (16.19 wt. %) when compared to the wood (1.32 wt. %) and the bark (7.49 wt. %). This is due to the leaf extract containing the compounds chlorophyll a ($C_{55}H_{72}O_5N_4Mg$) and b ($C_{55}H_{70}O_6N_4Mg$)^{184, 185} used in photosynthesis and known to be extracted from the leaf using ethanol. The recovery of Na in the wood (60.87 wt. %) and bark extracts (59.17 wt. %) is far larger than for the leaf (16.97 wt. %). This could be indicating the Na in the leaf could be contained in compounds not easily soluble in ethanol when compared to those in the wood and bark. The recovery of K in the extracts of the bark (4.56 wt. %) and wood (2.88 wt. %) is much lower than for the leaf extract (12.99 wt. %), although there is a variation in the K amount recovered in the extract.

Table 3.2 Summary of ICP-AES AAEM results for various biomass components along with fraction of AAEM recovered in the extract biomass components used in the experiment

Component	Mass concentration of Inorganic Species found in each sample reported as wt. % daf of the sample analysed.											
	Al	Ba	Ca	K	Na	S	Mg	Ti	Si	Fe	P	Sr
Raw Wood	0.0025%	0.0003%	0.1215%	0.0625%	0.0233%	0.0075%	0.0328%	0.0001%	0.0201%	0.0037%	0.0194%	0.0024%
Washed Wood	0.0015%	0.0001%	0.1230%	0.0620%	0.0095%	0.0063%	0.0336%	0.0001%	0.0128%	0.0028%	0.0192%	0.0025%
Wood Extract	0.0258%	0.0080%	0.0393%	0.0860%	0.3373%	0.0420%	0.0121%	0.0007%	0.1747%	0.0229%	0.0242%	0.0003%
Raw Bark	0.0029%	0.0008%	2.7042%	0.1529%	0.2150%	0.0152%	0.0736%	0.0001%	0.0327%	0.0051%	0.0288%	0.0338%
Washed Bark	0.0030%	0.0007%	3.3986%	0.1793%	0.1084%	0.0165%	0.0859%	0.0001%	0.0373%	0.0059%	0.0359%	0.0408%
Bark Extract	0.0025%	0.0009%	0.0143%	0.0372%	0.6682%	0.0097%	0.0266%	0.0004%	0.0107%	0.0018%	0.0061%	0.0003%
Raw Leaf	0.0176%	0.0013%	0.8897%	0.5458%	0.6450%	0.0676%	0.1364%	0.0018%	0.0739%	0.0085%	0.1145%	0.0091%
Washed Leaf	0.0236%	0.0015%	1.2737%	0.6723%	0.7283%	0.0846%	0.1564%	0.0025%	0.0982%	0.0099%	0.1503%	0.0131%
Leaf Extract	0.0023%	0.0007%	0.0083%	0.2415%	0.4136%	0.0234%	0.0820%	0.0002%	0.0084%	0.0051%	0.0212%	0.00002%
	Mass fraction for each inorganic species recovered in the extract as a mass % of the original “raw” component daf content.											
Wood	41.41%	62.10%	0.61%	2.88%	60.87%	19.54%	1.32%	39.49%	39.29%	27.84%	4.83%	0.37%
Bark	18.31%	24.87%	0.11%	4.51%	59.17%	11.55%	7.49%	59.07%	5.75%	7.50%	5.07%	0.14%
Leaf	3.65%	14.94%	0.28%	12.99%	16.97%	9.59%	16.19%	3.15%	3.06%	17.27%	5.13%	0.07%

3.4 Fluidized-bed material

The material selected for the fluidized-bed is commercially available thermal sand, which can be purchased in 20 kg quantities and is mainly used in the under floor heating industry. The sand was initially passed over a 700 μm screen to remove any large lumps or impurities that may have been present in the raw material, >99.9 wt. % passed through this screen. It was then sieved mechanically into five size fractions, these were <125 μm , 125–250 μm , 250–355 μm , 355–425 μm and finally >425 μm . The sieves used were standard Tyler series sieves available for laboratory use. Figure 3.1 shows the results of the size distribution generated by the initial sieving of the sand material, with size fraction of 125–250 μm being used throughout the experimental program.

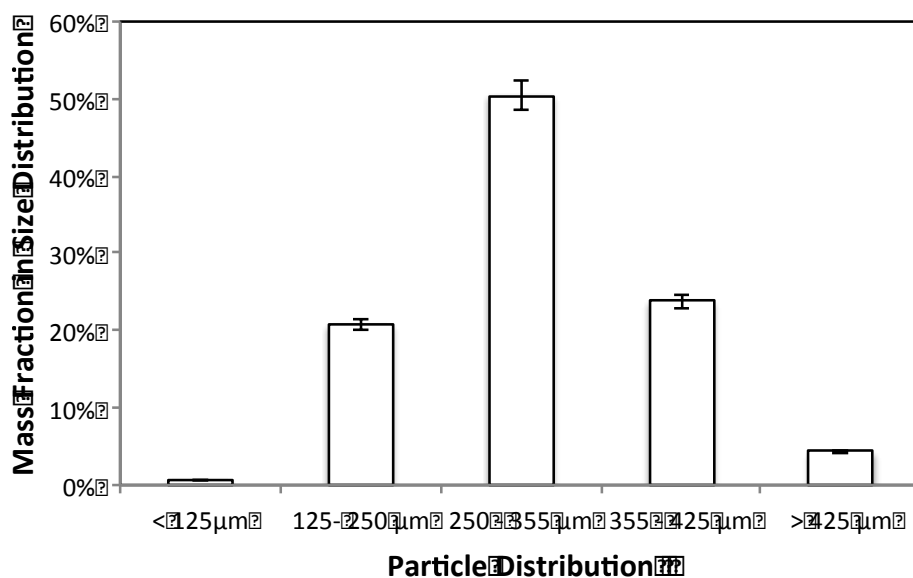


Figure 3.1 Original sand material size distribution for the purchased thermal sand

This material was then subjected to three washing cycles, consisting of four aliquots of demineralised water per cycle to remove water-soluble impurities and loose

debris. The washing took place in a large pyrex beaker continuously mechanically stirred for one hour at room temperature. The speed of the mechanical stirrer was adjusted to ensure the sand and water came into intimate contact but not sufficient to produce large abrasive action between the sand particles. The wash water from each cycle was decanted through a 125 μm Tyler screen to ensure that no sand would be lost. The sand was then recovered from the screen and placed in an oven at 50 °C where it was allowed to dry for several hours. Once the washing cycle was complete, the dry sand was spread onto large stainless steel trays to a thickness of approximately 5–10 mm and placed into an induction furnace. The furnace was set at a ramp rate of 5 °C/min where it was calcined at 600 °C in the presence of air (nominally 2 Normal litres per minute) for six hours to remove any organic material present. Once calcined, the sand was removed and allowed to cool to room temperature. A further two washing cycles were performed using the procedure outlined above. Once dry, the sand was placed in airtight containers to reduce the likelihood of contamination occurring during storage.

Table 3.3 is a summary of the results for the ICP-AES analysis performed on the selected fluidized-bed material. Outline of the analysis technique used is found in 3.8.6. From Table 3.3 the purity of the sand used in the experimental program had a purity >99.5 wt. % silica.

Table 3.3 Summary of ICP-AES analysis results for the sand bed material used throughout the experimental program, showing the chemical analysis for the major elements present.

Inorganic Species	Mass Fraction (wt. %)
Al	0.080
Ba	0.002
Ca	0.011
Fe	0.011
K	0.089
Mg	0.007
Na	0.080
P	0.010
S	0.022
Si	99.674
Sr	0.000
Ti	0.015

3.5 Characterisation of the fluidized-bed sand material

Because little was known about the sand bed material, it was subjected to a number of tests such as bulk density (free and packed), surface area and particle size distribution (D_{10} , D_{50} and D_{90}) within the initial size distributions measured above. These values are required for a more accurate calculation of the minimum fluidisation velocity using the Ergun equation.¹⁸⁶⁻¹⁸⁸

3.5.1 Free and packed bulk density and porosity

The bulk density of the material was measured using a modified measuring cylinder, which was cut at the 10 ml mark to ensure it could be filled to a constant volume. The procedure followed to determine the free packed bulk density was: the initial mass of the measuring cylinder before the sand material is poured into it is obtained and noted; sand material is poured into the cylinder and the excess is removed, scraping the top, using a spatula to ensure a level surface and a constant volume of 10 ml. The new mass of the cylinder was noted and the free packed bulk density of the sand material was calculated. To determine the packed density, the cylinder was placed on a vibrating table for 30 minutes. Once the time had expired, the new volume of the sand material was read from the measuring cylinder and the packed bulk density could be calculated. Knowing the density of sand (2700 kg m^{-3}), the porosity of the packed and unpacked bulk sand could be calculated. Table 3.4 is a summary of the average results obtained for the different size distributions tested; the average error for the measurements was $\pm 3\%$.

Table 3.4 Summary of the measured free and packed bulk densities and the calculated free and packed bulk porosities for the fluidized-bed sand material size fractions.

Size Distribution	Free Bulk Density (kg m^{-3})	Packed Bulk Density (kg m^{-3})	Free Bulk Porosity (Volume %)	Packed Bulk Porosity (Volume %)
< 125 μm	1265	1512	53.1	44.0
125–250 μm	1423	1595	47.3	40.9
250–355 μm	1483	1612	45.1	40.3
355–425 μm	1478	1594	45.3	41

3.5.2 Surface area and particle size distribution of original screened bed material

Three small representative samples from each of the size distributions were obtained by using a sample riffler. Each of these samples was then subjected to a size distribution analysis using a Malvern Mastersizer 2000 laser diffraction analyser following the procedures outlined in the operating manual. Table 3.5 is a summary of the Malvern analysis results acquired; the data had an error $\pm 1\%$.

Table 3.5 Summary of the Malvern Mastersizer results for each of the original sand distributions analysed.

Size Distribution	D ₁₀ (µm)	D ₅₀ (µm)	D ₉₀ (µm)	Specific Surface Area (m ² g ⁻¹)
<125 µm	67	130	227	0.057
125 - 250 µm	176	244	340	0.025
250 - 355 µm	257	353	485	0.018
355 - 425 µm	316	434	592	0.014
>425 µm	388	531	730	0.012

3.5.3 Minimum fluidisation velocity of the selected sand bed material

Laboratory bench scale fluidisation tests were performed on the 125–250 µm material only; this was the selected size distribution used throughout the research program followed. The minimum fluidisation velocity is an important measurement required to ensure the sand bed material is completely fluidized during all the pyrolysis experiments performed.

Fluidisation tests were performed using a 150 mm diameter column with a 74 µm mesh screen at the bottom of it. The screen was used to prevent the sand material

coming in contact with the 5mm glass beads used to evenly distribute the fluidising air in the conical transitional section of the column. The fluidising medium used during the experiments was instrument air having a dew point <-6 °C and having an average molecular mass of 28.97. The pressure drop across the column and bed material was measured using a water-filled manometer. The air flowrate through the bed was measured using a calibrated rotameter and increased from 0 to 70 STP litres per minute. The height of the bed and the corresponding pressure drop was recorded. Figure 3.2 is a plot of the bed column pressure drop vs. the fluidisation air flowrate obtained for the sand bed fluidisation experiments.

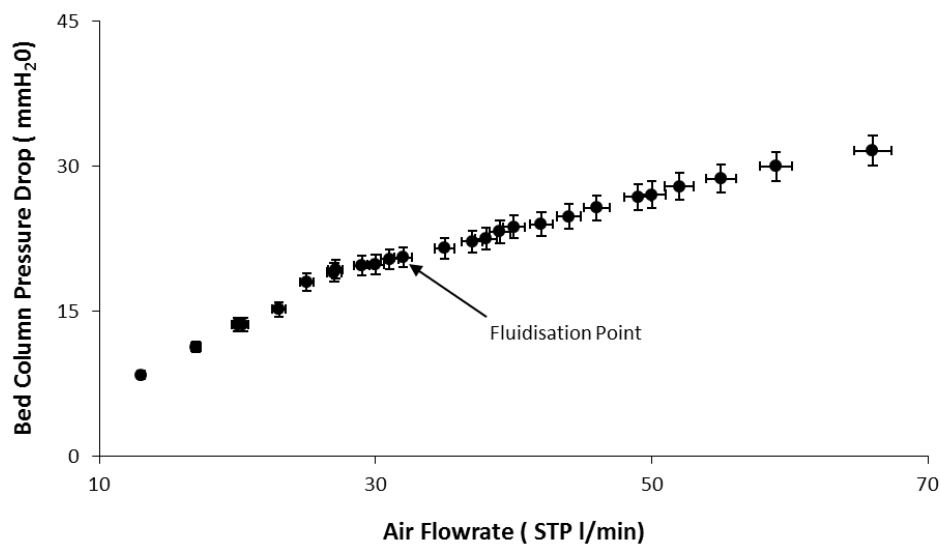


Figure 3.2 Results for the bed column pressure drop vs. air flowrate for 125–250 μm sand bed material

From Figure 3.2 the minimum fluidisation point is estimated to be 32 STP litres per minute of air, giving a minimum fluidisation velocity of 0.032 m sec^{-1} ; this equates to a particle Reynolds number <0.3 . When substituting the values for the porosity and D_{50} measured and reported above in Table 3.5 into the Ergun equation, a value

of 0.031 m sec^{-1} is obtained. These values (calculated and measured) are in agreement with each other, validating the minimum fluidisation velocity measured and the assumption that the particle Reynolds number will be <1 . The reduced Ergun equation was then used to calculate the required gas flowrates for the minimum fluidisation velocity of the bed material during the experimental program followed. The fluidising gas flowrate was taken at 1.5 to 2.5 times the required minimum calculated.

3.6 Fluidized-bed pyrolyser reactor set up

Figure 3.3 is a schematic diagram of the type of fluidized-bed pyrolyser used throughout the research program. The reactor is extensively manufactured from quartz and can be operated at a maximum continuous temperature of $900 \text{ }^{\circ}\text{C}$.

The induction furnace is cylindrical in shape with a 100 mm diameter opening running through the core. The furnace is used to provide the heat source required for the pyrolysis reactions to occur. To ensure no movement of the reactor occurs during any experiment, the reactor is securely anchored in the vertical position using external clamps; this also ensures an even flow distribution of gas through the fluidized-bed during the experiment.

The induction furnace has its own Programmable Logic Controller (PLC) and feedback control systems, giving the furnace the ability to control not only the final required temperature but also the ramp temperature rate, which can be adjusted from 1 to $100 \text{ }^{\circ}\text{C}/\text{min}$. This control system provided the ability to perform slow pyrolysis experiments in the reactor from room temperature to the required experimental bed

temperature at various specified heating rates up to 100 °C/min. The bed temperature was monitored via a separate inserted thermocouple to ensure both the heat rate and bed temperature required were achieved. For fast pyrolysis experiments the final temperature of the furnace was manually adjusted to ensure that the bed temperature, measured via the inserted thermocouple, was within 5 °C of the desired experimental temperature.

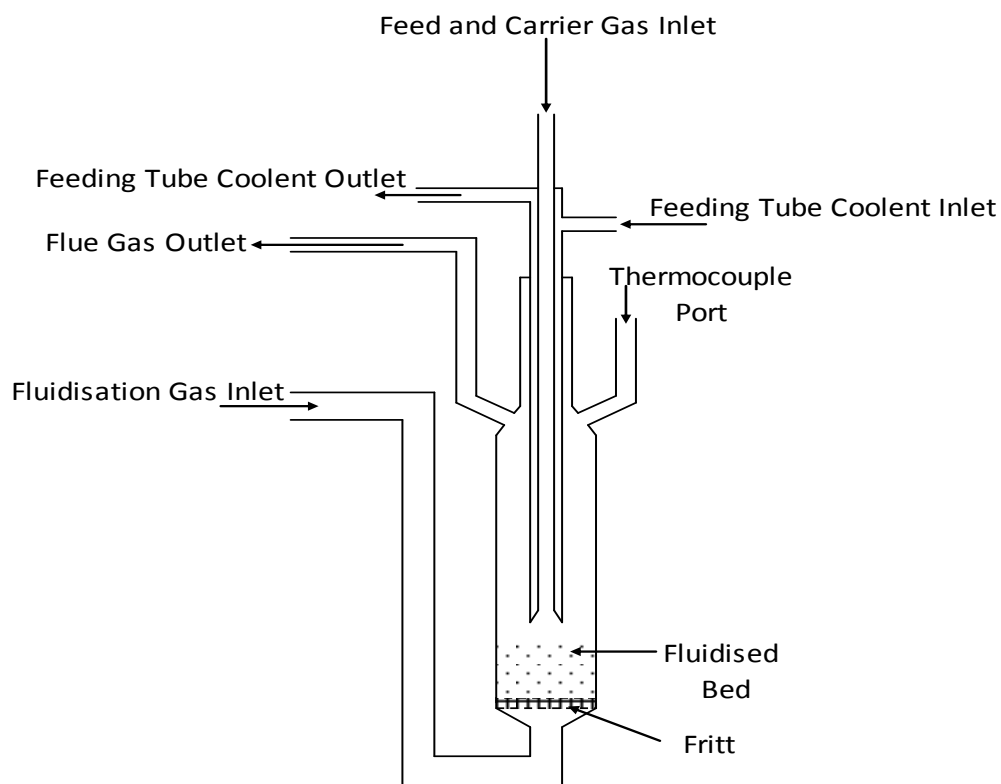


Figure 3.3 Schematic diagram of fluidized-bed pyrolyser reactor used throughout the research experimentation.

To ensure the bed temperature in the reactor will have the best chance of being constant, the reactor frit was placed near the bottom of the isothermal zone in the furnace. The isothermal zone was found by inserting a thermocouple into the centre of the furnace, noting the depth from the top of the furnace and the temperature at that position. The temperature reading was allowed to stabilise for 15 minutes

before being recorded. These calibration curves were done over a number of furnace set temperatures to ensure there is no difference over the temperature range. Figure 3.4 is the results of the calibration curves drawn. From this graph the isothermal zone for the furnace used ranges from 170 to 320 mm from the top of the furnace. The frit in the reactor was placed at the 290 mm mark and was kept at this distance throughout the experimental program followed.

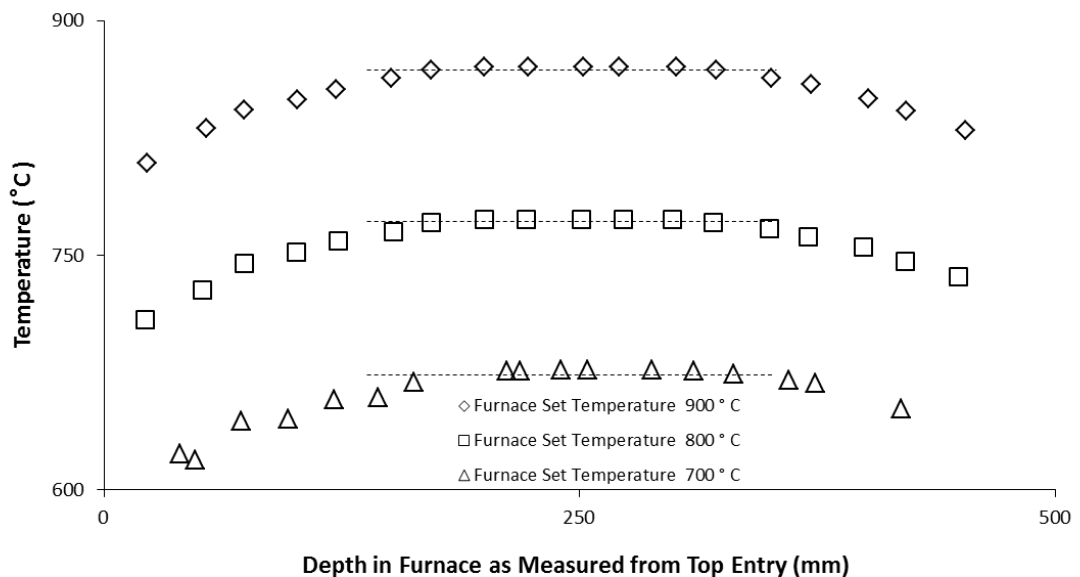


Figure 3.4 Plot of furnace temperature vs. distance from top of furnace showing the isothermal zone (dashed lines) performed at furnace set temperatures of 700, 800 and 900 °C

The inlet feed tube was gas cooled using compressed instrument air having a dew point <-20 °C. The flowrate of the instrument air was adjusted until the outlet temperature of the air was less than 50 °C. This was performed to ensure that no pyrolysis occurred within the feeding tube itself. To minimise short-circuiting of the cooling gas in the feeding tube, an internal central baffle was installed running 90%

of the total length of the feeding tube. The feed tube insertion depth into the reactor was adjusted to be located at a fixed distance (5mm) from the fluidized-bed. This could be performed since there was a constant charge of 19.5–20 g of constant size distribution (125–250 μm) sand bed material used in each of the experiments. The fluidisation gas flowrate was adjusted throughout the experiments within the range 3 to 5 Normal litres per minute. This equates to 1.5 times the minimum fluidisation velocity at 300 °C and 2.5 times the minimum fluidisation velocity at 700 °C.

3.7 Experimental procedures

This section details the experimental methodology used in the actual experiments performed. Four main types of experiments were performed throughout the experimental program:

- Fast pyrolysis of biomass solids (“washed” and “raw”);
- Slow pyrolysis of biomass solids (“washed” and “raw”);
- Fast pyrolysis of the “extract” of the biomass components;
- Drying of biomass in a fluidized-bed dryer.

3.7.1 Fast pyrolysis of biomass solids

Fast pyrolysis experiments were performed in the fluidized-bed reactor set-up as described in 3.6 above at an estimated heating rate of >200 K/sec. The biomass solids encompassed the washed and raw biomass components of leaf, bark and wood. The temperature range investigated during the experiments was 200–700 °C for raw and 200–600 °C for washed biomass.

The induction furnace was heated to the approximate temperature required for the experiment. Once the furnace was at the pre-set temperature, the empty reactor was weighed. An aliquot (19.5–20 g) of sand bed material (125–250 μm) was pre-weighed and placed into the reactor after which the reactor was weighed again and the amount of sand bed material was determined.

The fluidisation gas, feeding tube, off gas and feeding tube cooling connections to the reactor were made and the thermocouple was inserted into the reactor sand bed, taking care not to allow the thermocouple to contact the frit or the sides of the reactor. The fluidisation gas (Ar) was set and adjusted to the required set point (3 to 5 Normal litres per minute) and the reactor was then placed into the furnace at the correct position and clamped. The feeding tube cooling air was turned on and set to a nominal flow of 3 Normal litres per minute.

The reactor was left in the furnace for 15 minutes to allow it to thermally stabilise; the stability was determined using the inserted thermocouple. During this stabilising time the feeding tube cooling air exit temperature was checked and the air flowrate adjusted until the exit temperature was below 50 °C. The furnace temperature was adjusted to ensure the bed temperature required for the experiment was within 5 °C. Once achieved, the reactor was allowed to sit for a further 15 minutes to become thermally stable.

The biomass sample (washed or raw) was pre-weighed, normally (1.95–2 g) for most experiments, and placed into the previously weighed sample holder. The sample holder was again weighed and connected to the sample feeding system. The feeding

system was purged with the inert gas used for the experiment for three to five minutes to remove any air contained in the sample. The rate achieved during the biomass sample feeding was in the range 0.3 to 0.5 g/min. The main overall driver for the feeding rate of the sample was the fluidized-bed temperature in the reactor. This temperature could not deviate by more than 5 °C from the required set point.

Once the biomass sample was fed into the reactor, the holding time for the experiment was started. This was nominally 15 minutes for most of the experiments but was adjusted from one to 40 minutes in some of the experiments to determine the effect of holding time on the pyrolysis reaction and agglomeration. At the end of the holding time the reactor was removed from the furnace and allowed to cool with the fluidisation gas to a temperature below 50 °C, after which the feeding tube and the flue gas connections were removed. The reactor was allowed to cool further to below 40 °C where the fluidisation gas was stopped. The inserted thermocouple was then removed and the reactor was weighed. The tar and condensate collected in the flue gas passage and sides of the reactor were burned off using a Bunsen burner, making sure no sample material was destroyed during this process. The reactor was again allowed to cool to room temperature. Once at room temperature the reactor was re-weighed and the contents were removed from the reactor. The contents, now termed “bed samples”, were collected and stored for further analysis.

3.7.2 Slow pyrolysis of biomass solids

Slow pyrolysis experiments were performed at 10 °C/min, in the same reactor as the fast pyrolysis experiments. The biomass solids encompassed the washed and raw

biomass components of leaf, bark and wood. The temperature range investigated during the experiments was 200–600 °C.

The empty reactor was weighed and the mass noted. A pre-measured aliquot (19.5–20 g) of sand bed material having a size distribution of 125–250 µm was placed into the reactor and, once again, the reactor was weighed and the mass recorded. Finally, an aliquot (1.95–2.0 g) of the biomass sample required for the experiment was added and the final mass of the reactor was determined.

The fluidisation and flue off gas connections were made on the reactor, after which the thermocouple was inserted into the sand bed, taking care not to allow the thermocouple to contact the sides or the frit of the reactor. The reactor was then placed into the furnace, which was at room temperature. The reactor was then clamped into the correct vertical position to prevent any movement during the experiment, along with ensuring an even distribution of the fluidized gas through the bed material. The fluidisation gas (Ar) was set and adjusted to the required set point.

The rate of temperature rise required for the experiment was programmed into the PLC of the furnace, along with the final temperature required. The furnace was turned on and the temperature of the bed was monitored and noted throughout the experiment. Once the bed temperature reached the required experimental temperature, the holding time was started. This ranged from 1 to 35 minutes and is noted where required; for most experiments it was kept at 15 minutes. Once the holding time elapsed, the reactor was removed from the furnace, allowed to cool to below 50 °C and the flue gas and feed tube connections were removed. The

fluidisation gas was allowed to flow until the reactor temperature was below 40 °C, after which it was stopped and the reactor was weighed. The tar and condensate were then burned off from the flue and sides of the reactor using a Bunsen burner, taking care not to degrade the sample material remaining in the reactor. Once the tar and condensate had been removed, the reactor was once again allowed to cool to room temperature, at which time the mass of the reactor was determined. The contents in the reactor were then deemed the “bed sample” and were collected for further analysis.

3.7.3 Fast pyrolysis of biomass “extract”

Fast pyrolysis experiments were performed on the “extract” material resulting from the ethanol leaching of the biomass components leaf, bark and wood, at an estimated heating rate >200 K/sec. The procedure used for the pyrolysis experiments followed the same as outlined in 3.7.1 above, with only two differences. First, the preparation of the sample and second, the method used to feed the sample into the reactor. The temperature range investigated during the experimentation was 170–600 °C.

The amount of extract fed into the reactor was back-calculated to be equivalent to that which is contained in the 1.95 to 2.0 g of the “raw” biomass component. The extract content values, used to back-calculate the extract requirement for the experiment, were bark 35.2 wt. % db, leaf 44.7 wt. % db and wood 12.2 wt. % db. These values were determined by other^{62, 63} researchers using the same feedstock from the same area. The amount of extract required was weighed using a Mettler Toledo microbalance and placed into a calibrated syringe. Then 24 times the initial

sample mass of ethanol was placed into the syringe and the syringe was shaken until all the extract was dissolved.

The syringe was connected to a small stainless steel injection pipe (4 mm ID) inserted into the existing air-cooled feeding tube. To assist in the dispersion of the ethanol extract mixture and also to ensure the entire sample was inserted into the reactor, entrainment gas, usually the same as the fluidisation gas, was injected into the smaller tube and set at flowrate of 0.5 Normal litres per minute. Figure 3.5 is a schematic representation of the feed set-up used. Before the syringe was connected to the injection system, the feed tube and syringe tubes were purged to ensure an inert atmosphere was present.

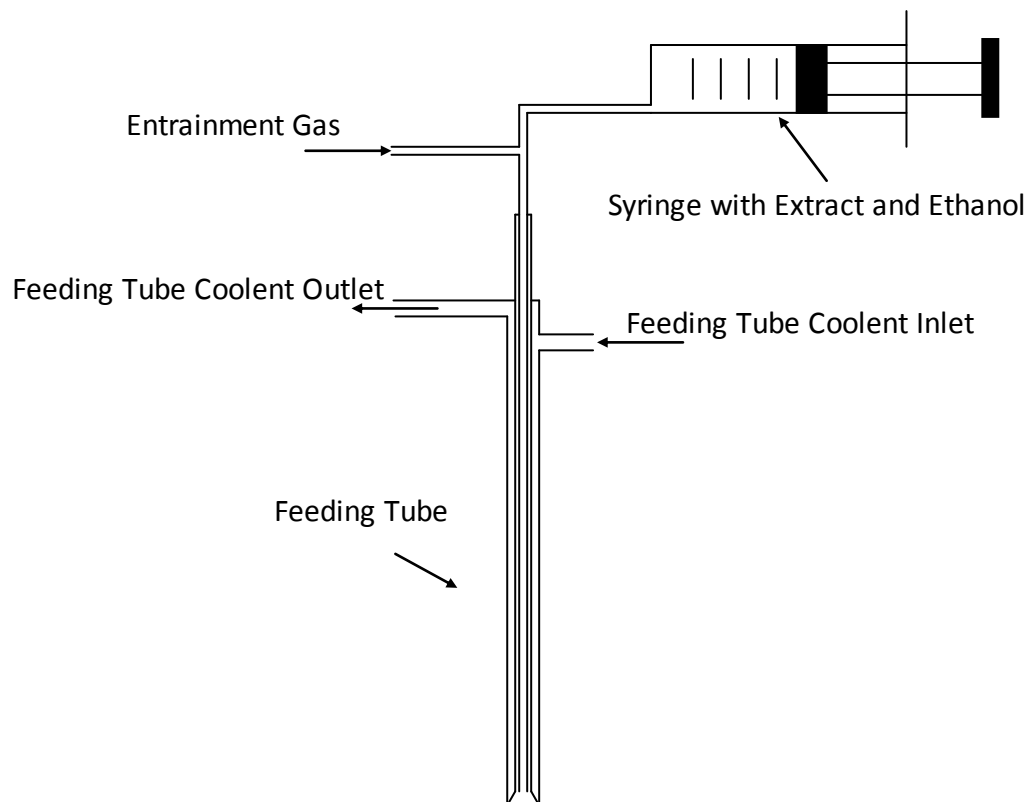


Figure 3.5 Schematic diagram for feeding ethanol diluted extract during fast pyrolysis.

The temperature in the reactor was monitored, via an inserted thermocouple, to ensure it did not deviate by more than 5 °C during the feeding of the sample. Once the full sample was injected, the holding time was started, usually 15 minutes unless otherwise stated. The procedure for removal and cooling of the reactor along with the final collection of the “bed sample”, were the same as described in 3.7.1 above.

3.7.4 Drying of biomass solids

Drying experiments were performed in the fluidized-bed reactor set-up as described in 3.6. The biomass solids encompassed the “raw” biomass component of leaf only.

The procedure followed was the exactly the same as that for fast pyrolysis described above in 3.7.1. The only differences were the temperature range was much lower and was performed at 120–250 °C and 2 fluidisation gases were used: firstly, air in the form of instrument air having a dew point <-20 °C, and secondly, argon.

3.7.5 Cleaning of the reactor

After each experiment the reactor was cleaned to reduce the risk of contamination between experiments. The cleaning of the reactor was achieved by following the procedure outlined below:

The reactor was inserted into the furnace at 600 °C for 30 minutes to combust any residual organic material. Once the 30 minutes had expired, the reactor was taken out of the furnace and allowed to cool to room temperature. The reactor was rinsed and then allowed to steep for a further 30 minutes with a 2 M solution of H₂SO₄.

The sulphuric acid solution was used to remove any salts that may have built up in

the reactor during the experiment. The reactor was then emptied and rinsed with three or four bed volumes of demineralised water to remove any contaminants and then returned to the furnace to dry. Once dry, the reactor was removed and allowed to cool to room temperature, covered and placed into storage for use at a future date.

3.8 Analytical techniques

3.8.1 Determining particle size distribution

To study the bed agglomeration phenomenon, the mass particle size distributions were determined for the bed samples collected after biomass pyrolysis experiments or after solvent treatments. Each sample was sieved into a series of nine size fractions (i.e., <106 μm , 106–125 μm , 125–355 μm , 355–500 μm , 0.5–0.71 mm, 0.71–1.0 mm, 1.0–1.7 mm, 1.7–3.15 mm and >3.15 mm) for determining its mass particle size distribution.

3.8.2 Determining the solvent-soluble and solvent-insoluble organic matter

Selected bed samples collected after biomass pyrolysis were washed using a mixed solvent of chloroform and methanol (ratio: 4:1), known to be good solvent for washing organic matter,¹⁸⁹ in order to determine the yields of “solvent-soluble organic matter” present in the bed samples.

The bed sample was placed into a flask and the mass determined. Twice the mass of a 4:1 chloroform methanol mixture was placed into the flask and hand-swirled for 10 minutes. After solvent washing of the bed sample was complete, solids and solution were separated using filtration. The solution collected was placed into an oven at 35 °C to evaporate the solvents. The yield (wt. % daf) of organic matter remaining after

solvent evaporation, normalised to the total mass (daf) of biomass fed into the pyrolysis reactor, is considered to be the yield of “solvent-soluble organic matter”. The bed samples after solvent washing were also collected via filtration followed by evaporating the residual solvents in an oven at 35 °C. The insoluble organic material was determined by combusting the rest of the bed sample using a controlled burning profile used in the original calcining of the sand bed material described in 3.4 above. For the solvent-washed bed sample, the weight loss after combustion was considered as the yield (wt. % daf) of “solvent-insoluble organic matter” in the bed sample collected from biomass pyrolysis, normalised to the total mass (daf) of biomass fed into the bed. The sum of the yields of “solvent-soluble organic matter” and “solvent-insoluble organic matter” is considered as the yield of “total organic matter” in the bed sample.

3.8.3 Proximate analysis.

Various samples were selected for proximate analysis. The char particles, when required, were separated from the bed samples via mechanical rubbing of the samples through a 106 µm Tyler screen in order to liberate the char from the sand bed material. The sand material was left on the screen while the liberated char was collected below the screen in a pan. The actual determination of the proximate analysis was performed in a METTLER Thermogravimetric Analyser (TGA) following a specific program adapted from the ASTM E 871-82 method.¹⁹⁰ The particular program followed is outlined below:

Approximately 10 mg of the char sample at room temperature was placed into the TGA crucible and allowed to heat up at a rate of 5 °C/min to 35 °C in an argon

atmosphere. The sample was held at this temperature for 10 minutes to allow the sample to purge completely and to give a constant starting temperature for the analysis. Once the 10 minutes elapsed, the sample was heated at 10 °C/min to 110 °C and held at this temperature for one hour to drive off moisture. The moisture content of the sample can be determined by the difference between the starting mass and the mass of the sample at this point. The sample was further heated in the argon atmosphere at 50 °C/min to a final temperature of 900 °C and kept at this temperature for a further 30 minutes. The mass loss at the end of the heat up and constant temperature holding time is determined to be the volatile content within the sample. The sample was then cooled at a rate of 10 °C/min to a temperature of 700 °C and allowed to equilibrate at this temperature for 10 minutes before the atmosphere in the TGA was changed from argon to air with a dew point <-20 °C. The sample was given a further 30 minutes in this atmosphere to allow for the complete combustion of the carbon material. The mass loss at this point is deemed to be the fixed carbon content and the residual mass is determined to be the ash content of the sample.

3.8.4 Ultimate analysis

Selected samples were subjected to chemistry analysis using a CHNS/O elemental analyser (model: PerkinElmer 2400 Series II) following the procedures outlined in the owner's operational manual.

3.8.5 UV spectra

Selected solutions resulting from the solvent washing of the bed sample described above in 3.8.2 were subjected to analysis using a UV-fluorescence spectrometer (model: Perkin-Elmer LS55B). The collection of UV-fluorescence spectra followed a procedure similar to that reported in a previous study.¹⁹¹ Briefly, the spectra were scanned at a speed of 200 nm min⁻¹, at a constant energy difference of -2800 cm⁻¹ and a slit width of 2.5 nm. The intensities of spectra were normalised as per g of biomass feed, enabling direct comparison among the solvent-soluble organic matter in bed samples collected from biomass pyrolysis under various experimental conditions.

3.8.6 Analysis of inorganic species

Specific samples were analysed for their inorganic species content. The specific inorganic elements measured were Al, Ba, Ca, K, Na, Mg, Ti, Si, Fe, P and Sr.

The procedure followed for the analysis of the inorganic species contained in the samples tested has been used in a previous study.¹⁹² In brief, 20–30 mg of sample was placed into a platinum crucible and inserted into an induction furnace in a specialised quartz container to prevent any contamination. The furnace thermocouple was inserted into the container. Air in the form of instrument air with a dew point <-20 °C was fed at nominal rate of 2 Normal litres per minute into the container to aid in the ash cycle. The heating profile used for the ash cycle was developed to ensure very little or none of the inorganic species in the sample was released during the ash cycle. The heating profile used for the ash cycle was pre-set

into the furnace PLC before the ash cycle was initiated. The heating profile allows for the initial heating of the sample from room temperature to 270 °C at a heating rate of 10 °C/min. The sample was then held at this temperature for 15 minutes before the temperature of the furnace further was increased to 315 °C at a heating rate of 5 °C/min and held at this temperature for a further five minutes. The furnace temperature was again increased to 370 °C at a heating rate of 5 °C/min and held at this temperature for a further five minutes. The temperature of the sample was finally increased to 600 °C at a heating rate of 10 °C/min and held for two hours at this final temperature. The furnace was then allowed to cool before the ash samples could be removed.

Once the samples had been removed from the furnace, they could be weighed and the ash content of the initial sample determined. The ash samples were then mixed with X-ray flux containing a mixture of lithium tetraborate (35.3 wt. %) and lithium metaborate (64.7 wt. %). The X-ray flux was added to the sample in a 30:1 mass ratio, lids were placed onto the crucibles and the crucibles were placed into a specialised quartz container. The container was placed into the centre of the furnace and the furnace thermocouple was attached to the container. The fusion of the sample occurred in the crucibles, which are heated from room temperature to 950 °C at a heat rate of 5 °C/min and held at this temperature for 2 hours, where after the furnace was switched off and allowed to cool before the crucibles could be removed

Once removed the crucibles were placed into Teflon vials where a known quantity of redistilled nitric acid solution (10 % v/v) was added to dissolve the fusion product

from the crucibles. The resulting solution was subjected to inductively coupled plasma-atomic emission spectroscopy (ICP-AES) analysis, performed at Murdoch University's Marine and Freshwater Research Laboratory using a Varian Vista Axial CCD Simultaneous ICP-AES instrument.

3.8.7 Determining organic material in sand bed

To determine the amount of organic material reporting to the lower size distributions (<355 μm) were combined and combusted. The combustion procedure used to measure this organic material was to insert the lower size distributions (<355 μm) into a quartz reactor and determine the initial mass; instrument air (dew point <-20 $^{\circ}\text{C}$) was then used to provide the fluidisation and combustion gas for the sample. The reactor was then inserted into an induction furnace which was set at a temperature to ensure that the resulting fluidized-bed temperature was lower than 625 $^{\circ}\text{C}$ but higher than 600 $^{\circ}\text{C}$. This temperature was also monitored by an inserted thermocouple in the reactor. At the end of the 30-minute holding time, the reactor was removed from the furnace and allowed to cool while the fluidising air was left running until the bed sample reached room temperature. The fluidisation air was stopped and the reactor was then weighed again. The difference in mass from the start to the end was determined; this change in the total mass represents the amount of organic material that reported to the lower (<355 μm) particle size distributions.

3.8.8 Imaging

Selected bed samples were also set into resin to prepare cross-sectional specimens for morphological characterisation using a scanning electron microscope (SEM,

model: Zeiss EVO 40XVP). Other bed samples were also examined directly under an optical microscope (model: Nikon) equipped with an externally connected camera for image acquisition.

CHAPTER 4 MECHANISTIC INVESTIGATION INTO BED AGGLOMERATION DURING BIOMASS FAST PYROLYSIS IN A FLUIDIZED-BED REACTOR

4.1 Introduction

The objective of this chapter is to carry out a series of experiments to investigate bed agglomeration during biomass fast pyrolysis in a laboratory-scale fluidized-bed reactor. The research program followed in this chapter is designed to obtain the direct experimental evidence on bed agglomeration during fast pyrolysis and to report essential data on the nature and characteristics of the bed agglomerates formed under various pyrolysis conditions. Based on the experimental evidence and data, in this chapter the fundamental mechanisms responsible for bed agglomeration during biomass pyrolysis in a fluidized-bed reactor are discussed and postulated.

4.2 Experimental method

Fast pyrolysis reaction experiments were performed in a fluidized-bed pyrolyser using mallee raw leaf biomass having a size fraction of 355–500 μm within the temperature range 300–700 $^{\circ}\text{C}$ with a holding time of 7.5 to 25 minutes. The fast pyrolysis was performed using the outlined procedure in 3.7.1 above, and the preparation of the raw leaf biomass was performed as outlined in 3.2. Analysis performed on selected samples was performed using the techniques outlined in 3.8 above.

4.3 Results and discussion

4.3.1 Evidence of bed agglomeration during biomass fast pyrolysis in a fluidized-bed reactor

Figure 4.1A presents the mass particle size distribution of the bed samples collected after biomass fast pyrolysis at various pyrolysis temperatures and a holding time of 15 minutes. It should be noted that the bed materials (silica sand) in the fluidized-bed pyrolysis reactor have sizes of 125–355 μm while the biomass particles fed into the reactor have sizes of 355–500 μm . It is therefore safe to conclude that any particles $>500 \mu\text{m}$ in the bed samples collected after biomass pyrolysis must be due to bed agglomeration. Indeed, Figure 4.1A clearly demonstrates that depending on pyrolysis temperature, there are various amounts (1.8–16.5 wt. %) of the materials in the samples collected after biomass pyrolysis having particle sizes $>500 \mu\text{m}$. There are also very small but appreciable quantities (<0.5 wt. %) of small particles of size $<125 \mu\text{m}$ generated, possibly due to the significant weight loss of biomass particles and/or fragmentation of biomass/char particles during pyrolysis.

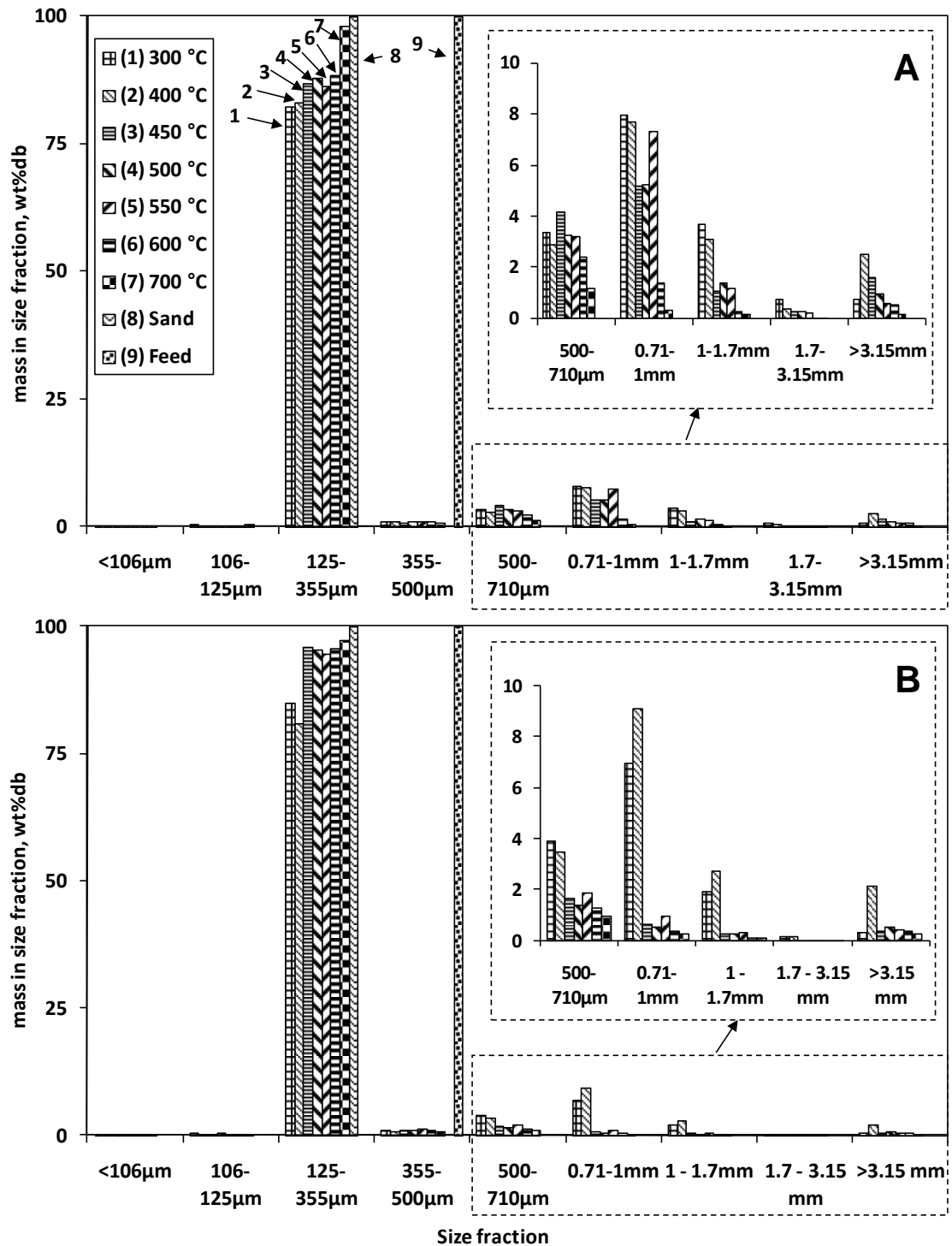


Figure 4.1 Particle size distribution of total materials in the bed after biomass fast pyrolysis (pyrolysis temperature: 300–700 °C; feeding time: 4 minutes; holding time: 15 minutes; sand particle size: 125–355 μm; biomass particle size: 355–500 μm). A) before solvent washing; B) after solvent washing

Figures 4.2A–4.2C present typical SEM images of the cross-sections of the bed agglomerates collected from the fluidized-bed pyrolysis reactor after the pyrolysis of

mallee leaf at 300, 500 and 700 °C and a holding time of 15 minutes. The images clearly show that the char particles in the agglomerates are generally of a partially-round shape, suggesting that these particles experienced at least partial melting during pyrolysis, even at a pyrolysis temperature as low as 300 °C. The SEM images in Figure 4.2A–4.2C clearly show that these agglomerates are either due to a) multiple char particles agglomeration with each other or b) multiple sand particles agglomeration with char particles. Figures 4.2D–4.2F further present optical images taken for the bed agglomerates under the same pyrolysis conditions. Similarly, the optical images also clearly show the agglomeration either among sand particles and biomass char particles or among multiple char particles. It is clear that the char particles experienced at least partial melting and the connection neck of the char-char or char-sand agglomerates being carbon-enriched organic matter. Therefore, it is important to note that bed agglomeration observed during biomass pyrolysis at 300–700 °C in this study is unlikely due to ash agglomeration. It is well known that ash agglomeration takes place during solid fuels combustion/gasification and requires the bed temperatures to be greater than 700 °C.¹⁹³⁻¹⁹⁶ The results clearly provide direct experimental evidence that bed agglomeration indeed takes place during biomass fast pyrolysis in a fluidized-bed reactor under the conditions in this study. Therefore, it is important to understand a) the dependence of bed agglomeration on pyrolysis temperature and holding time; b) characteristics of bed agglomerates and the organic materials responsible for bed agglomeration during biomass pyrolysis under various conditions and c) the fundamental mechanisms responsible for bed agglomeration.

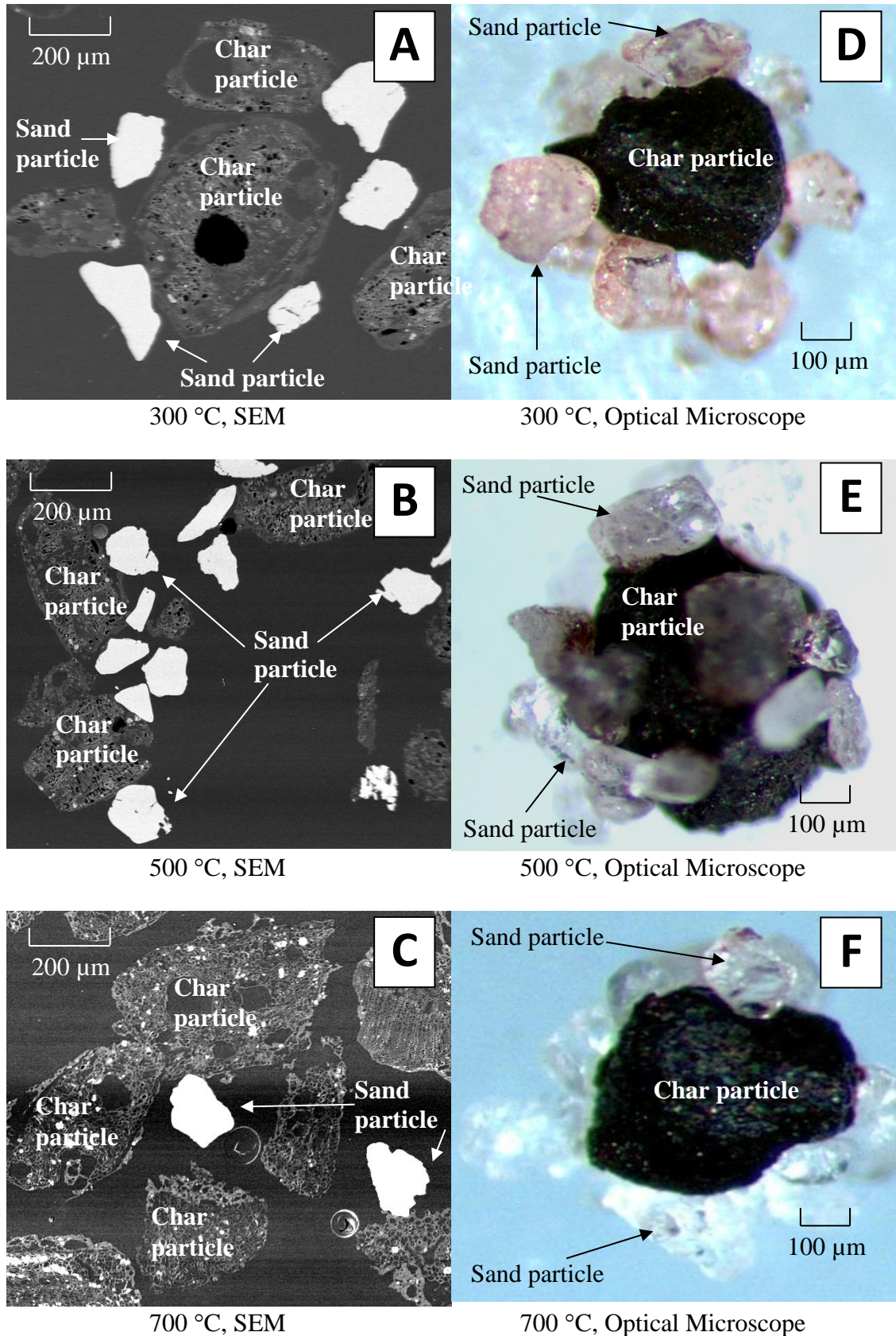


Figure 4.2 SEM and optical images of bed agglomerates (pyrolysis temperature: 300, 500 and 700 °C; holding time: 15 minutes); A, B and C: SEM images; D, E and F: optical images

4.3.2 Dependence of bed agglomeration on pyrolysis temperature and holding time

The data in Figure 4.1A demonstrates that bed agglomeration is strongly dependent on the bed temperature (300–700 °C).

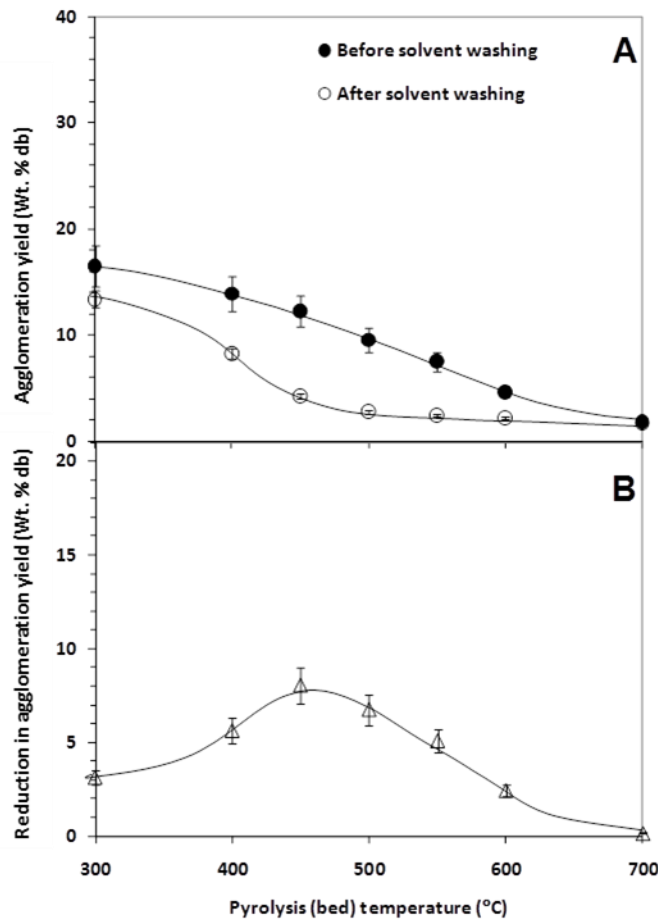


Figure 4.3 Dependence of agglomeration yield on pyrolysis temperature (holding time: 15 minutes)

For subsequent discussion, a term “agglomeration yield” is then defined to quantify the extent of bed agglomeration during biomass pyrolysis in the fluidized-bed reactor. The “agglomeration yield” (wt. % db) is defined as the mass (db) of materials >500 μm as the percentage of the total mass (db) of the bed sample after

pyrolysis. The agglomeration yield provides a reasonable estimation of the extent of agglomeration taken place in the bed because a) the sizes of sand and biomass particles are 125–355 μm and 355–500 μm , respectively, so that all materials $>500 \mu\text{m}$ must be deemed as bed agglomerates; and b) there are minimal amounts ($<0.5 \text{ wt. \%}$) of materials $<125 \mu\text{m}$.

Figure 4.3A presents the agglomeration yields during biomass pyrolysis in the fluidized-bed reactor at various pyrolysis temperatures at a constant holding time of 15 minutes (i.e., the series of datum points in filled circles with legend “Before solvent washing”). It is clear that the agglomeration yield decreases with pyrolysis temperature, from $\sim 16.5 \text{ wt. \%}$ at $300 \text{ }^\circ\text{C}$, to $\sim 9.5 \text{ wt. \%}$ at $500 \text{ }^\circ\text{C}$, $\sim 4.6 \text{ wt. \%}$ at $600 \text{ }^\circ\text{C}$ and merely $\sim 1.8 \text{ wt. \%}$ at 700°C , respectively.

A set of experiments was also carried out at a pyrolysis temperature of $500 \text{ }^\circ\text{C}$, varying the holding time from 7.5 to 25 minutes. The results are plotted in Figure 4.4A (i.e., the series of datum points in filled circles with legend “Before solvent washing”). The data shows that there is an initial decrease in the agglomeration yield with increasing holding time, from 13.3 wt. \% at 7.5 minutes to 9.5 wt. \% at 15 minutes. Increasing holding beyond 15 minutes leads to only slight change in the agglomeration yield.

This is also the reason that the same holding time of 15 minutes was used in the experiments for investigating the effect of pyrolysis temperature on bed agglomeration (see Figure 4.3A, the series of datum points in filled circles with legend “Before solvent washing”).

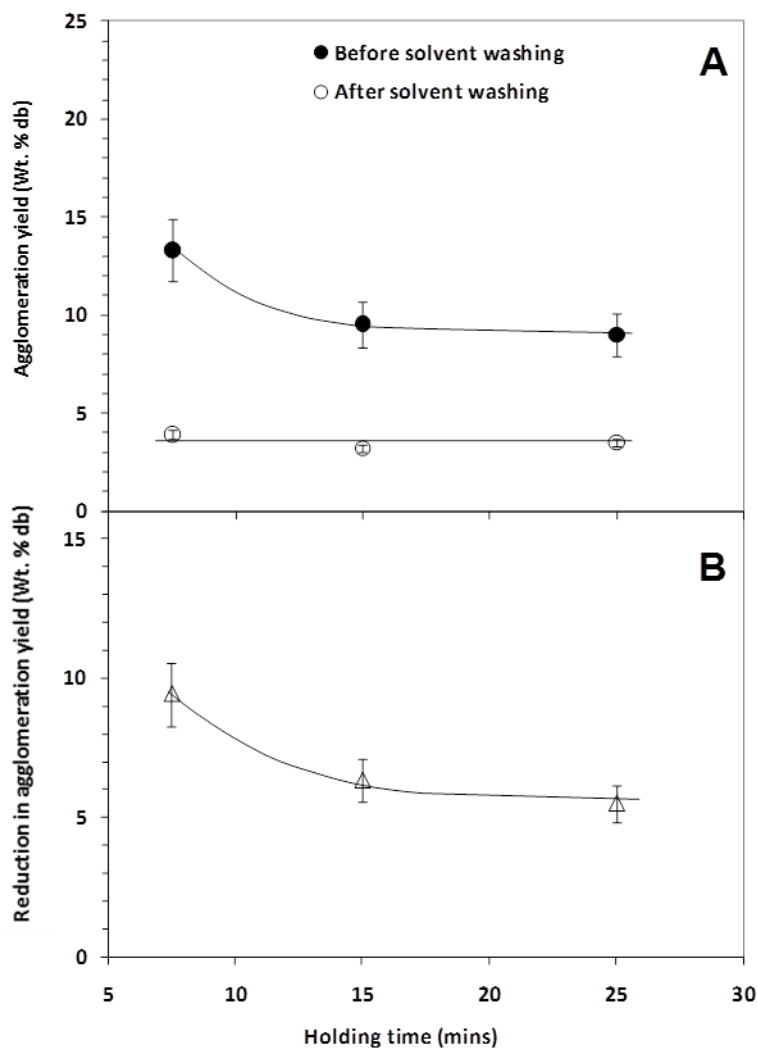


Figure 4.4 Dependence of agglomeration yield on holding time (pyrolysis temperature: 500 °C)

4.3.3 Characteristics of bed agglomerates and correlations between bed agglomeration and organic matter in bed samples

To investigate the characteristics of bed agglomerates, the bed samples collected after biomass pyrolysis were then washed using a mixed solvent of chloroform and methanol, aiming to remove any possible solvent-soluble organic matter that could aid in the agglomeration. The particle size distributions of the bed samples after solvent washing are presented in Figure 4.1B, which shows a significant shift in the

particle size distribution of bed samples to smaller particle sizes after solvent washing, hence reductions in agglomeration yields (see Figure 4.3A and Figure 4.4A (i.e., the series of datum points in unfilled circles with legend “After solvent washing”)). It is also evident that after solvent washing, there are still various amounts of agglomerates present in the bed samples (see Figure 4.3A and Figure 4.4A (i.e., the series of datum points in unfilled circles with legend “After solvent washing”, respectively)).

The net reductions in the agglomeration yields as result of solvent washing are then calculated and plotted in Figures 4.3B and 4.4B. At a holding time of 15 minutes, Figure 4.3B shows that the reduction in agglomeration yield due to solvent washing firstly increases from 3.5 wt. % at 300 °C to a maximum of ~8.1 wt. % at 500 °C and then decreases rapidly as the pyrolysis temperature increases further. At 700 °C, solvent washing apparently leads to little (merely 0.2 wt. %) reduction in agglomeration yield. After solvent washing, the yield of the remaining agglomerates in bed samples decreases slightly with increasing pyrolysis temperature from 300 to 400 °C and rapidly from 400 to 500 °C, then levels off as the pyrolysis temperature increases further. At a given pyrolysis temperature (500 °C, see Figure 4.4B), the reduction in agglomeration yield due to solvent washing decreases with increasing holding time initially (from 7.5 to 15 minutes) then levels off with further increase in holding time. Figure 4.4A also suggests that holding time has no apparent effect on the yield of remaining agglomerates in the bed samples after solvent washing.

Since solvent washing removes at least some of the organic matter in the bed samples, the yields of solvent-insoluble, solvent-soluble and total organic matter in

the bed samples were then quantified. Figure 4.5 presents the yields of the different types of organic matter in bed samples collected from biomass pyrolysis at various temperatures and a holding time of 15 minutes, normalised to the total mass (daf) of biomass feed.

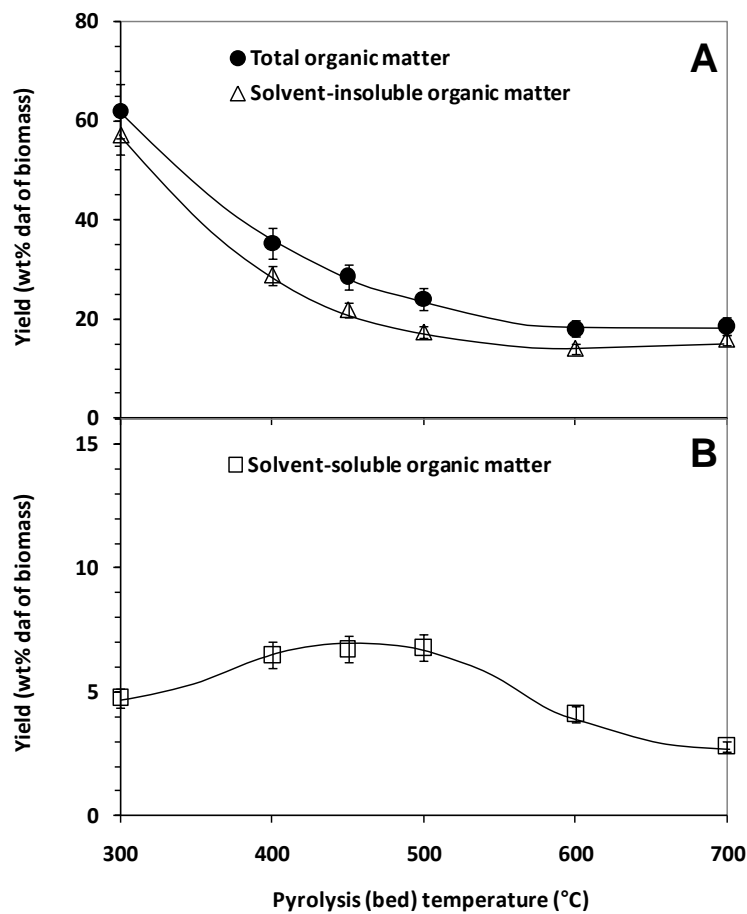


Figure 4.5 Yield of total organic matter, solvent-soluble organic matter and solvent-insoluble organic matter as a function of pyrolysis temperature (holding time: 15 mins).

It can be seen from Figure 4.5A that the yields of solvent-insoluble organic matter decrease with increasing pyrolysis temperature, following a similar trend observed in the effect of temperature on the yield of remaining agglomerates in the bed samples after solvent washing (see Figure 4.4A). However, the yield of solvent-soluble

organic matter initially increases from 300 to 500 °C then decreases with further increasing pyrolysis temperature. Interestingly, the trend is also similar to that seen in the effect of pyrolysis temperature on the reduction in agglomeration yield as results of solvent washing. At a given pyrolysis temperature (500 °C, see Figure 4.6B), both the yields of solvent-soluble organic matter and solvent-insoluble organic matter decrease with increasing holding time initially (from 7.5 to 15 minutes) then level off with increased holding time.

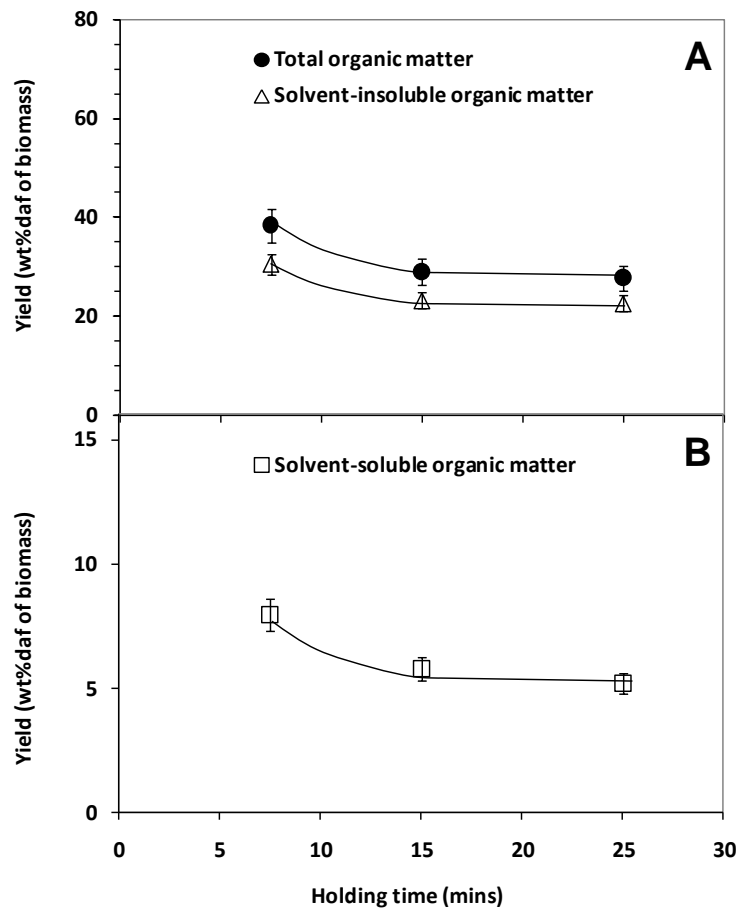


Figure 4.6 Yield of total organic matter, solvent-soluble organic matter and solvent-insoluble organic matter as a function of holding time (pyrolysis temperature: 500 °C).

Attempts were then made to investigate the correlations between the reduction in agglomeration yield due to solvent washing and the yields of solvent-soluble organic

matter (i.e., via plotting the data in Figures 4.3B and 4.4B against the corresponding data in Figures 4.5B and 4.6B). Similarly, the data in Figures 4.3A and 4.4A (i.e., the yields of remaining agglomerates in bed samples after solvent washing) are also plotted against the corresponding data in Figures 4.5A and 4.6A (i.e., the yields of solvent-insoluble organic matter).

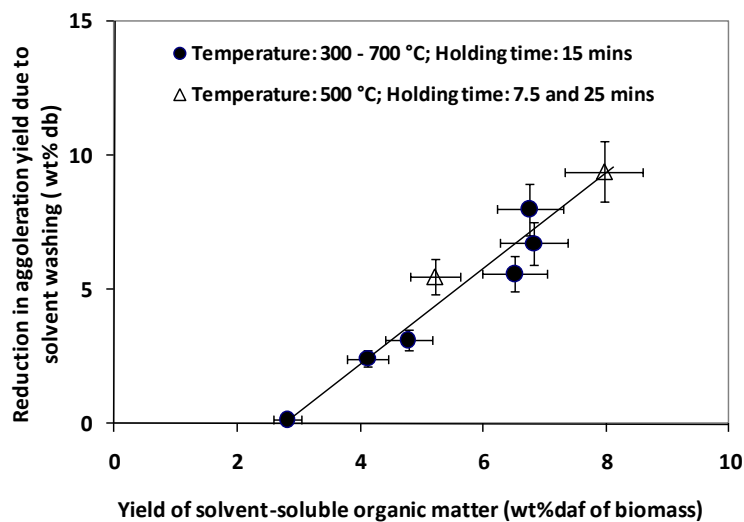


Figure 4.7 Correlation between the yield of agglomeration (after the solvent washing of bed materials collected from biomass pyrolysis) and the yield of solvent-insoluble organic matter

As shown in Figures 4.7 and 4.8, both correlations are broadly linear, clearly suggesting that the respective (solvent-soluble or solvent-insoluble) organic matter is indeed responsible for the formation of the corresponding bed agglomerates during biomass pyrolysis

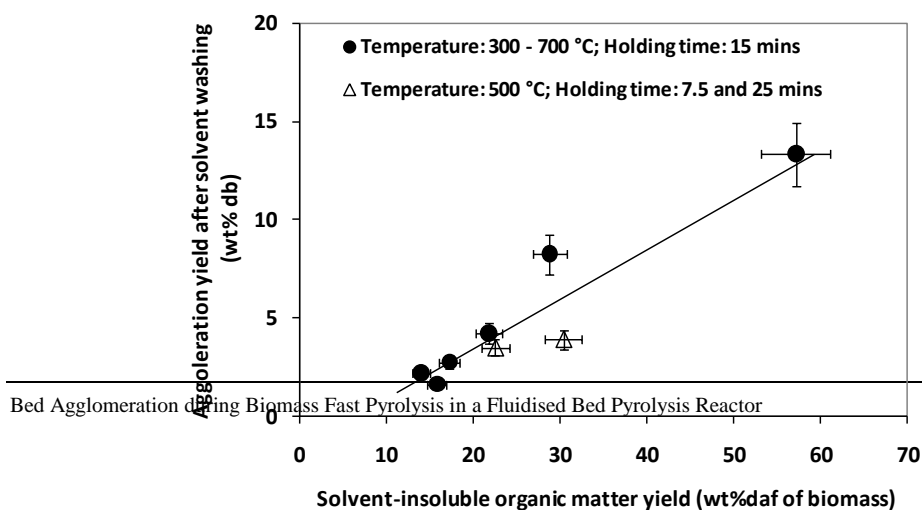


Figure 4.8 Correlation between the reduction in the yield of agglomeration (due to the solvent washing of bed materials collected from biomass pyrolysis) and the yield of solvent-soluble organic matter

For both solvent-soluble and insoluble organic matter, the correlations do not pass through zero, as shown in Figures 4.7 and 4.8. The data suggests that a minimal amount of organic matter is required for bed agglomeration to take place.

4.3.4 Possible mechanisms responsible for bed agglomeration during biomass pyrolysis

The data presented in this paper so far provides essential experimental evidence for understanding the nature of bed agglomerates formed and the mechanisms responsible for ash agglomeration during biomass gasification in a fluidized-bed reactor. It is clear in the SEM and optical microscope images (Figures 4.2A–4.2F) that the bed agglomeration is due to some organic matter which acts as sticky agent for forming agglomerates, producing the carbon-enriched connection necks in either char-char or char-sand agglomerates during biomass pyrolysis. The data in Figures 4.3–4.8 further suggest that there are two different types of agglomerates in the bed samples. One is the bed agglomerate formed due to solvent-soluble organic matter and such agglomerates dissemble upon solvent washing. The other type of bed agglomerate is the remaining agglomerates in bed samples which are formed as results of solvent-insoluble organic matter produced from biomass pyrolysis.

To understand the relative importance of bed agglomeration caused by solvent-soluble and solvent-insoluble organic matter, the contributions of the two types of agglomerations to the total agglomeration are calculated and plotted in Figure 4.9, based on the data in Figure 4.4A and Figure 4.5A. The contribution of agglomeration due to solvent-insoluble organic matter dominates at the low pyrolysis temperatures (e.g. ≈ 80 wt. % at $300\text{ }^{\circ}\text{C}$), decreases with pyrolysis temperature and reaches a minimum at $500\text{ }^{\circ}\text{C}$ (≈ 30 wt. %) then increases with a further increase in pyrolysis temperature. At $700\text{ }^{\circ}\text{C}$, the contribution is over 90 wt. % so that bed agglomeration is again dominantly due to solvent-insoluble organic matter.

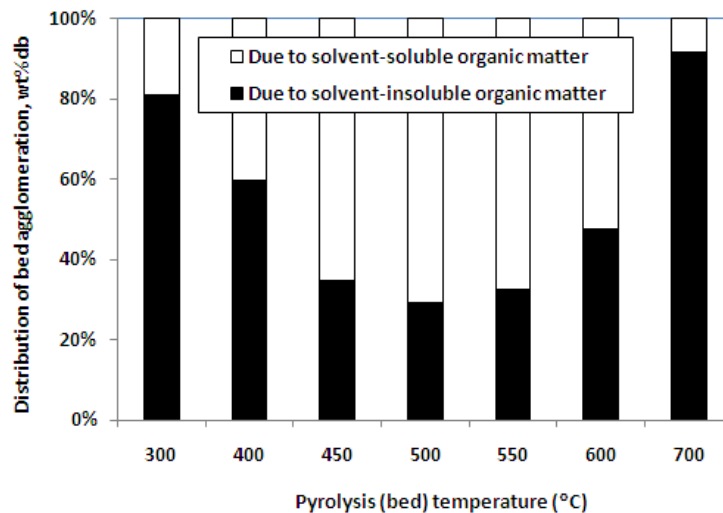


Figure 4.9 Distribution of bed agglomeration as a function of pyrolysis temperature (holding time: 15 mins)

On the contrary, the contribution of bed agglomeration due to solvent-soluble organic matter is low initially (≈ 20 wt. % at $300\text{ }^{\circ}\text{C}$), increasing rapidly and reaching a maximum as temperature increase from 300 to $500\text{ }^{\circ}\text{C}$ (≈ 70 wt. %) then decreasing

again. An increase in pyrolysis temperature above 600 °C leads to a drastic reduction in the bed agglomeration contributed by solvent-soluble organic matter.

It is important to note that initially there were only silica sand and biomass particles present in the fluidized-bed reactor. The biomass feed particles would be the only particles to have experienced thermal decomposition during fast pyrolysis, as the silica sand particles are inert. Therefore, the organic matter (both solvent-soluble and solvent-insoluble) must be a product of physical and/or chemical transformation of biomass during pyrolysis in the reactor. As shown in Figure 4.3A, the agglomeration yields due to solvent-insoluble organic matter are very high at a pyrolysis temperature as low as 300 °C. As pyrolysis reactions are not intensive at such a low temperature, the biomass particles must have undergone at least a partial melting process that makes the particles become sticky to enable bed agglomeration. This is also consistent with the previous experimental observations that cellulose/biomass particles may experience a melting process upon rapid heating.^{197,}
¹⁹⁸ Certainly, melting appears to take place at high pyrolysis temperatures as well, as supported by the experimental observation in Figure 4.2 (i.e., the char particles in the agglomerates having partially round shapes).

As pyrolysis temperature increases from 300 to 600 °C, biomass pyrolysis reactions become more intensified, leading to a continuous decrease in the yield of total organic matter (i.e., char yield of biomass pyrolysis). This in turn results in a decrease in bed agglomeration that is contributed by solvent-insoluble organic matter (see Figures 4.4 A and 4.5A). Due to the fact that the pyrolysis reactions are more intensive at pyrolysis temperatures 400–500 °C,^{199, 200} this leads to a drastic

reduction in the bed agglomeration due to solvent-insoluble organic matter around this temperature range.

Table 4.1 Elemental analysis of chars collected at various pyrolysis temperatures and a holding time of 15 minutes

Pyrolysis temperature (°C)	Elemental analysis (wt. % daf)				
	C	H	N	S	O*
300	68.14	4.82	1.56	0.57	24.91
450	74.02	3.37	2.41	0.39	19.82
500	76.82	2.78	2.52	0.39	19.82
550	78.73	2.43	2.99	0.30	15.55
600	78.75	2.31	3.17	0.28	15.49
700	86.06	1.34	3.78	0.12	8.80

* determined by difference

This is further supported by the data in Table 4.1, which clearly shows that the char samples, which are the dominant solvent-insoluble organic matter in the bed samples after solvent washing, have indeed become increasingly carbonised. The yield of solvent-soluble organic matter (see Figure 4.5B) and the agglomeration contributed by solvent-soluble organic matter (see Figure 4.4B) increases with pyrolysis temperatures up to 500 °C then decreases rapidly as temperatures further increase (e.g., 600 and 700 °C). It should be noted that the solvent-soluble organic matter in question remains in the bed sample rather than be released as part of the volatiles during biomass pyrolysis. Therefore, the solvent-soluble organic matter is most likely produced via two mechanisms. One is as part of the reacting biomass particles, which experience at least partial melting, and the other is as heavy tars, which were not released to gaseous phase under the pyrolysis conditions. The first

mechanism appears to be dominant at low temperatures (e.g., 300 °C) while the second mechanism appears to be dominant at high pyrolysis temperatures. This is supported by the experimental data in Figure 4.10 on the UV spectra of the solvent solutions produced by the washing of the bed samples. The data are reported as the relative intensity of the synchronous spectra normalised to the total mass (daf) of biomass feed. Figure 4.10 clearly shows that the yield of aromatics in the solvent-soluble organic matter indeed also follow a similar trend (i.e., increasing with pyrolysis temperature up to 500 °C then decreasing rapidly as temperatures further increase). As secondary cracking reactions of biomass tars become more pronounced at temperatures >500 °C,²⁰¹ the solvent-soluble organic matter would have experienced thermal cracking, resulting in the formation of large aromatic ring systems possibly re-combined into the solid “char” as part of the insoluble organic matter. This is reflected in the substantial reductions in not only the yield of solvent-soluble organic matter in the bed samples (see Figure 4.5B) but also the bed agglomeration yield contributed by solvent-soluble organic matter (see Figure 4.4B).

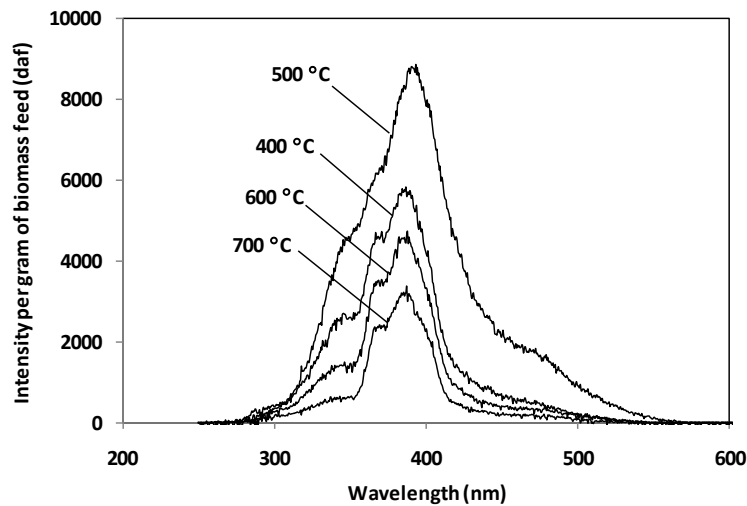


Figure 4.10 UV fluorescence synchronous spectra of the solutions obtained from the solvent washing of bed materials collected from biomass pyrolysis at 400–700 °C (holding time: 15 minutes). The UV intensities are normalised to the amount of biomass fed into the pyrolysis reactor.

4.4 Conclusions

This chapter reports an experimental investigation into bed agglomeration during biomass pyrolysis in a fluidized-bed reactor operated at a temperature range of 300–700 °C. The results clearly show that bed agglomeration takes place, forming char-char and char-sand agglomerates connected by carbon-enriched connection necks. The yield of bed agglomerates decreases with increasing pyrolysis temperature. Two types of bed agglomerates are identified: one is formed due to solvent-soluble organic matter and can be disassembled via solvent washing while the other is the remaining agglomerates which are formed as a result of solvent-insoluble organic matter produced from biomass pyrolysis. There is a broadly linear correlation between the yield of each type of bed agglomeration and the yield of the corresponding type of organic matter in the bed samples. The distribution of the two types of agglomerations is also strongly dependent on the pyrolysis temperature.

The contribution to bed agglomeration due to solvent-insoluble organic matter dominates at low pyrolysis temperatures (e.g., 300 °C), after which it decreases with an increase in pyrolysis temperature and reaches a minimum at 500 °C, then increases with a further increase in pyrolysis temperature. The contribution of bed agglomeration due to solvent-soluble organic matter follows an opposite trend. At pyrolysis temperatures above 600 °C, there is a drastic reduction in the bed agglomeration contributed by solvent-soluble organic matter due to thermal cracking reactions so that solvent-insoluble organic matter dominates bed agglomeration. Overall, bed agglomeration is formed due to sticky agents produced during biomass pyrolysis, including both the partial molten pyrolysing biomass particles and/or the organic matter (solvent-soluble and solvent-insoluble) as products of biomass pyrolysis reactions.

CHAPTER 5 DIFFERENCES IN BED AGGLOMERATION BEHAVIOUR DURING THE FAST PYROLYSIS OF MALLEE BARK, LEAF AND WOOD IN A FLUIDIZED-BED REACTOR AT 500 ° C

5.1 Introduction

The key focus of this chapter is to investigate the agglomeration behaviour among different biomass components during fast pyrolysis in a fluidized-bed pyrolyser operating at industrial conditions.

5.2 Experimental method

Fast pyrolysis reaction experiments were performed in a fluidized-bed pyrolyser using the mallee biomass components raw, washed and extract of leaf, wood and bark at a temperature of 500 °C and constant holding time of 15 minutes. The preparation and the procedures used in the fast pyrolysis experiments are detailed in chapter 3 above.

5.3 Results and discussion

5.3.1 Fast pyrolysis of raw mallee wood, leaf and bark

Figure 5.1 presents the particle size distributions (PSDs) of the bed materials collected from the fast pyrolysis of wood, leaf and bark in the fluidized-bed reactor at 500 °C and a holding time of 15 minutes. The PSDs of the bed materials for bark and leaf are also included in Figure 5.1 after the collected materials were washed

with solvent (chloroform and methanol mixed in a 4:1 ratio). Due to the fact that the sizes of the sand and biomass samples are 125–355 μm and 355–500 μm , respectively, the samples in the size fractions of 500–710 μm , 0.71–1.70 mm, 1.70–3.15 mm and >3.15 mm must have been produced due to bed agglomeration.

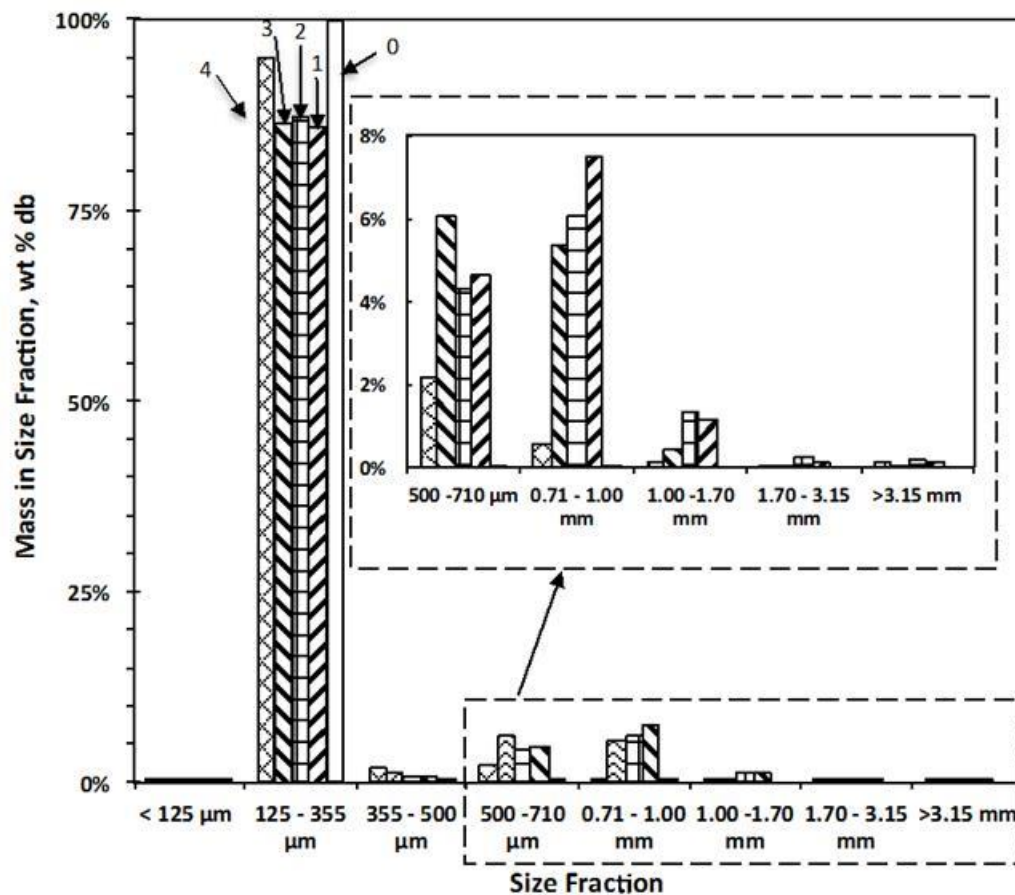


Figure 5.1 Particle size distributions (PSDs) of the bed materials collected from the fast pyrolysis of wood, bark and leaf in a fluidized-bed pyrolysis reactor at 500 °C and 15 minute holding time. Legends: 0 – bed material from wood pyrolysis, before the collected material being washed using solvent; 1 – bed material from bark pyrolysis, before the collected material being washed using solvent; 2 – bed material from leaf pyrolysis, before the collected material being washed using solvent; 3 – bed material from bark pyrolysis, after the collected material being washed using solvent; 4 – bed material from leaf pyrolysis, after the collected material being washed using solvent. The PSDs of sand (125–355 μm) and biomass (355–500 μm) fed to the reactor are omitted in the figure.

The results in Figure 5.1 show that the fast pyrolysis of wood, leaf and bark has resulted in significant difference in bed agglomeration. Fast pyrolysis of leaf and

bark leads to significant bed agglomeration but that of wood results in little agglomeration. In addition, the data also clearly shows that solvent washing of the bed materials can disintegrate at least some of the agglomerates from the fast pyrolysis of bark and leaf. There are also obvious differences between the reductions in the particle size distributions from the bark and leaf components. While solvent washing leads to a significant reduction in the PSD of the collected bed materials from leaf pyrolysis, such a reduction appears to be much less significant in the case of bark pyrolysis. The results suggest that the nature of the agglomerates from the fast pyrolysis of bark and leaf may be significantly different.

Figures 5.2A–5.2D present the images of various samples acquired using an optical microscope for leaf and bark particles before pyrolysis and typical agglomerates formed after fast pyrolysis of the bark and leaf. It can be seen that agglomerates are mainly formed via char-char binding and char-sand binding (see Figures 5.2B and 5.2D). Particularly, the agglomerate during bark pyrolysis appears to be formed via sand particles attached to the char particle itself (Figure 5.2B) while the agglomerate formed during leaf pyrolysis (Figure 5.2D) consists of a large amount of leaf char and sand particles inter-sintered. This could be due to the difference in shape as indicated in Figures 5.2A and 5.2C. The bark particles (Figure 5.2A) are more cylindrical or rectangular in nature while the leaf particles (Figure 5.2C) have shapes much closer to cubes. Therefore, the bark particles have much larger aspect ratios so that these particles provide less contact among the char particles produced but more contacts between the char particles and sand particles.

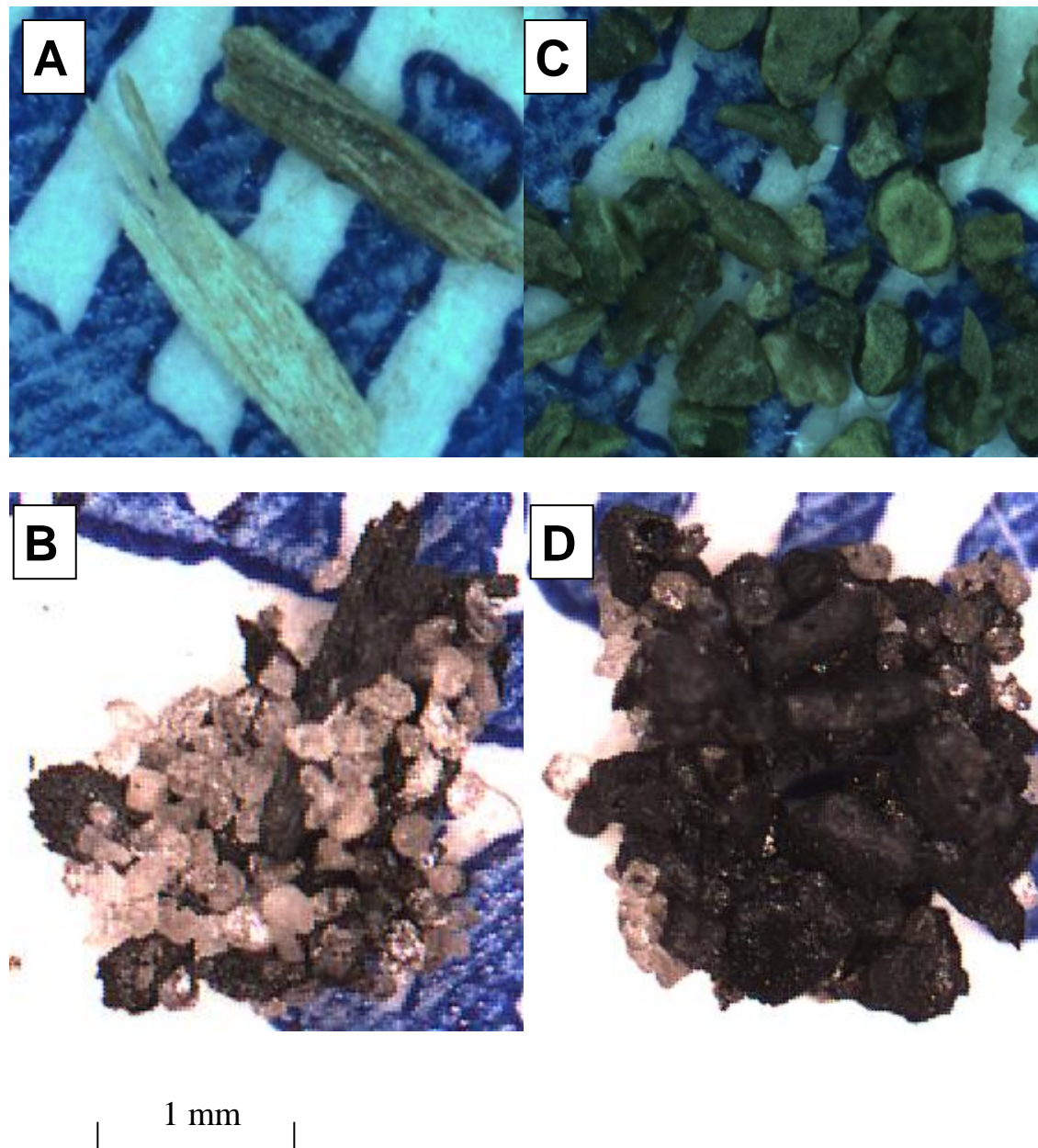


Figure 5.2 Optical images of various samples. Legend: (A) bark particles (355–500 μm) before pyrolysis; (B) a typical bed agglomerate in the size fraction of 1.70–3.15 mm collected from bark pyrolysis; (C) leaf particles (355–500 μm) before pyrolysis; and (D) a typical bed agglomerate in the size fraction of 1.70–3.15 mm collected from leaf pyrolysis. The blue marks underneath the sample are the marks of millimetres.

5.3.2 Fast pyrolysis of ethanol-washed mallee leaf and bark

The raw wood, bark and leaf samples were washed using ethanol to prepare a set of ethanol-washed biomass samples. The purpose of ethanol washing was primarily to

remove the extractives (ethanol-extractable) in the biomass components so that the effect of these ethanol-extractable components on the pyrolysis behaviour of the raw biomass materials can be explored. Figure 5.3 presents the yields (on a carbon basis) of the extract from the ethanol washing of the raw wood, leaf and bark. It can be seen that the yield of extract from the wood component is small (3.6 wt. % daf on a carbon basis) and those from the leaf and bark are substantial (18.9 and 15.9 wt. % daf on a carbon basis, respectively). Considering the little bed agglomeration during wood pyrolysis and the low yield of extract of wood, the experimental program was then conducted using the ethanol-washed leaf and bark samples only.

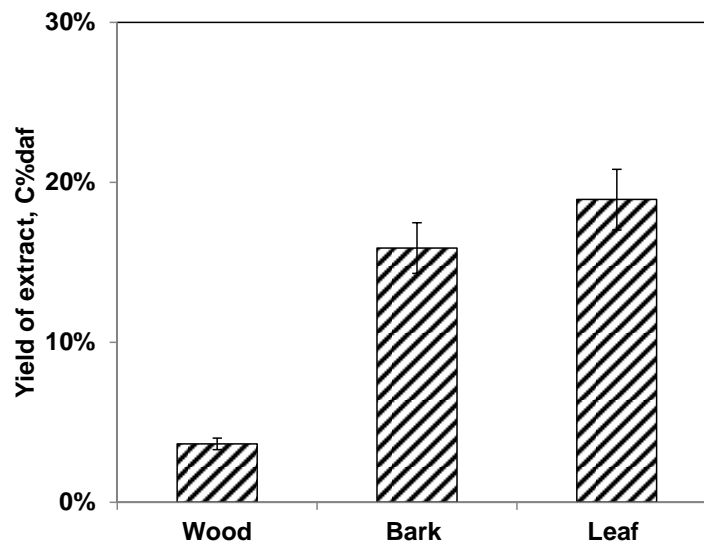


Figure 5.3 Yield of extract (C% daf) from the washing of wood, bark and leaf using ethanol at room temperature for 4 hrs.

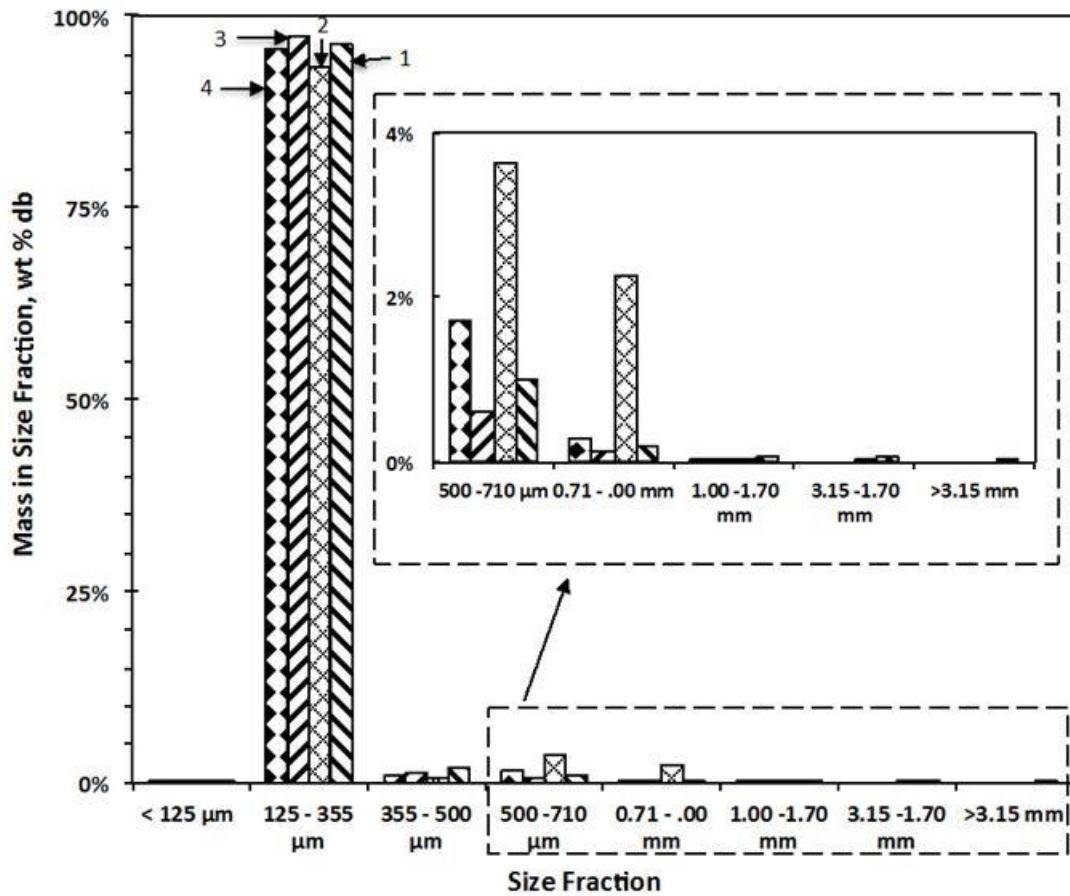


Figure 5.4 PSDs of the bed materials collected from the fast pyrolysis of ethanol-washed bark and leaf in a fluidized-bed pyrolysis reactor at 500 °C and 15 minute holding. Legends: 1 – bed material from ethanol-washed bark pyrolysis, before the collected material being washed using solvent; 2 – bed material from ethanol-washed leaf pyrolysis, before the collected material being washed using solvent; 3 – bed material from ethanol-washed bark pyrolysis, after the collected material being washed using solvent; 4 – bed material from ethanol-washed leaf pyrolysis, after the collected material being washed using solvent. The PSDs of sand (125–355 μm) and biomass (355–500 μm) fed to the reactor are omitted in the figure.

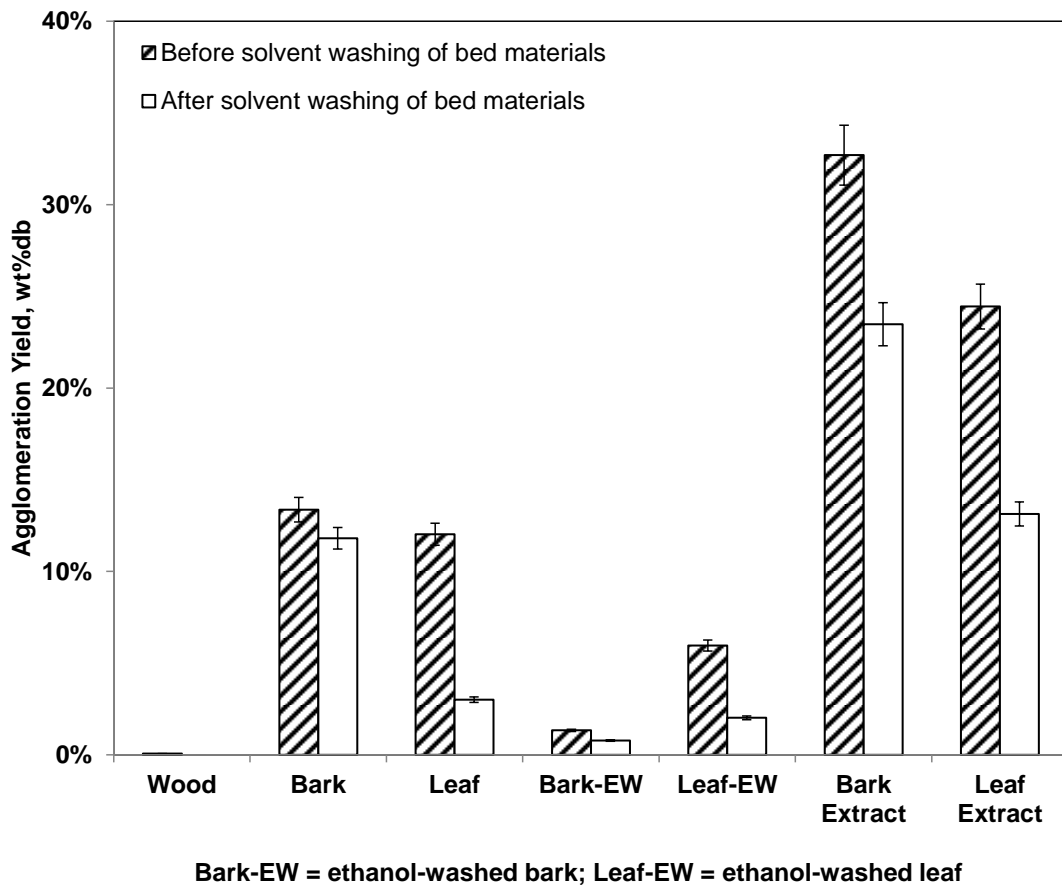


Figure 5.5 Bed agglomeration yields during the fast pyrolysis of various feeding materials in a fluidized-bed reactor at 500 °C and 15 minute holding time. The feeding materials include wood, bark, leaf, ethanol-washed bark (bark-EW), ethanol-washed leaf (leaf-EW), bark extract and leaf extract.

Figure 5.4 shows the PSDs of the collected bed materials from the fast pyrolysis of the ethanol-washed bark and leaf samples under the same pyrolysis conditions. It is interesting to see that compared to the PSDs in Figure 5.1, the bed materials collected from the pyrolysis of ethanol-washed presence of particles have been reduced substantially in the size fractions of 500–710 μm , 0.71–1.70 mm, 1.70–3.15 mm and >3.15 mm, respectively. The results suggest that after ethanol washing of the raw leaf and bark, there are drastic reductions in bed agglomeration when compared to the results for the raw biomass materials.

The agglomeration yields during the fast pyrolysis of wood, bark, leaf, ethanol-washed bark and ethanol-washed leaf are plotted in Figure 5.5. It can be seen that the agglomeration yields are reduced from 13.4 to 1.3 wt. % and from 12.0 to 6.0 wt. % after ethanol washing of the biomass material, for bark and leaf, respectively. The results suggest that the extractives in the biomass materials may play a critical role in bed agglomeration during the fast pyrolysis of bark and leaf.

5.3.3 Direct fast pyrolysis of extracts obtained from the ethanol-washing of mallee leaf and bark

Compounds found in the ethanol extracts from the mallee leaf have been identified by various researchers²⁰²⁻²⁰⁷ and have been identified as limonene, globulol, citronellol, terpinol, cineole, pipertone, phellandrene and eudesmol. Compounds within the ethanol extracts of the mallee bark has been performed by various researchers²⁰⁸⁻²¹⁰ and some of the compounds identified were yangambin; 1-monopalmitin; 3,3-di-O-methylellagic acid sideroxylin; 2,6-dimethoxy-1,4-benzoquinone; and β -sitosterol. As can be seen by the compounds identified by the researchers, these compounds are large and complex in nature. More compounds are being discovered yearly as both the analytical and measurement techniques are improved.

Further experiments were then carried out to investigate bed agglomeration when the extracts obtained from the washing of raw leaf and bark were directly fed into the fluidized-bed pyrolysis reactor under similar conditions (pyrolysis temperature: 500 °C; holding time: 15 minutes). Figure 5.6 presents the PSDs of the collected bed samples under the experimental conditions. It should be noted that the amount of

extract samples injected in each experiment was back-calculated to represent the same amount of extract that would be fed into the reactor during the pyrolysis of the raw biomass component. The results in Figure 5.6 clearly show that direct pyrolysis of the extract samples obtained from both of the leaf and biomass components results in significant bed agglomeration because there are substantial amounts of large agglomerates in the size fractions of >3.15 mm. The data provides direct evidence that demonstrates the extractives in the raw biomass playing a key role in bed agglomeration during fast pyrolysis of these biomass materials. This is consistent with the observation that there is little bed agglomeration during rapid pyrolysis of the wood (see Figure 5.1) because the yield of extract sample is very low (see Figure 5.3). It should also be noted that the extract samples were injected into the reactor in the form of an ethanol solution. Blank experiments of direct injecting the same amount of solvent only (ethanol) into the reactor led to no bed agglomeration under the same pyrolysis conditions.

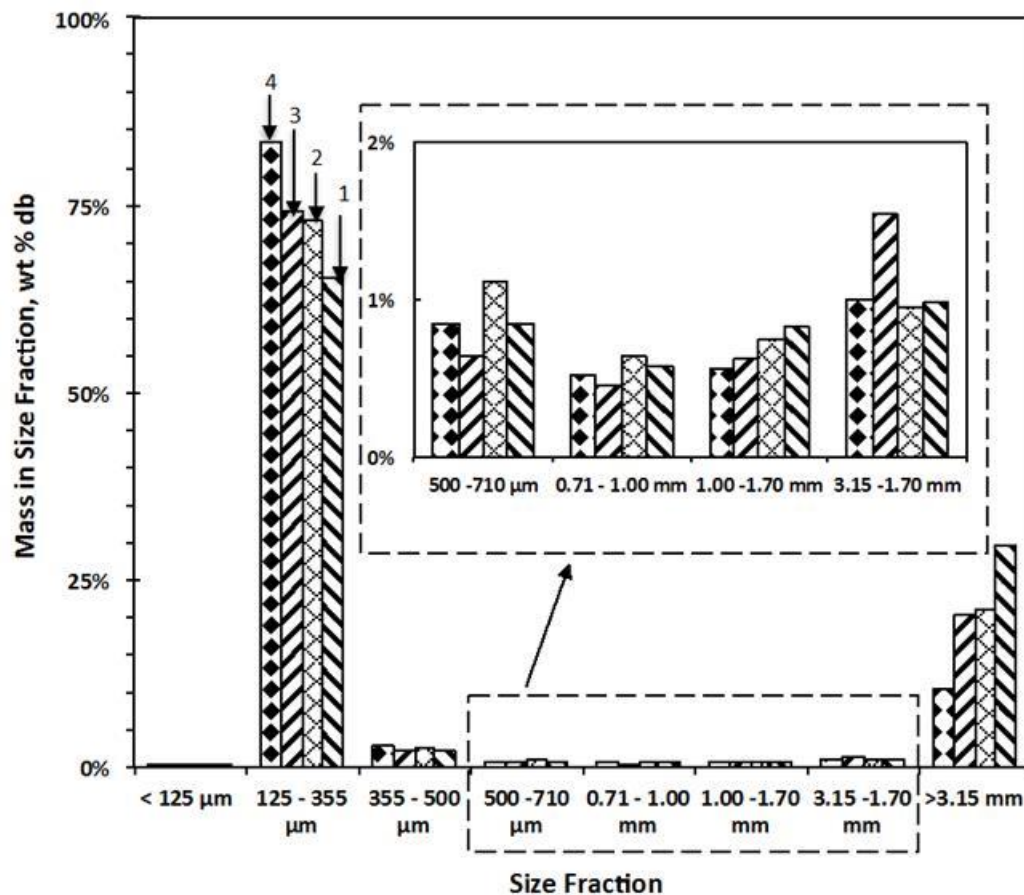


Figure 5.6 PSDs of the bed materials collected from the fast pyrolysis of the extracts from bark and leaf in a fluidized-bed pyrolysis reactor at 500 °C and 15 minute holding. Legends: 1 – bed material from bark extract pyrolysis, before the collected material being washed using solvent; 2 – bed material from leaf extract pyrolysis, before the collected material being washed using solvent; 3 – bed material from bark extract pyrolysis, after the collected material being washed using solvent; 4 – bed material from leaf extract pyrolysis, after the collected material being washed using solvent. The PSDs of sand (125–355 μm) in the reactor has been omitted from the figure.

Figure 5.6 also indicates the leaf and bark extracts having undergone fast pyrolysis have similar magnitude values for the size distribution in the size fractions of 500 μm–3.15 mm before and after washing with the chloroform : methanol solvent. The size fraction of >3.15 mm, however, differs greatly along with the 125–355 μm size fraction. This further indicates that the extract samples of bark and leaf react differently, most likely due to the leaf and bark extracts being composed of different compounds and composition.²¹¹⁻²¹⁶ The extract of the leaf contains smaller

molecular weight compounds than that of the bark extract as can be seen from some of the compounds listed above from each of the extracts. Nevertheless, the extracts seem to be interacting with sand in the fluidized-bed in a similar manner, forming very large amounts of >3.15 mm material relative to the other size fractions which remain similar in magnitude, except for the 125–355 μm (sand size fraction) which is decreasing at a proportional rate to the increasing >3.15 mm material. The results suggest that the sand is essentially being used to form the corresponding amount of large agglomerates of sizes >3.15 mm. This is consistent with the fact that after solvent washing, the sand distribution (125–355 μm) increases almost by the same amount as the >3.15 mm material decreases.

Figure 5.7A and 5.7B present the optical microscope images of the resulting agglomeration formed during the fast pyrolysis of the leaf (A) and bark (B) extract samples in the fluidized-bed at 500 °C and a holding time of 15 minutes. It can be seen that both of these extracts (leaf and bark) have almost completely intermixed with the sand particles to form these large agglomerates which are generally round in shape and tightly inter-packed sand particles. This shape indicates that these particles are forming by combining smaller agglomerated particles into much larger ones as they interact with the incoming sticky agent produced during the fast pyrolysis of the extract sample.

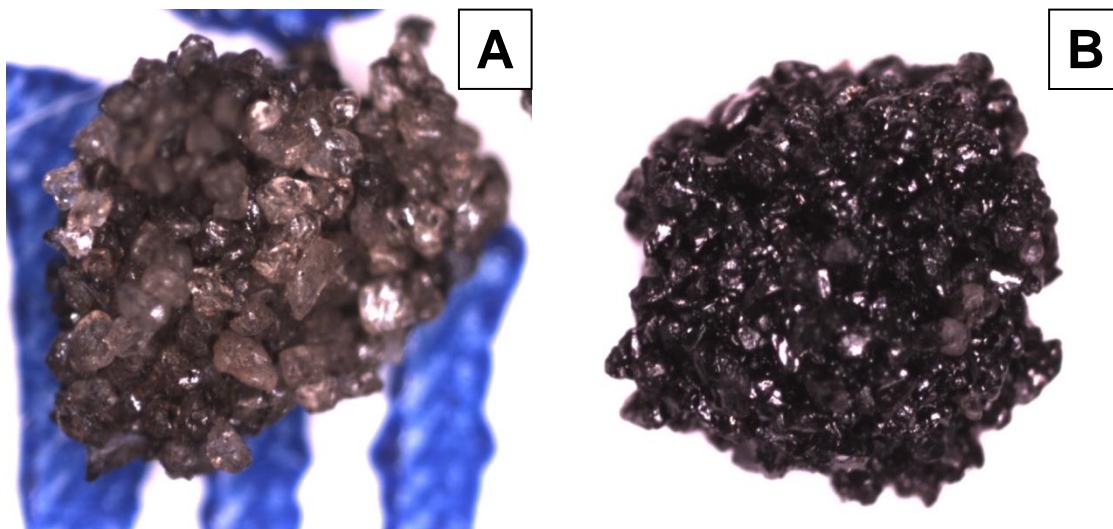


Figure 5.7 Optical images of typical bed agglomerates collected from the fast pyrolysis of leaf and bark extract sample in the fluidized-bed reactor at 500 °C and a holding time of 15 minutes. (A) agglomerated materials (>1.7 mm) resulting from the fast pyrolysis of leaf extract; (B) agglomerated materials (>1.7 mm) resulting from the fast pyrolysis of bark extract

5.3.4 Further discussion and practical implications

Figure 5.5 shows that when only injecting the extract into the fluidized-bed reactor at 500 °C under fast pyrolysis conditions, there has been a dramatic increase in bed agglomeration yield. Removing the extractive materials from leaf and bark (via ethanol washing) leads to substantial reductions in bed agglomeration yields.

Therefore, the results also clearly suggest that the extractive materials in leaf and bark biomass components play vital roles in producing sticky agents for the fluidized sand bed material to interact with. The potential mechanisms may include the thermochemical reactions of the extractive materials and interactions between these materials (or their pyrolysis products) and the pyrolysing biomass particles (or their pyrolysis products) that facilitate bed agglomeration. Compared to that of extractive materials, the pyrolysis of the raw biomass particles leads to a reduction in bed agglomeration. Therefore, the interaction between the pyrolysing extractive-free

biomass particles with the pyrolysing extractive materials hinders bed agglomeration. The results presented in this chapter show that there are significant differences in bed agglomeration behaviour during the fast pyrolysis of mallee wood, leaf and bark. While wood pyrolysis leads to minimal bed agglomeration, that of bark and leaf results in substantial bed agglomeration. It can therefore be concluded that when the whole biomass from mallee trees are used for bio-oil production via fluidized-bed pyrolysis, the leaf and bark components will be responsible for the potential bed agglomeration that can impact the durable operations of the reactor system.

5.4 Conclusions

There are significant differences in bed agglomeration behaviour during the pyrolysis of mallee wood, bark and leaf in a fluidized-bed reactor at 500 °C. Pyrolysis of wood component leads to insignificant bed agglomeration while the pyrolysis of leaf or bark biomass component results in substantial bed agglomeration. Removing extractive materials from leaf and bark via ethanol washing of the raw biomass samples resulted in insignificant bed agglomeration during the fast pyrolysis of the ethanol-washed leaf and bark in the fluidized-bed reactor under the same conditions. Direct pyrolysis of the extractive materials from leaf or bark leads to substantial bed agglomeration. The data in this chapter suggests when the whole mallee biomass is used for bio-oil production via fluidized-bed pyrolysis, the leaf and bark components are expected to result in bed agglomeration. The large amounts of extractive materials present in the leaf and bark play a critical role in bed agglomeration during the fast pyrolysis of these biomass samples.

CHAPTER 6 QUANTIFICATION OF INTERACTIONS BETWEEN SAND AND PYROLYSING BIOMASS PARTICLES IN FLUIDIZED-BED UNDER FAST PYROLYSIS CONDITIONS PERTINENT TO BIO-OIL PRODUCTION

6.1 Introduction

This chapter investigates the direct interaction between the biomass particle undergoing pyrolysis and the fluidized sand bed particle as it pertains to the conditions found in an industrial fluidized-bed pyrolyser (500 °C and above atmospheric pressure). The interaction is measured or quantified via a newly defined measurement parameter called sand loading (S_L) which has the units $\text{g}_{\text{sand}}/\text{g}_{\text{biomass (db)}}$.

6.2 Experimental method

Fast pyrolysis experiments were performed on the raw leaf biomass; preparation of the samples and procedures used in the fast pyrolysis are detailed above in chapter 3. The particle size distribution used for the sand bed material (125–250 μm) and the leaf biomass (355–500 μm) was constant for all experiments; the actual bed mass was kept constant for all experiments (19.5–20 g). The pyrolysis experiments were carried out at different holding times (1–35 minutes) using a constant feed mass (1.95–2 g), feed rate (≈ 0.3 g/min) and pyrolysis temperature of 500 °C. Various ratios of the biomass feed (on a dry basis (db)) to the sand bed material were performed (by adjusting the biomass feed mass only while keeping the mass of sand bed constant (19.5–20 g), at a holding time of 15 minutes). The size fraction used in

the experimentation (355–500 μm) is smaller than the usual feed into an industrial fluidized-bed pyrolyser >1 mm, this was performed to ensure that the resulting Biot number was <0.1 . With a Biot number <0.1 the effects of internal and external heat and mass transfer for the particle are minimised and can be ignored, as the particle is deemed thermally thin in nature.^{169, 217-219} By doing this we can get a true relationship between the interacting sand and biomass feed particles without the effect of thermal or mass transfer gradients across the particle. Samples before and after pyrolysis were subjected to analysis, the analysis performed is noted where and when required, and procedures used in the analysis are outlined in chapter 3 above.

6.3 Sand loading (S_L) as a key diagnosis parameter for bed agglomeration

A new parameter (i.e., sand loading (S_L)) is introduced in order to investigate the direct interaction between the pyrolysing biomass particles and the sand particles (as bed material). The sand loading (S_L) is defined as the mass of sand that sticks with the pyrolysing biomass particles in the bed to form bed agglomerates normalised to the total mass of biomass fed into the fluidized-bed reactor:

$$S_L = M_{S+}/M_{B0} \quad (6.1)$$

Where M_{B0} is the total mass of biomass feed (g, db). M_{S+} is the amount of sand (g) that is in the bed agglomerates.

Quantifying M_{S+} hence S_L can be done experimentally. As the sand particles have particle sizes of 125–250 μm , the mass of ash produced via the combustion of the bed sample of size >250 μm , excluding of ash in the recovered chars in the sample,

must be M_{S+} the mass of sand directly interacting with pyrolysing biomass particles in the bed.

6.4 Results and discussion

6.4.1 Distribution of char in bed agglomerates and non-agglomerate bed materials

In this chapter, the sand and biomass particles have particle sizes of 125–250 μm and 355–500 μm , respectively. Therefore, any material in the bed sample having a size greater than 500 μm must be bed agglomerates. It was also noted that there was little sample recovered in the size fraction of 250–355 μm . The amount of sample recovered in the size fraction of 355–500 μm is also minimal. In fact, the fluidisation velocity of the sand particle is much larger than that of the biomass char particle due to the substantial difference in particle densities of sand particles ($\approx 2700 \text{ kg/m}^3$) and bio-char ($\approx 250 \text{ kg/m}^3$). It was estimated that the char particles in these size fractions would be carried over by the fluidization gas if not forming agglomerates. Therefore, the samples collected in the size fraction of 250–500 μm should also be bed agglomerates, but the contribution from the size fraction to bed agglomerates is rather small. This can be clearly seen on the values of the bed agglomeration yield (Y_{AP}),²²⁰ presented in chapter 4 above, which is the mass of bed agglomerates as percentage of the total mass of the bed sample. As shown in Figure 6.1, the values of Y_{AP} are similar regardless of the particle size used $>250 \mu\text{m}$ or $>500 \mu\text{m}$ to measure the bed agglomerate yields.

Overall, the total amount of char in the bed sample after pyrolysis (i.e., M_C , g) consists of those in the bed agglomerates (denoted as M_{C+} , g) and those in the rest of bed sample, which is not bed agglomerates (denoted as M_{C-} , g):

$$M_C = M_{C+} + M_{C-} \quad (6.2)$$

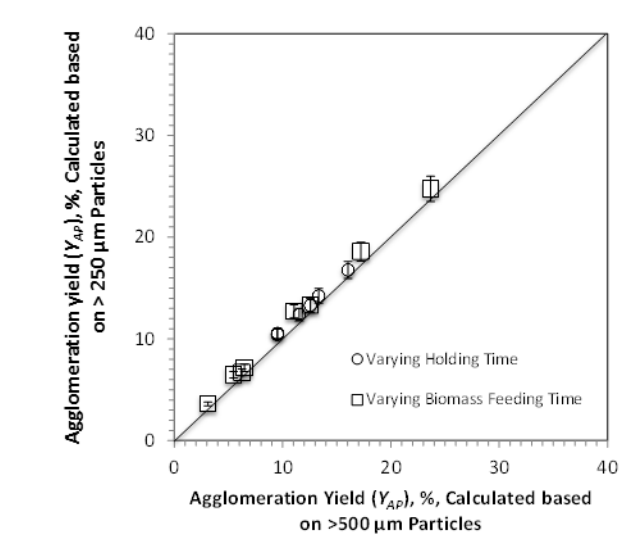


Figure 6.1 Comparison in bed agglomeration yield Y_{AP} , which is the mass of bed agglomerates as percentage of the total mass of the bed sample, considering either particles with sizes $>250 \mu\text{m}$ or particles with sizes $>500 \mu\text{m}$ as bed agglomerates

Figure 6.2 presents the data on char recovery from the bed materials $<250 \mu\text{m}$ normalised to the total char recovered from the whole bed sample (i.e., M_{C-} / M_C) under various pyrolysis conditions. From Figure 6.2 it can be seen that the results for the char recovery for either varying the feeding time (1–17 minutes) with a constant holding time of 15 minutes (panel A), or varying the holding time 1- 35 minutes at a constant feeding time of 6 minutes (panel B), the actual contribution of char in the bed materials $<250 \mu\text{m}$ to the total char recovery from the whole bed sample is insignificant ($\approx 2 \text{ wt. } \%$). Therefore, M_{C-} is also insignificant. We can then define char recovery (X_R , % db) from the fluidized-bed as char recovered from the

bed normalised to the total mass of biomass feed on a dry basis. The values of X_R under various conditions can be determined experimentally.

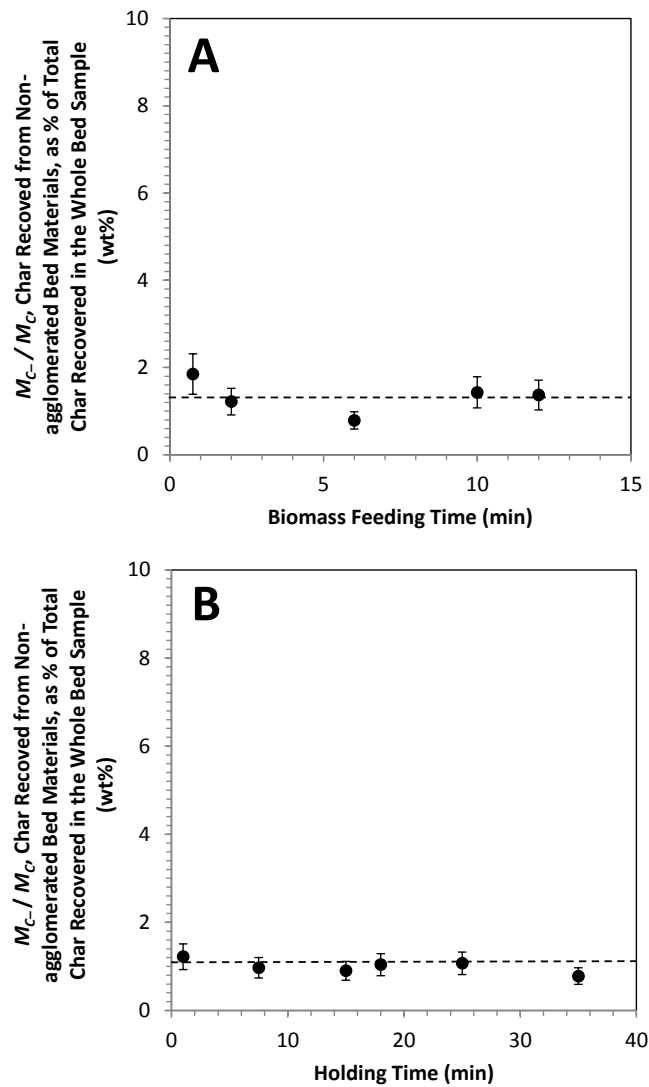


Figure 6.2 Contribution of char in the bed materials below 500 μm to the total char recovered from the whole bed sample (i.e., M_{C-}/M_C) during biomass fast pyrolysis in the fluidized-bed reactor at 500 $^{\circ}\text{C}$. Panel (A): with continuous biomass feeding at various periods of time (1–17 minutes) then followed with a constant holding time of 15 minutes; Panel (B): with a fixed feeding time of 6 minutes then followed with various holding times (1–35 minutes).

We then further have

$$M_C \approx M_{C+} \approx X_R M_{B0} \tag{6.3}$$

The total mass of bed agglomerates are the sum of the total mass of sand in bed agglomerates and the total mass of char in bed agglomerates, we have

$$M_{S+} = M_{T+S} - M_{C+} \quad (6.4)$$

where M_{T+S} is total mass of bed agglomerates (g) and M_{C+} is the total amount of char (g) in bed agglomerates. Substituting Equations (6.3) and (6.4) into Equation (6.1) yields that S_L can be calculated as

$$S_L = M_{T+S}/M_{B0} - X_R \quad (6.5)$$

Differentiating Equation (6.5) with respect to time, yielding

$$dS_L/dt = 1/M_{B0}^2 \cdot (M_{B0} \cdot dM_{T+S}/dt - M_{T+S} \cdot dM_{B0}/dt) - dX_R/dt \quad (6.6)$$

At a constant biomass feeding rate, $dM_{B0}/dt = 0$, therefore we have

$$dS_L/dt = 1/M_{B0} \cdot dM_{T+S}/dt - dX_R/dt \quad (6.7)$$

Equation (6.7) shows that the rate of bed agglomeration (dM_{T+S}/dt) and consequently the rate of sand loading (S_L) are affected by the char recovery from the bed as both of these variables are dependent on each other. Equation (6.7) also indicates that the rate at which the sand interacts with the pyrolysing biomass particles is dependent on the biomass pyrolysis reaction conditions occurring in the pyrolyser.

6.4.2 Kinetics of bed agglomeration during continuous holding after the completion of feeding

After the completion of biomass feeding, bed agglomerates formed undergo further evolution during continuous holding at the pyrolysis temperature. The further carbonisation of the organic matter, which is the sticky agent responsible for agglomerate formation, leads to further reduction in bed agglomeration²²⁰ as indicated in chapter 4 above. The relationship between sand loading (S_L) and holding time (t_h) may reveal further insights into the kinetics of bed agglomeration during continuous holding after the completion of feeding. Figure 6.3 plots the sand loading (S_L) as a function of holding time (t_h) after the completion of 6 minutes of feeding during pyrolysis at 500 °C. It is interesting to see that sand loading has a linear correlation with holding time.

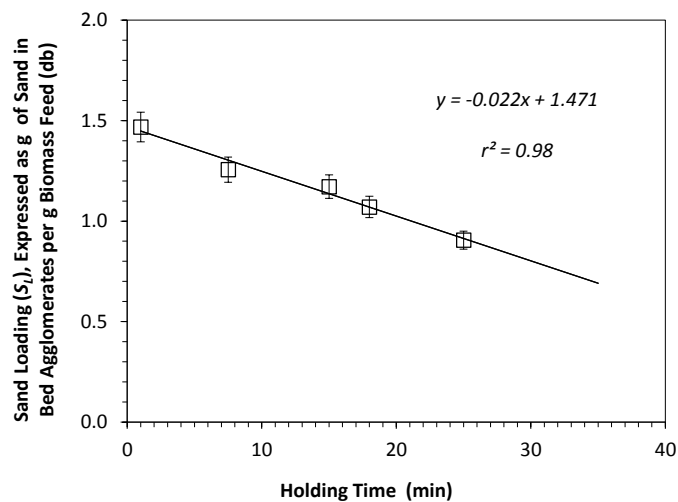


Figure 6.3 Sand loading (S_L), expressed as g of sand in bed agglomerates per g biomass feed (db), as a function of holding time during biomass undergoing pyrolysis at 500 °C

The results suggest that during holding at the pyrolysis temperature, the sand loading follows a zero-order reaction path with respect to holding time. In chemical reaction engineering, zero-order reaction kinetics are usually associated with catalytic

reactions,²²¹ in which the active sites on the catalyst are saturated so that the reactions are dictated by availability of active sites, instead of the concentration of the reactants. Therefore, the data in Figure 6.3 suggests that sand loading is a consequence of the pyrolysis reactions that produce sticky agents with “active sites” for sand particles to interact with for bed agglomeration to occur. Such “active sites” appear to lead to the formation of either char–char bonds (i.e., the “active sites” on the surfaces of different biomass particles interacting with each other) or char–sand bonds (i.e., the “active sites” on the surfaces of pyrolysing biomass particles interacting with the sand particles), as previously reported^{220, 222} in chapters 4 and 5 above.

Therefore, considering sand loading follows a zero–order reaction,^{223, 224} we have

$$d S_L/dt = -K_S \quad (6.8)$$

Integrating Equation (6.7) between the limits of holding time t_0 and t_h along with S_{L0} and S_L , we have

$$S_L - S_{L0} = -K_S(t_h - t_0) \quad (6.9)$$

Based on Equation (6.9) and the linear correlation in Figure 6.3, the values of K_S and S_{L0} can be determined from the slope and the intercept, which are 0.022 $\text{g}_{\text{sand}}/\text{g}_{\text{biomass}(\text{db})}$ per minute and 1.471 $\text{g}_{\text{sand}}/\text{g}_{\text{biomass}(\text{db})}$, respectively. As a consequence of pyrolysis reactions, S_L should be correlated with the pyrolysis reaction kinetics, which can be quantified as char recovery X_R over time. Therefore, the data on S_L as

a function of char recovery X_R are then plotted in Figure 6.4, which clearly shows that there is a linear correlation between S_L and X_R , with a slope of 0.04. It is also noteworthy that the extrapolation of the line goes through $(0,0)$, (i.e., at a zero char recovery ($X_R = 0$), the sand loading is zero).

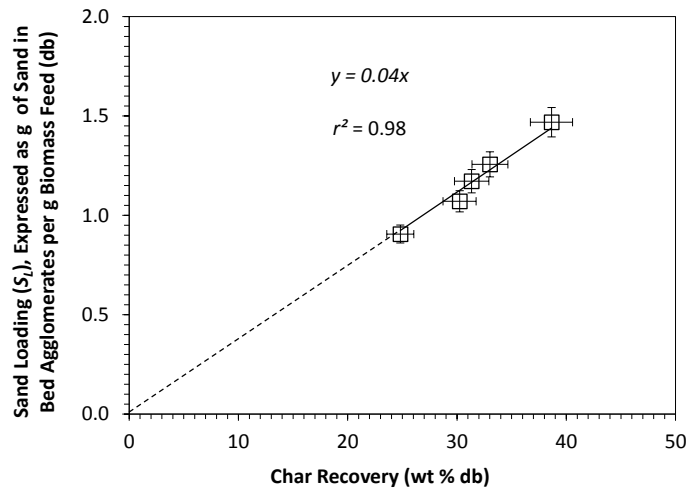


Figure 6.4 Plot of biomass sand loading (S_L) vs char recovery (X_R) for biomass pyrolysis at 500 °C after the completion of 6 minutes feeding and varying holding time (1–35 mins)

As the reaction kinetics for pyrolysis generally follows first-order kinetics, we have

$$dX_R/dt = -K_x X_R \quad (6.10)$$

Dividing Equation (6.8) by Equation (6.10), we have

$$dS_L/dX_R = K_S/K_X \cdot 1/X_R = K \cdot 1/X_R \quad (6.11)$$

Integrating Equation (6.11) over the limits S_{L0} to S_L and X_{R0} to X_R , we have

$$S_L = S_{L0} + K \cdot \ln(X_R/X_{R0}) \quad (6.12)$$

The initial char recovery (X_{R0}) can be found by plotting $\ln(X_R)$ vs holding time (t_h). From this plot the slope is the pyrolysis reaction constant (K_X) and the intercept is $\ln(X_{R0})$, where $\ln(X_{R0})$ represents the char recovery the instant the biomass particle is at 500 °C. Figure 6.5A is the plot of $\ln(X_R)$ vs holding time (t_h) for biomass pyrolysis at 500 °C with varying holding time (1–35 minutes). It can be found that $\ln(X_{R0}) = -0.9422$ and the pyrolysis reaction constant (K_X) is 0.0165 min^{-1} .

Furthermore, because the char recovery X_R was experimentally measured at different holding times, a plot of $\ln X_R/X_{R0}$ vs sand loading S_L can then be plotted in Figure 6.5B according to Equation (6.12). It can be seen that the initial sand loading S_{L0} is the intercept value (i.e., 1.461) and the slope of the line is the reaction constant K value (i.e., $1.293 \text{ g}_{\text{sand}}/\text{g}_{\text{biomass (db)}}$).

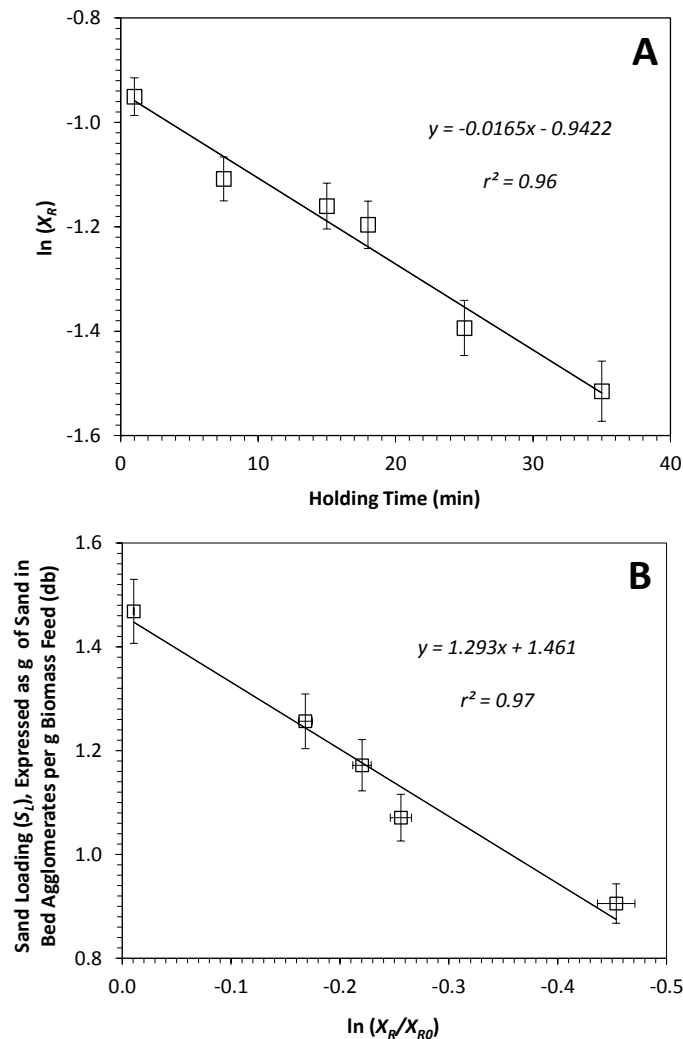


Figure 6.5 Plots of (A) $\ln(X_R)$ vs holding time (t_h) and (B) Sand load (S_L) vs $\ln(X_R/X_{R0})$ for biomass pyrolysis at 500 °C after the completion of 6 minutes feeding and various holding time (1–15 minutes)

Considering the values of K_X (0.0165 min^{-1} , see Figure 6.5A) and K_S ($0.022 \text{ g}_{\text{sand}}/\text{g}_{\text{biomass (db)}} \text{ per minute}$, see Figure 6.3), the reaction constant K is calculated to be $1.33 \text{ g}_{\text{sand}}/\text{g}_{\text{biomass (db)}}$, very close to the value of $1.293 \text{ g}_{\text{sand}}/\text{g}_{\text{biomass (db)}}$ determined experimentally in Figure 6.5B. In addition, the values of initial sand loading S_{L0} are also very close, being 1.471 (estimated in Figure 6.3) or 1.461 (estimated in Figure 6.5B) $\text{g}_{\text{sand}}/\text{g}_{\text{biomass (db)}}$, respectively. Therefore, for bed agglomeration, the sand is interacting with the pyrolysing biomass particles not in a random fashion but is indeed dependent on pyrolysis reactions occurring. This hypothesis is also verified

in the derivation of Equation (6.8) above where it was found that the sand that interacted with the biomass feed is dependent on the pyrolysis reactions occurring in the reactor.

6.4.3 Kinetics of bed agglomeration during biomass pyrolysis with continuous feeding

Section 6.4.2 shows that after the formation of bed agglomerates in the bed upon the completion of feeding, bed agglomeration follows a zero-order reaction during the continuous holding at the pyrolysis temperature. The “active sites” present in the binding agent as part of bed agglomerates diminish due to further pyrolysis reaction of the organic matter, resulting in a reduction in sand loading S_L and also bed agglomeration. However, the scenario is different to the case for bed agglomeration as a function of continuous feeding. As biomass is continuously fed into the fluidized-bed reactor, the sticky agent is being continuously generated from the biomass pyrolysis reactions occurring. As feeding time increases, the accumulated biomass fed into the fluidized-bed increases also.

The variable “biomass feed to sand ratio” (R) can then be derived at various feeding times as the ratio between the total accumulated mass of biomass (db) fed into the reactor and the total mass of sand in the fluidized-bed. The value of R varies from 1.5 to 25 wt. % under the conditions of the experiments in this study, corresponding to 0.5–17 minutes of continuous feeding, followed up with a constant 15 minute holding time in all experiments. Figure 6.6 presents the data on char recovery X_R as a function of biomass feed to sand bed ratio R .

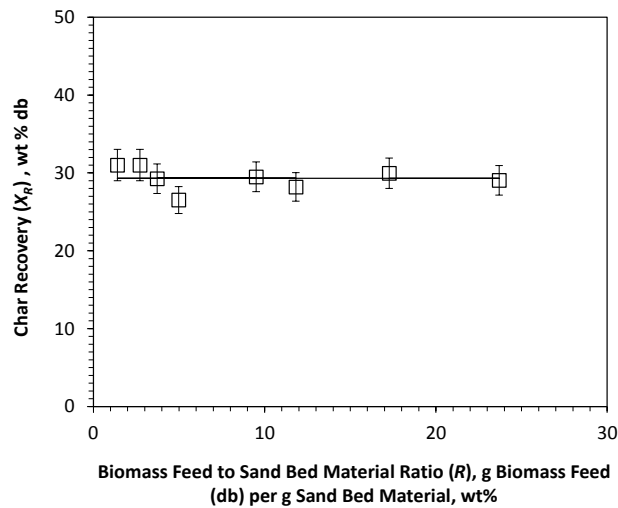


Figure 6.6 Char recovery (X_R) as a function of biomass feed to sand ratio (R), due to continuous feeding of biomass into the fluidized-bed reactor (R is between 1.5 and 25 wt. %) during fast pyrolysis

The data shows that the char recovery is independent of R as X_R remains constant over the range of R under the experimental conditions in this study. This suggests that upon continuous feeding, there is similar amount of char (relative to the amount of biomass feed) contributing to the formation of bed agglomerates. Figure 6.7 further presents the fraction of sand contained within the bed agglomerates as a function of biomass feed to sand bed ratio R .

The data shows that as the feeding of biomass continues (i.e., R increases), the fraction of sand in bed agglomerates continues to decrease up to $R = \sim 12$ wt. %, after which the sand fraction in bed agglomerates becomes relatively constant. A similar trend has been observed in Figure 6.8 for sand loading S_L as a function of R during continuous feeding.

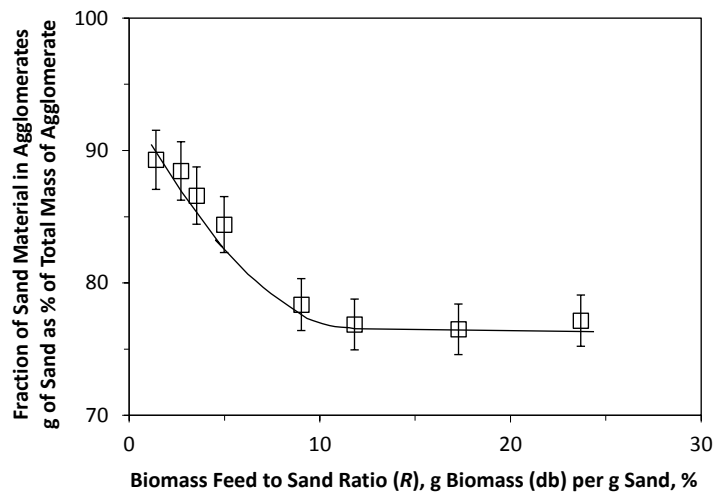


Figure 6.7 Fraction of sand in bed agglomerate as a function of biomass feed to sand ratio R , due to continuous feeding of biomass into the fluidized-bed reactor (R is between 1.5 and 25 wt. %) during fast pyrolysis

However, it is noted that the trend of S_L as a function of R is different to that of bed agglomeration yield Y_{AP} ,²²⁰ used in chapter 4 and 5 above, which is calculated based on the mass of bed agglomerates as percentage of the total mass of the bed sample.

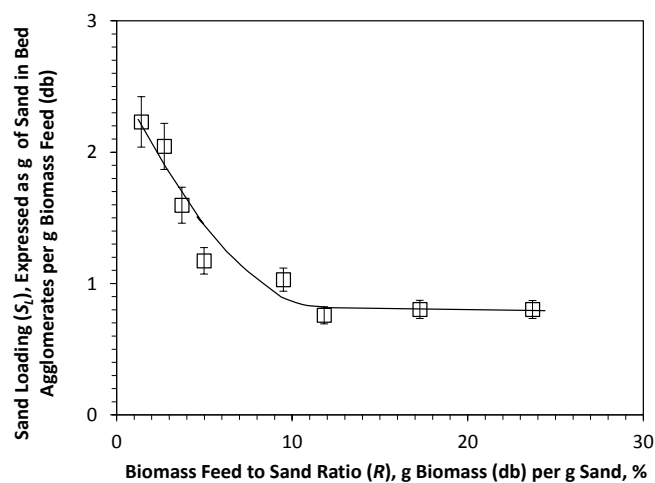


Figure 6.8 Sand loading S_L as a function of biomass feed to sand ratio R , due to continuous feeding of biomass into the fluidized-bed reactor (R is between 1.5 and 25 wt. %) during fast pyrolysis

As shown in Figure 6.9, Y_{AP} almost increases linearly with R . As biomass feeding continues, there is continuous decrease in the sand fraction in bed agglomerates and sand loading, suggesting that the sticky agent produced from biomass pyrolysis becomes more favourably to form char-char bonding, instead of char-sand bonding that increases S_L . The bed agglomerates formed at $R > \approx 12$ wt. % has a constant S_L , most likely due to the large bed agglomerates sinking to the bottom of the bed at a constant sand loading. Clearly, S_L is a more powerful diagnostic parameter for quantifying the actual interactions between sand and the pyrolysing biomass particles in the fluidized-bed than the previously used (chapters 4 and 5) bed agglomeration yield Y_{AP} .

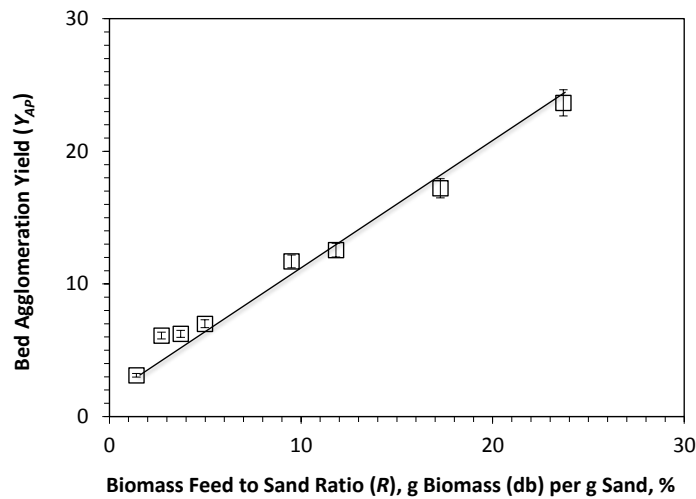


Figure 6.9 Bed agglomeration yield Y_{AP} as a function of biomass feed to sand ratio R , due to continuous feeding of biomass into the fluidized-bed reactor (R is between 1.5 and 25 Wt. %) during fast pyrolysis

If there is a relationship between the sand loading and the actual biomass feed ratio R , it may be mathematically represented as

$$S_L = K_R R^n \quad (6.13)$$

Taking natural logs of Equation (6.13), we have

$$\ln(S_L) = \ln K_R + n \ln(R) \quad (6.14)$$

Based on Equation (6.14), the relationship between $\ln(S_L)$ and $\ln(R)$ can then be plotted based on the experimental data, as shown in Figure 6.10. Indeed, $\ln(S_L)$ vs $\ln(R)$ yields a straight line in the figure. The data in Figure 6.10 shows that the slope of the line is -0.5 and the intercept is -1.24. It is noted that the slope of the line in Figure 6.10 yields the overall reaction order n and the intercept of the graph yields $\ln(K_R)$ from which the global reaction constant K_R can then be derived. Therefore, the interaction between sand and the pyrolysing biomass particles (upon continuous feeding) within the reactor seems to be in a negative order of 0.5. The negative order indicates that the concentration (indicated by the biomass feed to fluidized-bed mass ratio, R) inversely affects the sand loading (S_L) as the higher the concentration of the biomass feed to the fluidized-bed mass, the more the biomass feed will interact with itself to form char-char bonding rather than the actual sand bed material to form the char-sand bonding as indicated in Figures 6.7 and 6.8.

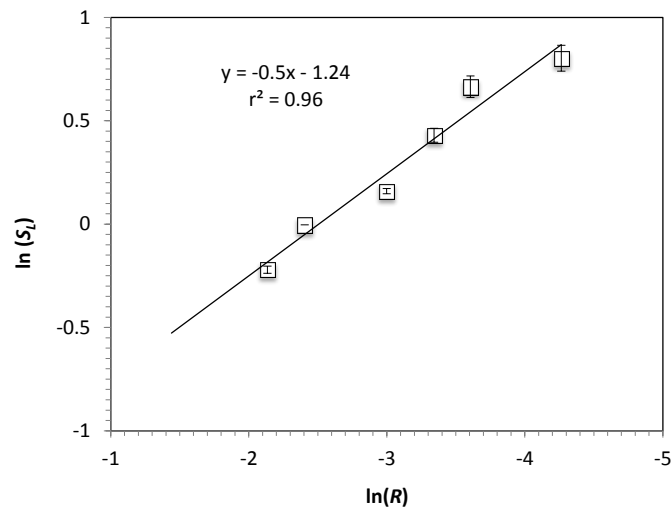


Figure 6.10 Relationship between $\ln(S_L)$ and $\ln(R)$, due to continuous feeding of biomass into the fluidized-bed reactor (R is between 1.5 and 25 wt%) during fast pyrolysis

It is also noted that the experiments performed at continuous feeding were done at a constant holding of 15 minutes after the completion of different feeding periods; the reaction order includes a constant holding time (i.e., $t_h = 15$ minute) and does not represent the actual order of reaction when there is no holding time (i.e., $t_h = 0$).

Therefore, the initial sand loading (S_{L0}) for each of the conditions tested can be back-calculated using Equation (6.12) with the calculated K value of 0.022 and with a constant holding time of 15 minutes. It is plausible to assume that the sand loading follows a zero-order reaction rate and the sand loading decreases in proportion to the holding time (as indicated by Figure 6.3). Figure 6.11 presents a plot of the back-calculated S_{L0} as a function of biomass feed to sand bed mass ratio R . A fitted curve in the figure shows that the overall global reaction for the interaction between sand and pyrolysing biomass particles during continuous feeding is -0.4 and the reaction constant K_R is 0.5.

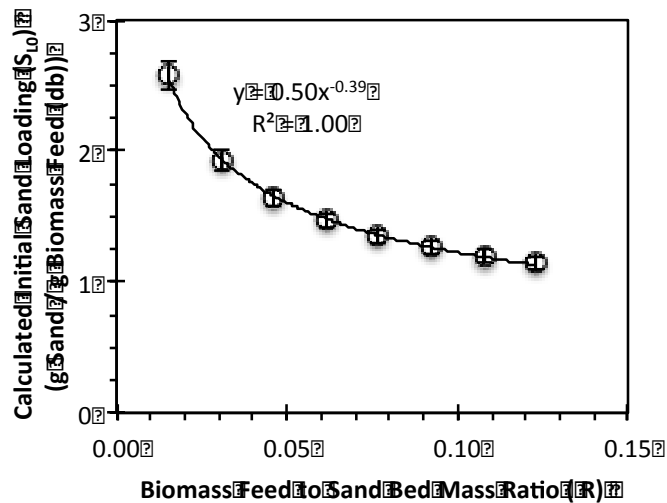


Figure 6.11 Back-calculated S_{L0} as a function of biomass feed to sand bed ratio R , due to continuous feeding of biomass into the fluidized-bed reactor (R is between 1.5 and 25 Wt%) during fast pyrolysis

At a given feeding rate (F) and feeding time (t_f), the biomass feed to sand bed ratio R can be mathematically expressed as

$$R = Ft_f / M_{S0} \quad (6.15)$$

Substituting Equation (6.15) and the values found from Figure 6.11 for S_{L0} into Equation (6.9) then the overall sand loading can be modelled in terms of feed rate (F), initial mass of the fluidized-bed (M_{S0}), feeding time (t_f) and holding time (t_h), using Equation (6.16) below.

$$S_L = K_R \cdot (Ft_f / M_{S0})^{-0.4} - K_S t_h \quad (6.16)$$

From the above results Equation (6.16) has an applicable range from $R = 0$ to $R = 12.5$ wt. % and for a particle diameter of 355–500 μm . Sand loading as a variable can be used in any situation in which there is agglomeration taking place during

pyrolysis or before combustion occurs, this being due to its definition being the amount of biomass that directly interacts with the fluidized-bed sand material.

6.5 Conclusions

This chapter introduced the diagnosis parameter sand loading (S_L) for examining the direct interaction of sand bed material with thermally thin (Biot number <0.1) pyrolysing biomass particles to form bed agglomerates during fast pyrolysis in a fluidized-bed reactor. The results and analysis in this chapter showed that bed agglomeration is not merely a random phenomenon but is dependent on biomass pyrolysis reactions and hence the pyrolysis conditions. During continuous feeding of biomass into the reactor, the correlation of S_L shows that the sand interacts with incoming biomass feed in a negative order of 0.4. At feed fractions below <12 wt. % of the bed mass, bed agglomeration is mainly driven by sand-char bonding, but char-char bonding becomes more important at higher feed fractions. Upon the completion of biomass feeding, the sand particles interact with the pyrolysing biomass particles accumulated in the bed in a zero-order reaction kinetic, which is only dependent on the holding time (t_h). Therefore, during holding, no new sand particles are connecting to the char particles in the bed material but are breaking off, thus reducing the sand loading (S_L).

CHAPTER 7 DIAGNOSIS OF BED AGGLOMERATION DURING BIOMASS PYROLYSIS IN FLUIDIZED- BED AT A WIDE RANGE OF TEMPERATURES

7.1 Introduction

The main focus of this chapter is to apply sand loading S_L to the diagnosis of bed agglomeration during biomass pyrolysis in fluidized-bed at a wide range of temperatures (200–700 °C).

7.2 Experimental method

The material used for the experimentation outlined in this chapter was ethanol washed, ethanol extract and raw leaf biomass. The size distribution used for the solid biomass was 355–500 μm . This size distribution was selected to ensure that the Biot number is <0.1 , under which conditions the effect of the intra-particle heat transfer can be ignored.^{169, 217-219} The biomass components underwent fast pyrolysis as detailed in chapter 3 above, where the pyrolysis temperature was varied from 300 to 700 °C, the mass of the biomass fed to the reactor (1.95–2 g or equivalent in the case of ethanol extract material), holding time (15 minutes), fluidized-bed mass (19.5–20 g) and sand bed material particle distribution (125–250 μm) were kept constant. Samples before and after pyrolysis were subjected to analysis, the analysis performed is noted where and when required, and procedures used in the analysis are outlined in chapter 3.

7.3 Results and discussion

7.3.1 Sand loading during biomass fast pyrolysis at a wide range of temperatures

Figure 7.1 presents sand loading as a function of pyrolysis temperature (200–700 °C) for the fast pyrolysis of raw biomass, ethanol-washed biomass and extract samples. For direct comparison, the values of sand loading for the pyrolysis of the ethanol-extracted biomass and extract samples have been back-calculated to be on the basis of the equivalent amount of raw biomass.

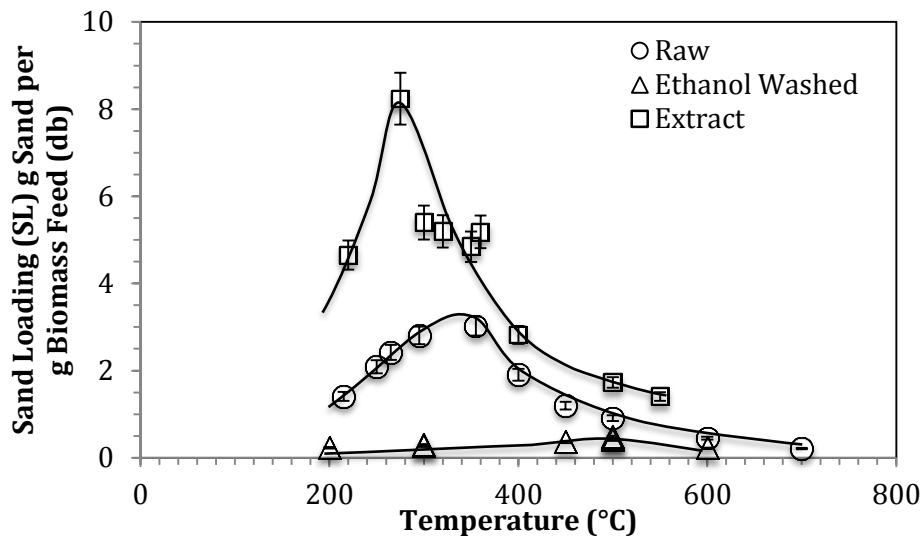


Figure 7.1 Sand loading as function of temperature for bed agglomeration during the fast pyrolysis of the raw biomass, extract and ethanol-washed biomass samples at different temperatures (200–700 °C)

There are several important observations from this figure. Firstly, it can be seen that over the wide temperature range (200–700 °C), the pyrolysis of the extract sample leads to the highest sand loading, followed by the raw biomass, then the ethanol-washed biomass. This is consistent with the data previously report on bed agglomeration during biomass fast pyrolysis at 500 °C²²⁵ in chapter 6 above. In addition, the data in Figure 7.1 clearly suggests that bed agglomeration during the

pyrolysis of the raw biomass is not just a simple addition of those of the two separated biomass components (ethanol-washed biomass and extract). Clearly, there are synergies between the two biomass components during raw biomass pyrolysis. The large sand loading values obtained from the pyrolysis of the extract are due to the fact that when it is injected alone there is no hindrance from the resulting biomass char or particle matrix.

Secondly, the sand loading increases with increasing temperature initially, reaches a maximum, then decreases with further increasing temperature. It is noted that sand loading is an indicator for ability of “active sites” (for forming bed agglomeration) with the sticky agent that is produced by biomass pyrolysis. At a given temperature, the production of sticky agents (therein the active sites) is the net result from the competition between sticky-agent-generating reactions (such as depolymerisation) that generate the sticky agents (therein the active sites) and sticky-agent-eliminating reactions (such as carbonisation) that eliminate the sticky agents (therein the active sites). At low temperatures, the sticky-agent-generating reactions (e.g., depolymerisation) are more important so that an increasing temperature leads to the production of more sticky agents (therein active sites) for bed agglomeration, resulting in an increase in the sand loading. At high temperatures, sticky-agent-eliminating reactions (e.g., carbonisation) are dominant so that an increasing temperature leads to the diminishing of sticky agents, resulting in a reduction in sand loading, at high pyrolysis temperatures. This suggests that either the amount of such “active sites” formed becomes less and/or the quality of “active sites” becomes less sticky as a result of intensive carbonisation reactions of samples (therein the sticky agents). However, it is interesting to note that the temperatures, at which the

maximum values of sand loading values are reached, are significantly different for different samples (i.e., $\approx 250\text{--}280$ °C for the extract sample, $\approx 310\text{--}350$ °C for the raw biomass sample and $\approx 490\text{--}510$ °C for the ethanol-washed biomass sample). It is clear that the raw biomass, ethanol-washed biomass and extract samples experience significantly different pyrolysis reactions in producing/eliminating the sticky agents that are responsible for bed agglomeration. The data in Figure 7.2 further confirms that the presence of extract in the sample has a significant effect on bed agglomeration, hence sand loading, and suggests that there may be synergies among different biomass components during raw biomass pyrolysis.

7.3.2 Determination of activation energy (E_a) of the sand loading (S_L) during biomass fast pyrolysis

During biomass fast pyrolysis in a fluidized-bed reactor at 500 °C pertinent to bio-oil production (as previously reported in chapter 6), sand loading (S_L) follows a zero-order rate equation with respect to the holding time (t_h) as $S_L = S_{L0} - K_S t_h$. At a constant holding time (t_h), sand loading (S_L) is a function of the amount of biomass continuously fed into the reactor and can be mathematically represented as $S_L = KR^{-0.5}$. Here, R is the biomass feed to sand ratio (i.e., the mass ratio of the biomass feed (db) to the total mass of biomass and sand in reactor) while K is the reaction constant ($g_{\text{sand}}/g_{\text{biomass (db)}}$). Therefore, for biomass fast pyrolysis at a wide range of temperatures, the reaction constant K can be considered to follow an Arrhenius equation that can be mathematically represented as

$$K = A_k \text{EXP} \left(\frac{E_a}{R_g T} \right) \quad (7.1)$$

where A_k is the frequency factor, E_a is the activation energy, R_g is the universal gas constant and T is the bed temperature in Kelvin.

In Equation 7.1, A_k is a function of both the total number and the alignment or orientation of collisions (i.e., sand and pyrolysing biomass particles in the reactor coming in contact) to form bed agglomerates (indicated by measured S_L). The orientation and the alignment determine if the surface of the particle has sufficient “sticky agent” to produce the sand-char or char-char bonding agglomerates (as previously observed in Chapters 4–6^{206, 211, 212}). The activation energy E_a can be considered as the minimum energy required for the particles to form “sticky agent”. Therefore, the fraction of particles containing the amount of energy required for the reaction is approximated by the term $EXP\left(\frac{E_a}{R_g T}\right)$.

Substituting Equation (7.1) into the generic sand loading equation developed in chapter 6 ($S_L = KR^{-0.5}$) and rearranging the equation, the relationship between sand loading and temperature is derived as

$$S_L/R^{-0.5} = A_k EXP\left(\frac{E_a}{R_g T}\right).$$

Taking natural log yields Equation (7.2)

$$\ln(S_L/R^{-0.5}) = \ln A_k - \left(\frac{E_a}{R_g}\right) \frac{1}{T} \quad (7.2)$$

Equation (7.2) suggests that when plotting $\ln(S_L/R^{-0.5})$ as a function of $1/T$, the slope of the line should represent $-E_a/R_g$ and the intercept should be $\ln A_k$. As shown in Figure 7.2, the plots of $\ln(S_L/R^{-0.5})$ vs $1/T$ are indeed linear for the raw biomass (panel A), ethanol-washed biomass (panel B) and extract (panel C) samples over the temperature range investigated. The reactions leading to bed agglomeration are initially endothermic then become exothermic at the high temperatures. Such observation is consistent with the results presented in Figure 7.1 where during the endothermic reaction, energy is absorbed from the system to produce the sticky agent.

During the exothermic reaction, the “sticky agent” is either being consumed (reduction in the amount of the “sticky agent” available for interaction) or carbonised (reduction in the “stickiness” of the agent).

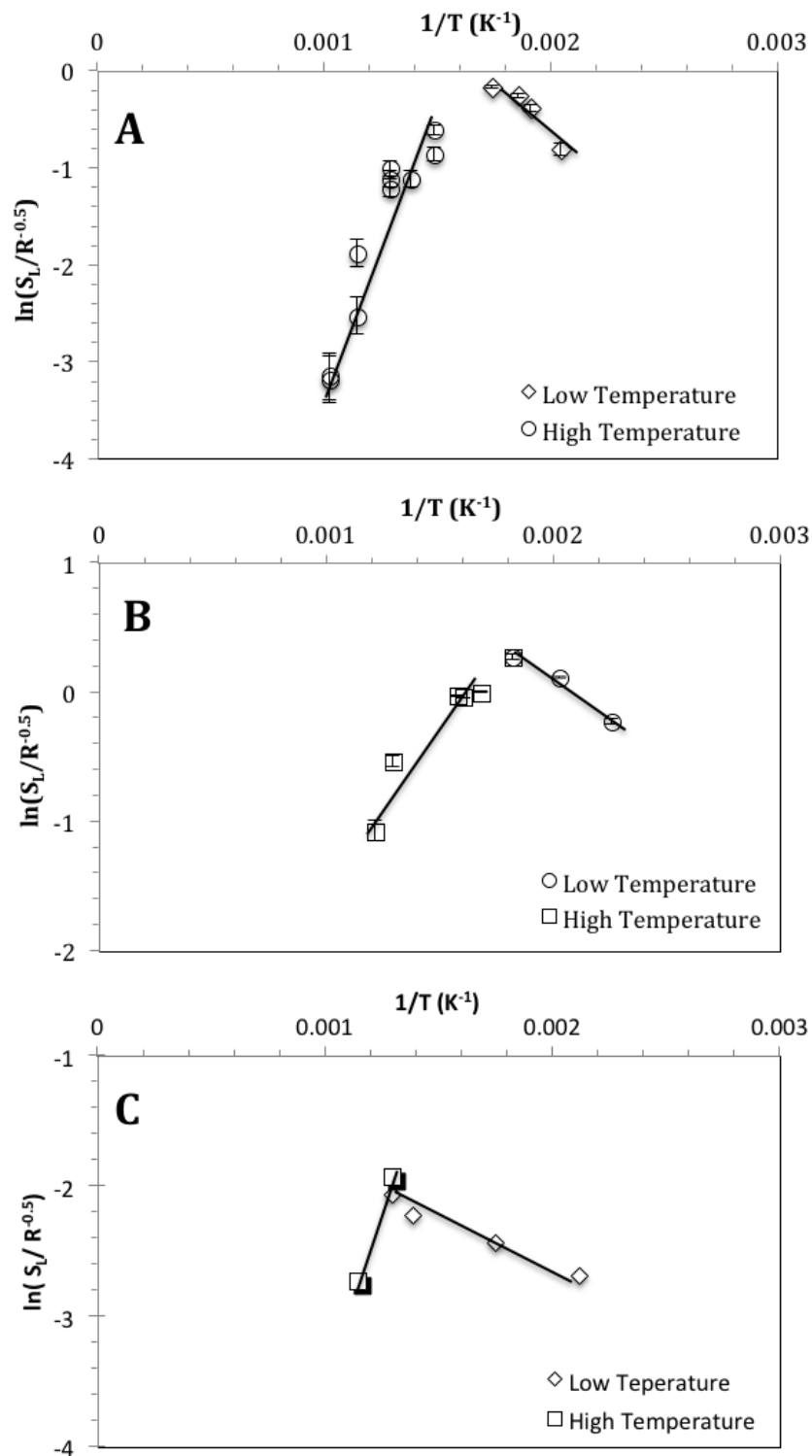


Figure 7.2 $\ln(S_L/R^{0.5})$ as a function of $1/T$ for bed agglomeration during the fast pyrolysis of the raw biomass (A), extract (B) and the ethanol-washed biomass (C) samples at 200–700 °C

Table 7.1 lists the results obtained from Figure 7.2 for the activation energies (E_a) and frequency factors (A_k). Both the activation energy and the frequency factor give insights into the bed agglomerations among pyrolysing biomass particles and sand particles.

Table 7.1 Activation energies (E_a) and frequency factor (A_k) determined based on sand loading (S_L) for bed agglomeration during the fast pyrolysis of the raw biomass, ethanol-extracted biomass and extract samples at 200–700 °C

Sample	Temperature °C	Slope E_a/R_g	Intercept $\ln A_k$	Activation energy (E_a), kJ mole ⁻¹	Pre-exponential factor (A_k), min ⁻¹
Raw biomass	200–310	-3314	5.8	27.6	3.4E+02
Raw biomass	350–600	5362	-8.4	-44.6	2.2E-04
Ethanol-washed biomass	200–500	-781	-1.0	6.5	3.6E-01
Ethanol-washed biomass	500–600	5390	-8.9	-44.8	1.4E-04
Extract	200–275	-1651	3.4	13.7	3.0E+01
Extract	275–600	1994	-3.3	-16.6	3.7E-02

The activation energies (E_a) at low temperatures are positive (endothermic), varying from 27.6 kJ mole⁻¹ for the raw biomass, to 13.7 kJ mole⁻¹ for the extract sample and then to 6.5 kJ mole⁻¹ for the ethanol-washed biomass. Removing the extract from the raw biomass leads to a drastic reduction in the activation energy (from 27.6 to 6.5 kJ mole⁻¹). Although activation energy for the ethanol-washed biomass is lower than that for the raw biomass, the actual sand loading values obtained for the ethanol-washed is far lower than that for the raw biomass, due to the considerably

lower frequency factor for the ethanol-washed biomass ($3.6\text{E}-01$) in comparison to that for the raw biomass ($3.4\text{E}+02$).

Furthermore, the activation energy (13.7 kJ mole^{-1}) for sand loading during the pyrolysis of the extract sample is lower than that during the pyrolysis of the raw biomass (27.6 kJ mole^{-1}). However, the frequency factor for sand loading during the pyrolysis of the extract sample ($3.0\text{E}+01$) is lower than that during the pyrolysis of the raw biomass sample ($3.4\text{E}+02$) by one order of magnitude. Figure 7.3 presents the mass of bed agglomeration normalised to the equivalent amount of biomass fed into to the reactor during the pyrolysis of extract and raw biomass at 170 to 275 °C during the build-up phase of the sand loading values.

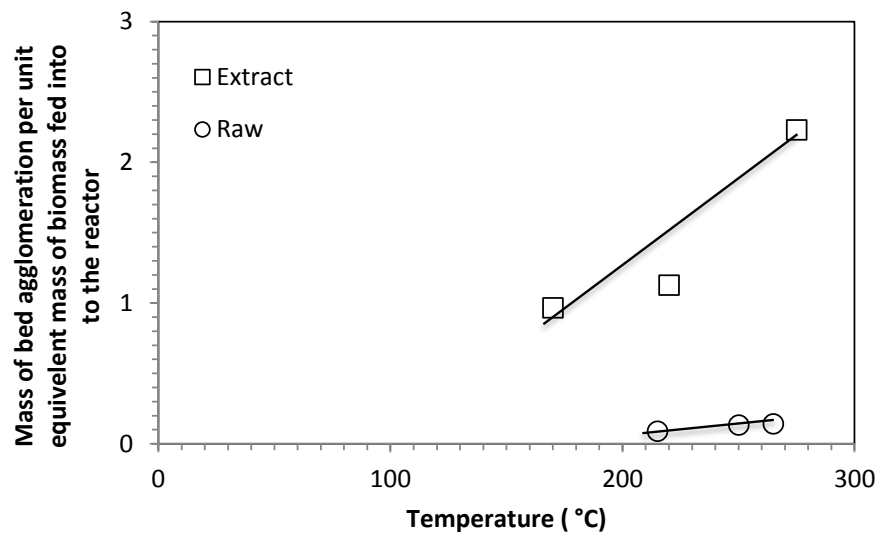


Figure 7.3 Mass of bed agglomeration per unit equivalent mass of biomass fed into the reactor during the fast pyrolysis of the raw biomass and extract samples at 170–275 °C during the build-up phase of the sand loading showing relative slopes

It can be seen from figure 7.3, that the relative difference in the sand interaction (ratio of slopes) during the pyrolysis of the extract sample is higher than that during the pyrolysis of the raw biomass sample by one order of magnitude. The results

suggest that the pyrolysing extract picks up large amounts of the sand particles from the bed material, leading to a reduction in the collisions available for the fresh incoming feed material to interact with. These are in consistence with the observation made in chapter 5 above, that the extracts are primarily responsible for sand loading and there is a substantial interaction between the extract and the nascent char/biomass particles during pyrolysis. Sand loading (S_L) is strongly dependent on the content of extracts in biomass, for example, fast pyrolysis of wood leads to little bed agglomeration (observed in chapter 5 above) because the content of extracts in wood is low (<3%).

7.3.3 Overall equation of sand loading (SL) for bed agglomeration during biomass pyrolysis at a wide range of temperatures

Under continuous feeding conditions, sand loading is a function of biomass feed to sand ratio (R) and the holding time (t_h) in the form of $S_L = K_R R^{-0.4} + K_S t_h$ as indicated in chapter 6 above. Considering $S_L = KR^{-0.5}$ and a holding time of 15 minutes in the experiments, the overall sand loading can be calculated as

$$KR^{-0.5} = K_R R^{-0.4} + 15K_S \quad (7.3)$$

Equation (7.3) indicates that the ratios of K_R/K_S and K/K_S must be constant due to the fact that the biomass feed to sand ratio R remains constant during sample holding in the reactor at the pyrolysis temperature. From chapter 6 above the values of K , K_R and K_S for biomass leaf fast pyrolysis at 500 °C are $K_R/K_S = 0.5/0.022$ and that for $K/K_S = 0.29/0.022$. These ratios can then be used to back-calculate the corresponding K_S and K_R at the reaction temperatures. The activation energy and pre-exponential constants can also be found using Equation (7.2).

Figure 7.4 presents the plot of the natural logs of the back-calculated K_R and K_S as a function of inverse temperature ($1/T$) for the raw biomass leaf. The activation energy and the pre-exponential factor can also be determined. It is interesting to note that the activation energy is similar to that determined from the data presented in Figure 7.2.

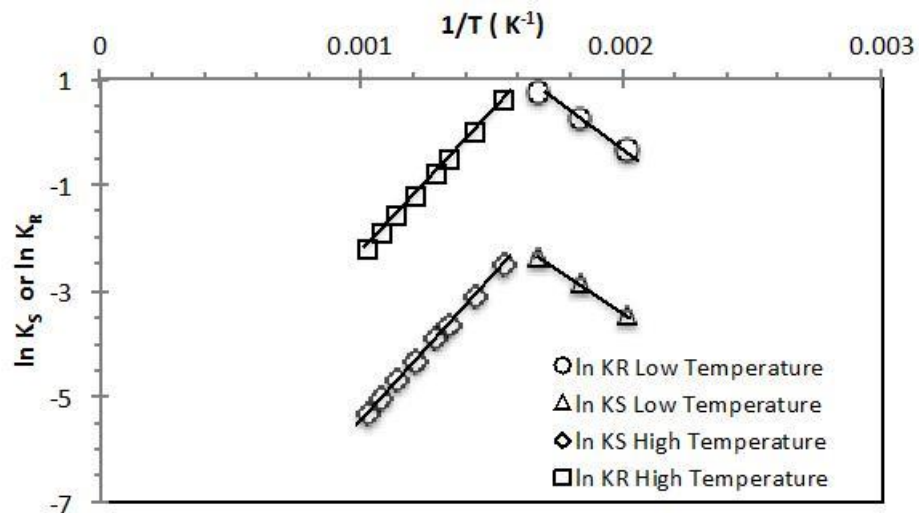


Figure 7.4 $\ln K_R$ or $\ln K_S$ as a function of $1/T$ for bed agglomeration during fast pyrolysis at 200–600 °C

This is expected because it is the same reactions that govern bed agglomeration and result in sand loading. The results presented in Figure 7.4 clearly confirm that sand loading is not a random event in the fluidized-bed reactor but a direct consequence of the reactions occurring during pyrolysis.

The activation energy and the frequency factor determined based on the data in Figure 7.4 can then be used to calculate the overall sand loading for the pyrolysing raw leaf biomass as a function of holding time t_h and biomass feed to sand ratio R for the two temperature ranges, as Equation (7.4a) for 200–310 °C and Equation (7.4b) for 350–700 °C below

$$S_L = 601EXP\left(\frac{-3300}{T}\right)R^{-0.4} - 24.5EXP\left(\frac{-3300}{T}\right)t_h \quad (7.4a)$$

$$S_L = 0.00045EXP\left(\frac{5300}{T}\right)R^{-0.4} - 0.00002EXP\left(\frac{5300}{T}\right)t_h \quad (7.4b)$$

where the biomass feed to sand ratio R is related to biomass feed rate (F), feeding time (t_f) and initial sand bed mass (M_{S0}) as $R = \frac{Ft_f}{M_{S0}}$. This would suggest that the sand loading is an actual product of the biomass pyrolysis reactions occurring and its modelling may be taken into account in the overall model of biomass pyrolysis in a fluidized-bed reactor. As shown in Figure 7.5, the model predictions are broadly in good agreement with the experimental data, except at the turning point around 310 °C, this could be due to the fact that the reactions within this region are turning from endothermic (27.6 kJ mole⁻¹) to exothermic (-44.6 kJ mole⁻¹) in nature.

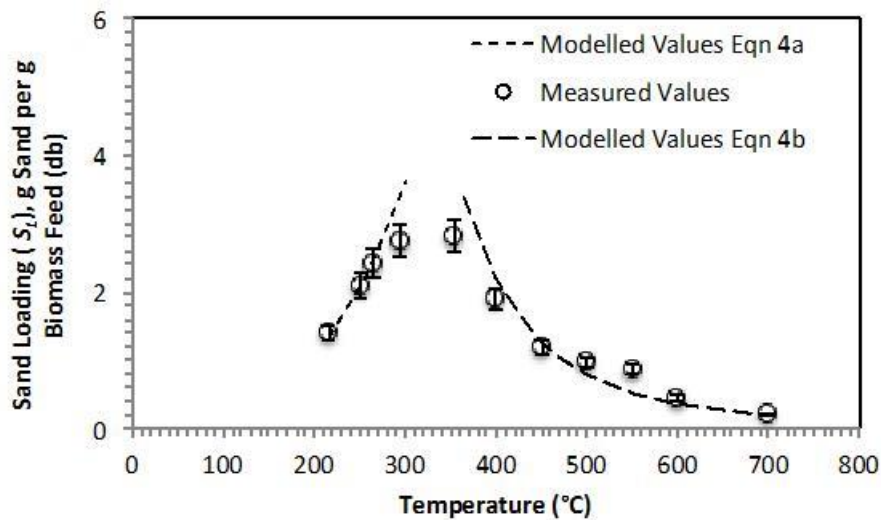


Figure 7.5 Modelled sand loading for bed agglomeration during the fast pyrolysis of the raw biomass in a fluidized-bed reactor at different temperatures 200 – 700 °C

This would suggest that there is a very large interaction between the sticky agent produced and the char matrix during pyrolysis in this temperature region (310 to 350 °C), which could likely be attributed to the formation of complex intermediates,

which firstly increase the sand loading dramatically then decrease it as the temperature reaches 350 °C.

7.4 Conclusions

Sand loading as a powerful analysis tool is successfully applied for the diagnosis of the interactions between the pyrolysing biomass particles and sand material to form bed agglomeration during fast pyrolysis of biomass feedstock at 200–700 °C. The reaction between the raw leaf biomass particles undergoing pyrolysis and the sand bed material is endothermic (27.6 kJ mole⁻¹) at low temperatures (200–310 °C) and the sand loading increases from 0.2 to 4 g_{sand}/g_{biomass (db)}. At high temperatures (350–700 °C), the reaction turns to exothermic (-44.6 kJ mole⁻¹) and the sand loading value decreases from 4 to below 0.23 g_{sand}/g_{biomass (db)} at 700 °C. The results further confirm that the extracts in biomass are responsible for bed agglomeration, hence sand loading, as the removal of extracts from the raw biomass leads to a drastic reduction in sand loading from a peak of 8.24 g_{sand}/g_{biomass (db)} at 275 °C to 0.42 g_{sand}/g_{biomass (db)} at 500 °C. The extracts interact with the biomass particles during pyrolysis to increase the activation energy from 13.7 kJ mole⁻¹ (extract only) to 27.6 kJ mole⁻¹ for the raw biomass sample.

CHAPTER 8 BED AGGLOMERATION DURING THE DRYING OF MALLEE LEAF IN FLUIDIZED-BED

8.1 Introduction

While there has been a large amount of reports on the performance and modelling of biomass drying in fluidized-bed dryers,²²⁶⁻²³³ potential bed agglomeration issues during biomass drying has not been reported and explored. Consequently, the objective of this chapter is focused on quantifying the interaction between biomass particles and sand bed particles, responsible for bed agglomeration, during the drying of mallee leaf in a fluidized-bed dryer in air or inert (argon) atmosphere at 120–250 °C.

8.2 Experimental method

The material used for the experimentation outlined in this chapter was raw leaf biomass. The size distribution used for the solid biomass was 355–500 µm. This size distribution was once again selected to ensure that the Biot number is <0.1, under which conditions the effect of the intra-particle heat transfer can be ignored.^{169, 217-219} The biomass components underwent fast drying as detailed in chapter 3 above, the drying temperature was varied from 120 to 250 °C and the mass of the biomass fed to the reactor (1.95–2 g), holding time (15 minutes), fluidized-bed mass (19.5–20 g) and sand bed material particle distribution (125–250 µm) were kept constant. The feed rate to the reactor was kept constant at ≈0.3 g per minute. The reactor before and after the drying experiment was weighted. Biomass recovery

(X_{Rb} , wt. % db) from the drying reactor was then determined as biomass recovered from the bed after drying normalized to the total mass of biomass feed on a dry basis.

8.3 Results and discussion

8.3.1 Biomass recovery after drying in fluidized-bed and evidence of bed agglomeration

Figure 8.1 is a plot of biomass recovery (X_{Rb}) as a function of drying temperature (120–250 °C) in the fluidized-bed. At drying temperatures <200 °C, the biomass recovery after drying is high, but at drying temperature >200 °C the biomass recovery decreases rapidly.

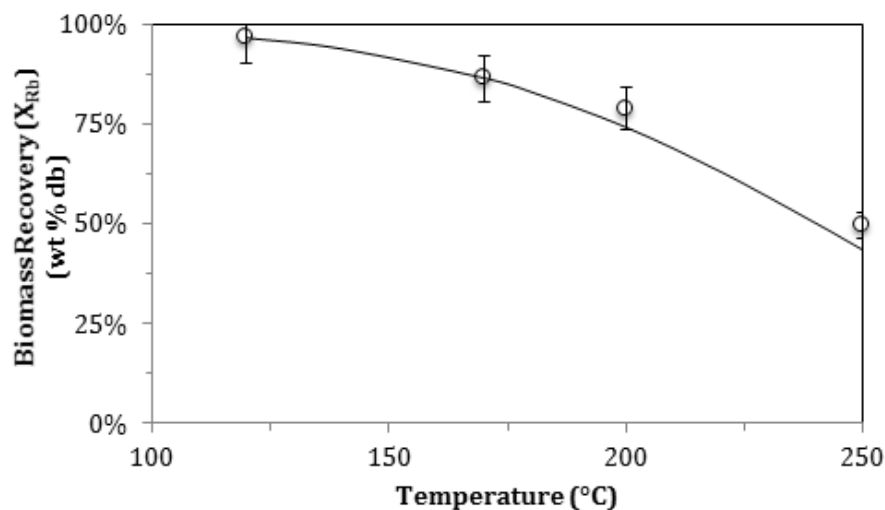


Figure 8.1 Biomass recovery (X_{Rb}) as a function of drying temperature (120–250 °C) in a fluidized-bed reactor in an air atmosphere

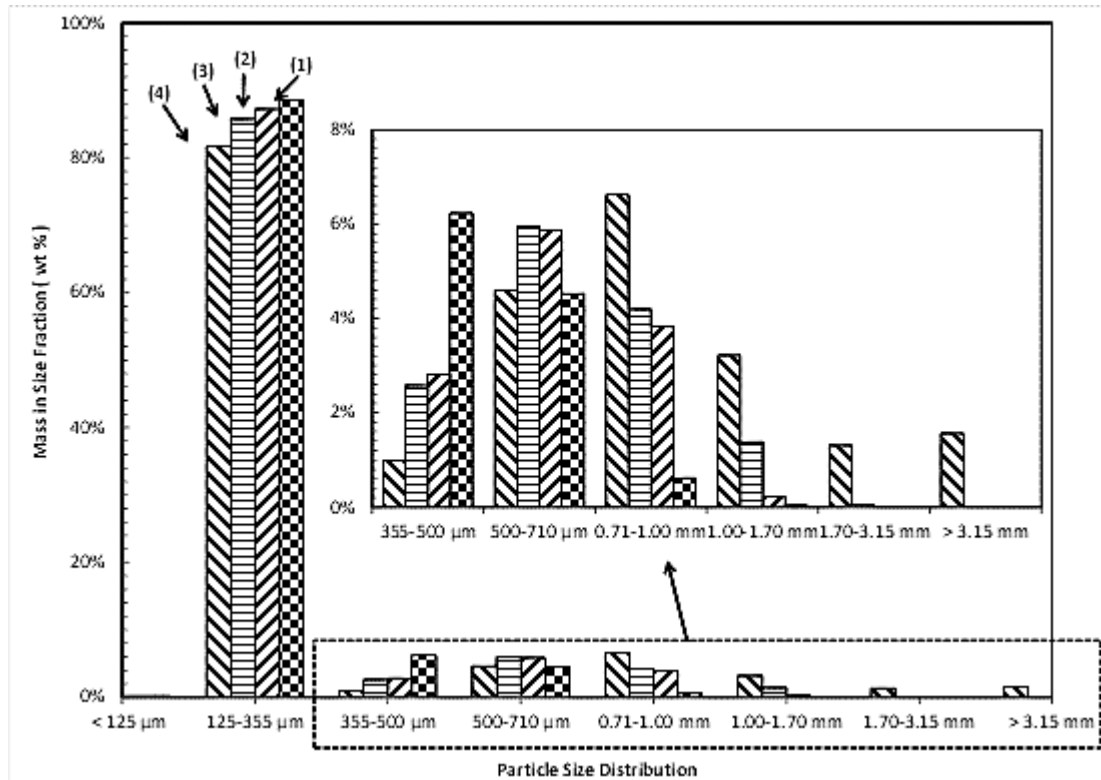


Figure 8.2 Particle size distribution results of bed samples collected after the drying of mallee leaf in a fluidized-bed reactor under air atmosphere at (1)120 °C, (2)170 °C, (3)190 °C and (4)250 °C

Therefore, upon drying in the fluidized-bed, a proportion of the biomass samples were carried out by the fluidisation gas, due to changes in the properties of biomass particles such as loss of moisture, possible attrition or effect of potential pyrolysis (at temperatures above 200 °C). The results show that the drying temperature needs to be kept below 170 °C for a biomass recovery of >90 wt. % (db).

Figure 8.2 presents the particle size distribution of bed samples collected from the drying of mallee leaf in the fluidized-bed reactor at 120–250 °C. The particle size of the original biomass fed into the fluidized-bed was 355–500 μm and that of the bed sand material was 125–250 μm so that any particles of sizes >500 μm must be bed agglomerates formed during biomass drying. This study then deploys bed agglomeration yield (Y_{AP} , wt. %), which was previously defined^{220, 234} and used in

chapters 4,5 and 6 above as the total mass of bed sample with size $>500 \mu\text{m}$ normalised to the mass of the total bed sample, for quantifying bed agglomeration. Figure 8.3 presents Y_{AP} as a function of bed temperature during the drying of mallee leaf at 120–250 °C. The results in Figures 8.2 and 8.3 clearly demonstrate that bed agglomeration does occur during the drying of mallee leaf in fluidized-bed at 120–250 °C. Furthermore, as shown in Figure 8.3, Y_{AP} increases with increasing bed temperature.

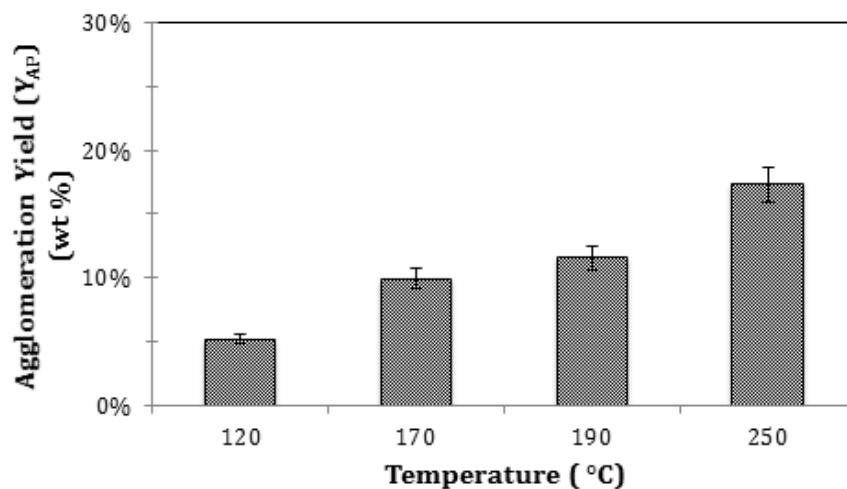


Figure 8.3 Bed agglomeration yield Y_{AP} (wt. %) as a function of drying temperature during the drying of mallee leaf in a fluidized-bed reactor at 120–250 °C in an air atmosphere

8.3.2 Nature of bed agglomerates during mallee leaf drying in fluidized-bed

The observation of bed agglomeration in Figures 8.2 and 8.3 is surprising because bed agglomeration during biomass drying in fluidized-bed was not reported previously. For bed agglomeration to take place a sticky agent would have been produced during biomass drying and such a sticky agent is responsible for the formation of bed agglomerates. Figure 8.4 further presents the typical optical

microscopy images of bed agglomerates collected after the experiment of mallee leaf drying at 170 °C.

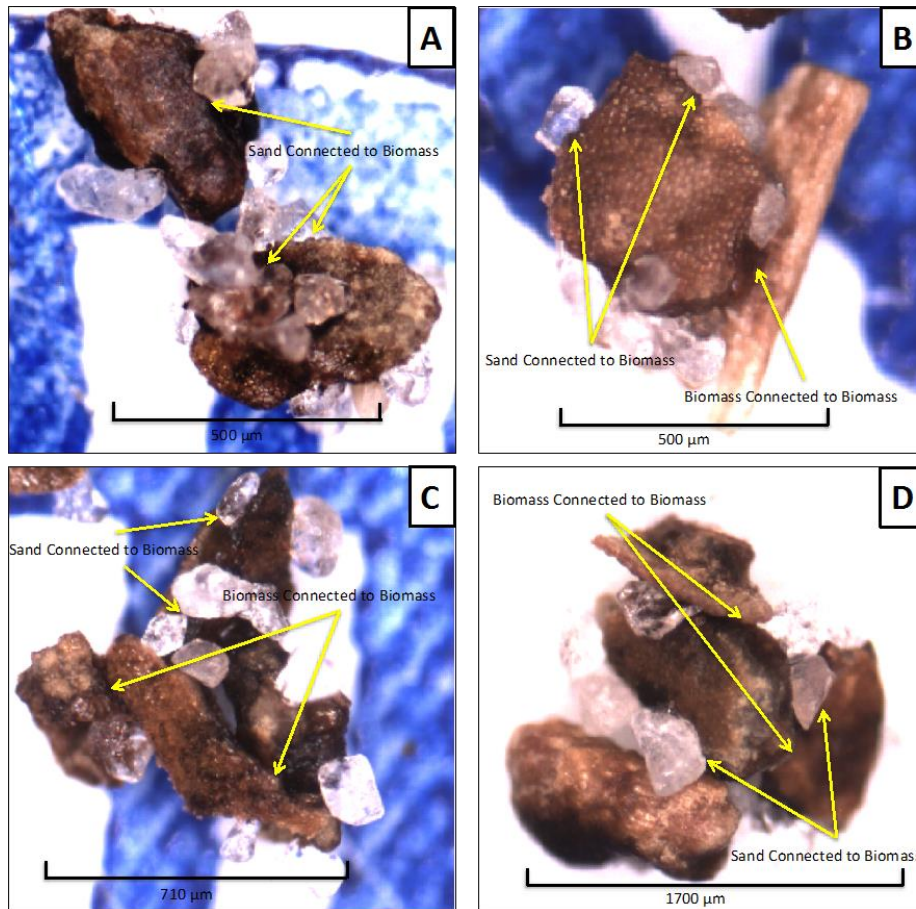


Figure 8.4 Typical optical microscope images of bed agglomerates in the bed samples collected after the drying of leaf in a fluidized-bed reactor at 170 °C under air atmosphere; panel A: bed agglomerate with sand-biomass binding of multiple particles in the size fraction of 500–710 μm; panel B: bed agglomerate with both sand-particle and biomass-biomass binding of multiple particles in the size fraction of 500–710 μm; panel C: bed agglomerate with both sand-biomass and biomass-biomass binding of multiple particles in the size fraction of 710–1000 μm; panel D: bed agglomerate with both sand-biomass and biomass-biomass binding of multiple particles in the size fraction of 1000–1700 μm

It can be seen that bed agglomeration that takes place at such low temperatures is mainly contributed by a mixture of biomass-biomass and biomass-sand bonding of multiple particles. It is noted that there are also signs of bubbling on the surface of the biomass particles and the particle surfaces also become smooth (see Figure 8.4B

and to a lesser extent Figures 8.4C and 8.4D). It appears that during the drying of mallee leaf, the sticky agents seem to be formed within the biomass particles and then diffuse to the surface of biomass particles to form a coating.

From chapter 5 above at 500 °C significant bed agglomeration takes place during the fast pyrolysis of mallee leaf (containing 18.9 wt. % extractives) but little bed agglomeration can be observed during the fast pyrolysis of mallee wood (containing 3.6 wt. % extractive), suggesting that the extractives in biomass play an important role in facilitating bed agglomeration. The results in this chapter further show that even at temperatures as low as 120 °C, sticky agent responsible for bed agglomeration can also be produced in the process of drying mallee leaf. The extractives appear also to play an important role, as bed agglomeration during the drying of mallee wood was not observed in a set of separate experiments. In addition, the data in Figure 8.3 shows that during mallee leaf drying, Y_{AP} increases with increasing bed temperature, suggesting that the production of the sticky agent responsible for bed agglomeration increases with increasing temperature.

8.3.3 Sand loading as a function of temperature during the drying of mallee leaf in fluidized-bed

Figure 8.5 presents the experimental results on sand loading (S_L) during the drying of mallee leaf in fluidized-bed at 120–250 °C in air and argon atmospheres. It can be seen that at temperatures <200 °C, the values of S_L are insensitive to atmosphere. This suggests that the mechanisms responsible for producing the sand loading (i.e., the actual interactions with the biomass and the sand, leading to bed agglomeration) are similar. Therefore, S_L and R during mallee leaf drying at temperatures <200 °C

are also likely to follow the correlation previously derived in chapter 6 for similar reaction conditions under an inert atmosphere, ($S_L = KR^{-0.5}$) for a 15 minute holding time, where K is the relational proportional constant and can be determined experimentally and R is the ratio of total biomass feed (db) to the total mass of sand in the bed.

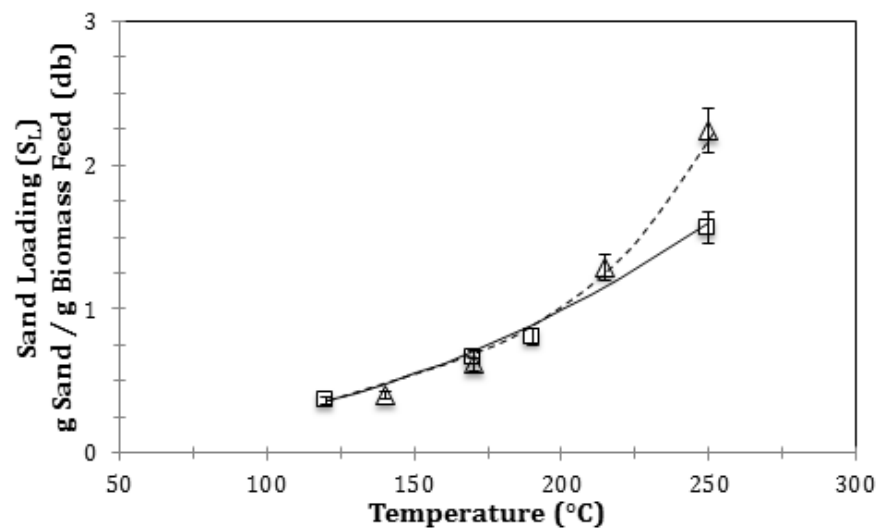


Figure 8.5 Modelled and measured sand loading values for raw leaf undergoing drying in an inert (argon) and air atmosphere in a fluidized-bed reactor at 120–250 °C. Legend: (Δ) measured values for biomass drying in inert atmosphere; (□) measured values for leaf drying in air atmosphere; (dash curve) modelled values for biomass drying in inert atmosphere; and (solid curve) modelled values for biomass drying in air atmosphere.

Indeed, as shown in Figure 8.6, the plot of the natural log of ($S_L/R^{-0.5}$) against inverse temperature ($1/T$) is a straight line. The activation energies, which can then be derived from Figure 8.6 and are presented in Table 8.1, are 19.3 and 29.3 kJ mole⁻¹ for bed agglomeration at 120 to 250 °C, under air and argon atmosphere, respectively.

Table 8.1 Activation energies (E_a) and pre-exponential constants (A_k) for bed agglomeration during mallee leaf drying in fluidized-bed at 120–250 °C under air and argon atmosphere

Temperature	Atmosphere	Slope E_a/R_g	Intercept $\ln A_k$	Activation Energy (E_a) , kJ mole ⁻¹	Pre-Exponential Factor (A_k), min ⁻¹
120–250 °C	air	-2368	3.82	19.7 ± 1.3	46 ± 3
120–250 °C	inert, argon	-3528	6.34	29.3 ± 2.4	570 ± 37

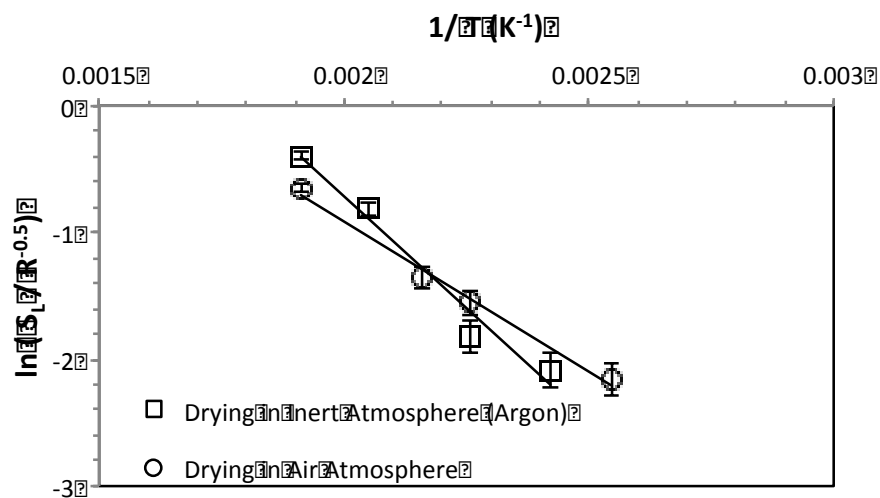


Figure 8.6 Plot of $\ln(S_f/R^{-0.5})$ as a function of $1/T$ during leaf drying in a fluidized-bed reactor at 120–250 °C under inert atmosphere (argon) and air atmosphere

In reaction engineering,²³⁵ activation energy (E_a) and pre-exponential factor (A_k) represent the energy and collisions required to form “intermediate complexes”, respectively. In this case, such “intermediate complexes” are bed agglomeration or the sand-biomass and biomass-biomass bonding. Activation energy E_a can be considered as the energy required to form sticky agents responsible for bed agglomeration while A_k is a measure of the collisions that result in the correct alignment (steric or having sufficient “sticky agent” or a good degree of “stickiness”

within the “sticky agent” available for the sand or biomass to interact with).

Therefore, the differences in E_a and A_k during mallee leaf drying in air and inert atmosphere suggest that the presence of O_2 during mallee leaf drying affects the generation and properties of sticky agents and hence bed agglomeration.

Based on the data, the overall Equations (8.1) and (8.2) can then be derived for estimating the sand loading which occurs during the drying of mallee leaf in air and inert (argon) atmosphere, respectively.

$$S_L = 46 e^{\frac{-2368}{T}} R^{-0.5} \quad (8.1)$$

$$S_L = 570 e^{\frac{-3528}{T}} R^{-0.5} \quad (8.2)$$

where T is the bed temperature (Kelvin) and R is the ratio of total biomass feed to total sand bed mass (fraction).

The modelled sand loading can then be predicted using Equations (8.1) and (8.2) during the drying of mallee leaf in fluidized-bed and the results (predicted) are then plotted along with experimental data (measured) in Figure 8.5. It can be seen from both experimental data and model prediction that drying in air or argon exhibits little difference in S_L at temperatures <200 °C. At temperatures ≥ 200 °C, atmosphere shows distinct effect on sand loading, suggesting that the thermochemical reactions of mallee leaf to generate sticky agents that are responsible for bed agglomeration follow different pathways. The results in this study clearly demonstrate that bed agglomeration takes place even at temperatures <200 °C during mallee leaf drying in

fluidized-bed. Therefore, such bed agglomeration issues during mallee leaf drying cannot be ignored.

8.4 Conclusions

During the drying of mallee leaf in fluidized-bed, bed agglomeration takes place even at temperatures below 200 °C. Such bed agglomeration can be modelled using sand loading (S_L) that was previously devised for investigation into bed agglomeration during biomass pyrolysis in fluidized-bed. It was also found that S_L during biomass drying follows a similar generic equation ($S_L=KR^{-0.5}$) that was previously derived (chapter 6) for bed agglomeration during biomass pyrolysis, where K is analogous to the Arrhenius equation and R is the ratio between the total accumulated mass of biomass fed and the total mass of sand in the fluidized-bed. The kinetic data (i.e., activation energies E_a and pre-exponential factor A_k) for bed agglomeration during mallee leaf drying under both air and argon atmosphere are also derived.

CHAPTER 9 INFLUENCE OF BIOMASS PARTICLE SIZE ON BED AGGLOMERATION DURING BIOMASS PYROLYSIS IN FLUIDIZED-BED

9.1 Introduction

This chapter further investigates the interaction between pyrolysing biomass particles and sand in fluidized-bed responsible for bed agglomeration during pyrolysis at 500 °C, considering a wide range of biomass particle sizes.

9.2 Experimental method

The leaf and bark components were separated from mallee trees harvested in Western Australia. The samples were dried, milled, then sieved to yield a series of biomass samples of different size fractions: <106, 106–150, 150–250, 250–355, 355–500, 500–710, 710–1000, 1000–2000 and 2000–4000 µm, with the corresponding average particle sizes of 53, 128, 200, 303, 428, 605, 855, 1500 and 3000 µm, respectively. The sand used was prepared as outlined in chapter 3 above.

A set of fast and slow pyrolysis experiments were carried out using the biomass samples prepared as indicated above, following the procedures outlined in chapter 3. After the feeding was completed, the reactor was held at 500 °C for further 15 minutes; this gives a total reaction time of approximately 21.5 minutes for the fast pyrolysis and approximately 61.5 minutes for the slow pyrolysis experiments. For both fast and slow pyrolysis experiments, the temperature time histories for all intents and purposes were consistent within the fast and slow pyrolysis and as such

the results within the slow or fast pyrolysis experiments are comparable with each other.

9.3 Results and discussion

9.3.1 Effect of biomass particle size on sand loading

Figure 9.1 shows that sand loading initially increases with an increase in biomass particle size, reaches a maximum at a transit biomass particle size of $\approx 430 \mu\text{m}$ and decreases with further increase in biomass particle size. It should be noted that S_L quantifies the products produced from biomass pyrolysis to form the “active sites” or “sticky agent” that are responsible for forming bed agglomerates.

Figure 9.1 shows that the actual values for S_L are dependent on pyrolysis conditions (fast or slow) and biomass used (leaf or bark). This result is also verified by the previous research reported into the differences in the agglomeration behaviour of the different biomass components in chapter 5 above. There is also a transition particle size ($\approx 430 \mu\text{m}$), suggesting that there is a change in the mechanism for the transfer of “sticky agent” from the surface of the biomass particle to interact with the sand particles. Based on experimental data on heat transfer coefficient (h) and the thermal conductivity of biomass¹⁵⁵, the critical particle size is estimated to be $\approx 500 \mu\text{m}$ at a critical Biot number of 0.1 for the biomass particles.

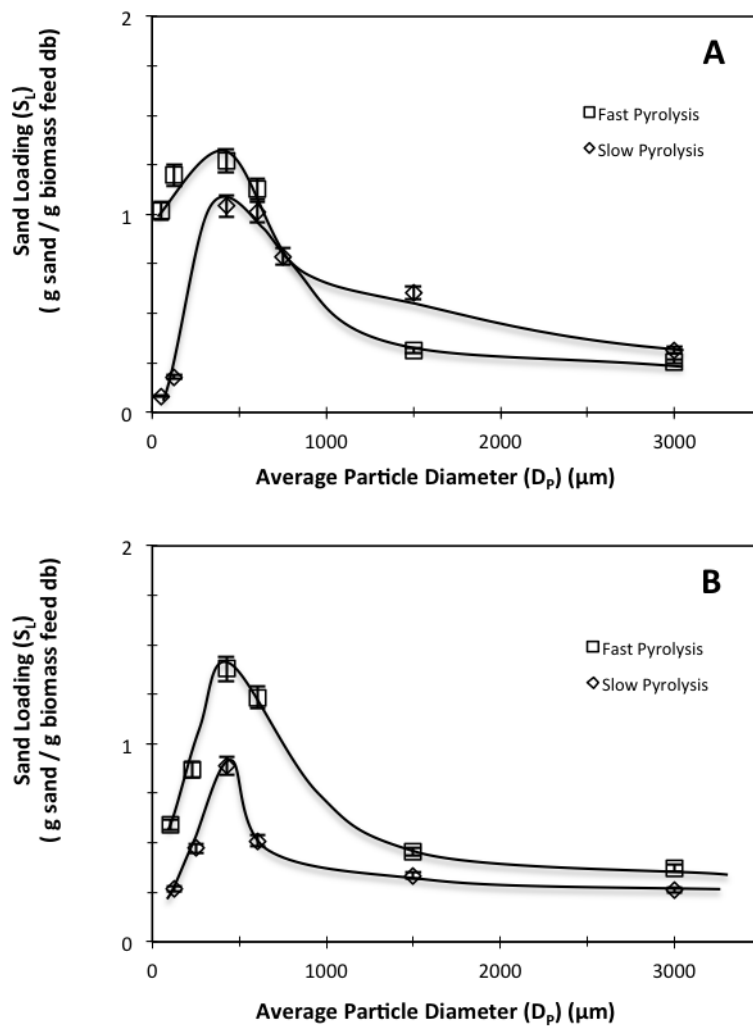


Figure 9.1 Sand loading (S_L) as a function of biomass particle size (D_p) during the pyrolysis of leaf (panel A) and bark (panel B) in fluidized-bed at 500 °C under fast or slow heating conditions.

Figure 9.1 shows that for the pyrolysing biomass particles the transition is around 430 μm , which is consistent with this estimation. Such a transition diameter during biomass fast pyrolysis reflects a change from a “thermally thin” regime where thermal and mass transfer effects can be ignored to “thermally thick” regime where such effects cannot be ignored.

9.3.2 Sand loading and mass transfer of sticky agent

As previously reported in chapters 6, 7 and 8 above, the amount of “sticky agent” produced is dependent on the pyrolysis reaction conditions and as such the actual sand loading should be a function of the overall biomass conversion ($X_C C_0$). The bed material can be considered as “inert”, as it has no concentration of sticky agent present and cannot generate any; therefore, the only place sticky agent can be generated is in the biomass particle undergoing pyrolysis, thus providing the concentration gradient required for mass transfer to occur. Therefore, once the “sticky agent” is produced within a pyrolysing biomass particle (high concentration of sticky agent), the value of S_L reflects the net results of the diffusion of the “sticky agent” through the particle and the convective transfer from the particle surface to interact with sand to form bed agglomerates. In other words, S_L may be modelled as an overall mass transfer phenomenon, considering diffusive transfer coefficient (D_{AB}) of the amount of “sticky agent” produced during biomass pyrolysis through the particle and the convective mass transfer coefficient (K_c) from the particle surface (high concentration of sticky agent accumulated) to interact with sand (low sticky agent concentration).

Based on mass transfer theory²³⁶, the dimensionless Sherwood number ($S_h = K_c D_p / D_{AB}$), Reynolds number ($R_e = \rho D_p V / \mu$) and Schmidt number ($S_c = \nu / D_{AB}$) follows a generic correlation $S_h = k R_e^\alpha S_c^\beta$. Here K_c is the mass transfer coefficient (length time⁻¹), D_p is the average particle diameter (length), D_{AB} is diffusion coefficient (length² time⁻¹), ρ is particle density (mass length⁻³), μ is fluid viscosity (mass length⁻¹ time⁻¹), V is fluid velocity (length time⁻¹), k is a dimensionless

proportional constant while α and β are constants measured experimentally. If we assume that the physical properties are consistent within the reaction sets, since the experiment temperatures and time histories are the same, then S_L can be modelled as an overall mass transfer phenomenon, then

$$S_L = k_s S_h = k_s k R_e^\alpha S_c^\beta = K_M D_P^N \quad (9.1)$$

where K_M is the overall proportional constant [$(g_{\text{sand}}/g_{\text{biomass}}) \text{ time}^{-1} \text{ length}^{-N}$] at total reaction time, S_L is sand loading ($g_{\text{sand}}/g_{\text{biomass}}$) and N is a constant dependent on the reaction conditions (dimensionless). Taking natural logs of the equation yields

$$\ln S_L = \ln K_M + N \ln D_P \quad (9.2)$$

Therefore, a plot of the natural log of S_L against the natural log of the particle size D_P will yield a slope equal to the exponential constant (N) and the intercept equal to $\ln K_M$.

Indeed, as shown in Figure 9.2 for the pyrolysis of biomass with various sizes at 500 °C and 15 minutes under either slow or fast heating conditions, the plot of $\ln S_L$ against $\ln D_P$ yields a straight line. The slopes and intercepts of the lines in Figure 9.2 are then derived and summarised in Table 9.1. It is interesting to see that when biomass particle sizes are $\leq 430 \mu\text{m}$, the values of N for the slow pyrolysis of both the bark (0.98) and leaf (1.23) are close to 1. This indicates that the diffusion and convective mass transfer of the “sticky agent” produced by the pyrolysis reactions are in “balance” for biomass particles of sizes $\leq 430 \mu\text{m}$. In other words, under slow

pyrolysis conditions, $S_L \approx K_M D_P$ so that S_L is proportional to biomass particle size.

The overall “sticky agent” produced by the pyrolysis reactions is a direct consequence of the individual biomass particle mass to area ratio:

$$R_{M:A} = \frac{M_P}{A_P} = \frac{\Phi_V \rho \frac{\pi}{6} D_P^3}{\Phi_A \pi D_P^2} = \frac{\Phi_V \rho D_P}{6 \Phi_A} = \frac{\Phi_V C_0 D_P}{6 \Phi_A} \quad (9.3)$$

where $R_{M:A}$ is the ratio of the mass or mole to the area of the particle (mass or moles length⁻²), M_P is total mass of the particle (mass or moles), A_P is the area of the particle (length²), ρ is the density of particle (mass or moles length⁻³), Φ_V is the volumetric shape factor (dimensionless), Φ_A is the area shape factor (dimensionless) and C_0 is the initial concentration of reactants present in particle (moles length⁻³).

Sand loading S_L may be related to the ratio of particle mass to the surface area, yielding

$$S_L = f(R_{M:A}) = K \frac{\Phi_V X_S C_0 D_P}{6 \Phi_A} = K_M D_P \quad (9.4)$$

Where K is the proportional constant ($\text{g}_{\text{sand}}/\text{g}_{\text{biomass}}$) length² mole⁻¹ time⁻¹) and X_S is the overall conversion of initial reactants to “sticky agent”. Equation (9.4) indicates that S_L is directly proportional to the overall flux of the “sticky agent” generated within the particle and then leaving the surface to interacting with sand.

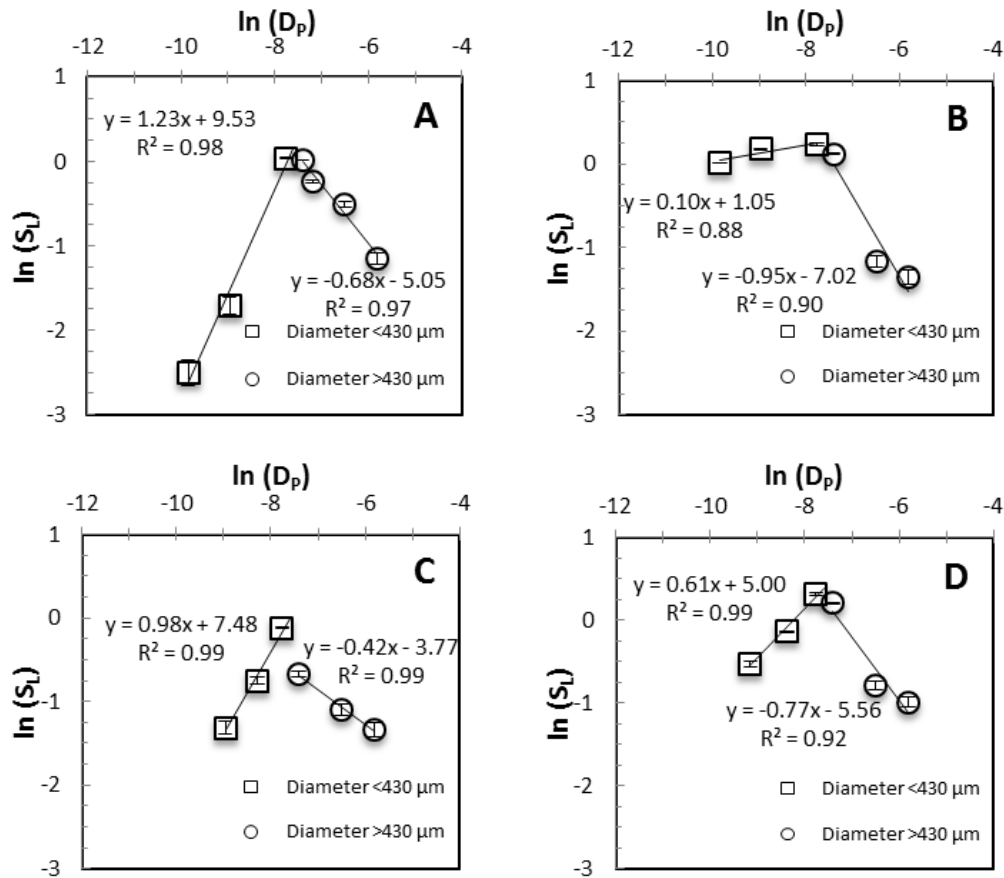


Figure 9.2 $\ln(S_L)$ as a function of $\ln(D_p)$ during the pyrolysis of leaf and bark with various particles sizes (53–3000 μm) at 500 °C. Panel A: slow pyrolysis of leaf; panel B: fast pyrolysis of leaf; panel C: slow pyrolysis of bark; and panel D: fast pyrolysis of bark.

Table 9.1 Values of N and K_M for sand loading during the pyrolysis of biomass particles

biomass	pyrolysis	particle size (D_p), length	slope (N)	intercept ($\ln K_M$)	K_M ($\text{g}_{\text{sand}}/\text{g}_{\text{biomass}}$) $\text{time}^{-1} \text{length}^{-N}$
leaf	slow ^a	$\leq 430 \mu\text{m}$	1.23	9.53	1.38e+04
leaf	slow ^a	$> 430 \mu\text{m}$	-0.68	-5.05	6.41e-03
leaf	fast ^b	$\leq 430 \mu\text{m}$	0.10	1.05	2.86e+00
leaf	fast ^b	$> 430 \mu\text{m}$	-0.95	-7.02	8.94e-04
bark	slow ^a	$\leq 430 \mu\text{m}$	0.98	7.48	1.77e+03
bark	slow ^a	$> 430 \mu\text{m}$	-0.42	-3.77	2.31e-02
bark	fast ^b	$\leq 430 \mu\text{m}$	0.61	5.00	1.48e+02
bark	fast ^b	$> 430 \mu\text{m}$	-0.77	-5.56	3.85e-03

^a slow pyrolysis at $10 \text{ }^\circ\text{C min}^{-1}$, ^b fast pyrolysis at $>200 \text{ K s}^{-1}$

In addition, Figures 9.1 and 9.2 indicate that at biomass particle size $<430 \mu\text{m}$, $N > 0$ so that S_L increases with particle size and the convective mass transfer controls the amount of “sticky agent” that has presented at or left the surface of the particle to interact with sand. At biomass particle size $>430 \mu\text{m}$, $N < 0$ so that S_L decreases with particle size and the diffusive mass transfer controls the amount of “sticky agent” that interacts with sand or the flux of the sticky agent becomes constant.

9.3.3 Diffusive mass transfer of sticky agent

At biomass particle size $>430 \mu\text{m}$, S_L is controlled by the mass transfer of the “sticky agent” through the particle, which would allow for a constant molar or mass flux through the biomass particle to interact with the sand bed material. According to Fick’s law of diffusion²³⁶, $N_A = -D_{AB} \frac{dC_S}{dD_P}$, and Equation (9.1), we have

$$S_L \propto N_A \text{ or } S_L = K_M D_P^N = K_A N_A = -K_A D_{AB} \frac{dC_S}{dD_P} \quad (9.5)$$

where D_{AB} is the diffusivity coefficient ($\text{length}^2 \text{ time}^{-1}$), N_A is the flux of sticky agent or pyrolysis products from the biomass particles undergoing pyrolysis ($\text{g_mole} \text{ sticky agent} \text{ length}^{-2} \text{ time}^{-1}$), C_S is the overall concentration of “sticky agent” produced ($\text{g_mole length}^{-3}$) and K_A is the proportional constant and represents the fraction of the molar flux that directly interacted with the sand bed material to form the sand loading measured. The concentration of the sticky agent produced (C_S) depends on the actual initial reactant concentrations (C_0) produced from the pyrolysis reaction, which is first order in nature. Assuming similar average selectivity of “sticky agent” in the pyrolysis products, one may have $X_S/X_C =$

constant = K_{X_S} where X_C is the biomass conversion. The overall concentration of the “sticky agent” (C_S) produced, can be calculated by $C_S = K_{X_S}C$, where the concentration of the reactants (C) can be determined by $C = X_C C_0$. The biomass conversion X_C (interacting with the sand bed material) can also be represented by ($1 - X_R$) where X_R represents the char recovery in the bed sample. Applying this to Equation (9.5) yields

$$K_M D_P^N = K_A D_{AB} K_{X_S} C_0 \frac{dX_R}{dD_P} \quad (9.6)$$

Figure 9.3 is a plot of char recovery (X_R) as a function of biomass particle size (D_P) for the pyrolysis of leaf (Figure 9.3A) and bark (Figure 9.3B) at 500 °C in fluidized-bed under various conditions. It can be seen that X_R is a function of D_P and has a natural log fit and indicates that the overall conversion of the biomass is first order in nature over the reaction conditions investigated.

Integrating Equation (9.6) from the transitional particle diameter, the diameter at which the sand loading is being effected by the mass and heat transfer effects, (D_{PTr}) ($\approx 430 \mu\text{m}$) to the particle diameter (D_P) and from the corresponding transitional char recovery (X_{RTTr}) to the char recovery (X_R) at D_P , we have

$$K_M \int_{D_{PTr}}^{D_P} D_P^N dD_P = K_A D_{AB} K_{X_S} C_0 \int_{X_{RTTr}}^{X_R} dX_R$$

$$K_M \frac{(D_P^{N+1} - D_{PTr}^{N+1})}{(N+1)} = K_D (X_R - X_{RTTr}) \quad (9.7)$$

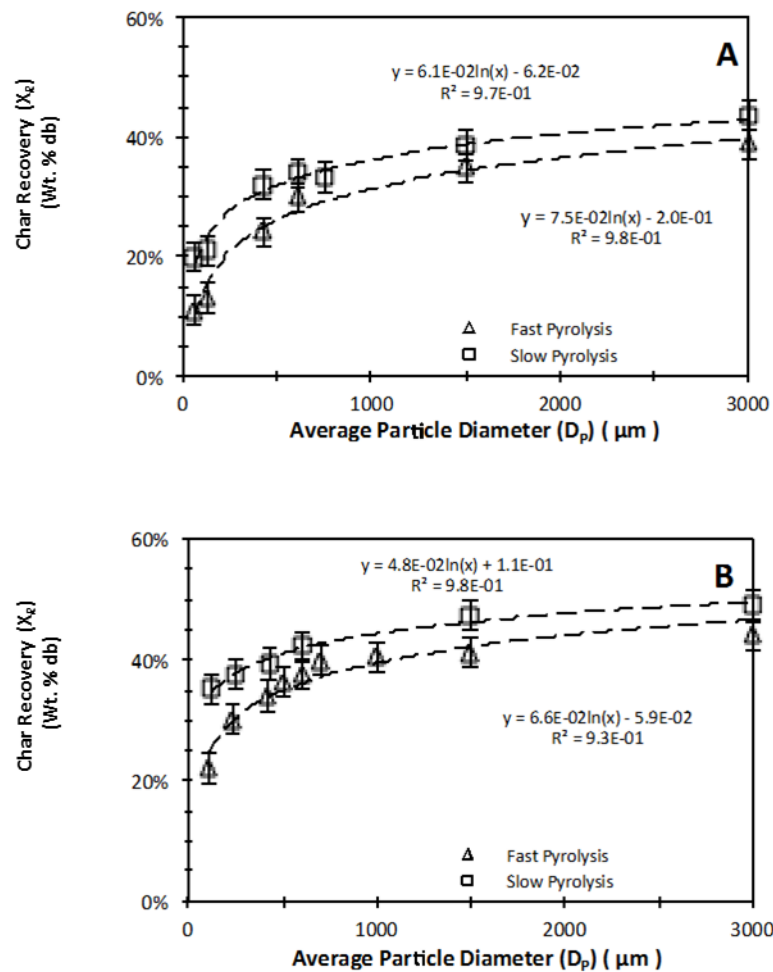


Figure 9.3 Char recovery (X_R) as a function of particle size (D_p) during the pyrolysis of leaf (panel A) and bark (panel B) in fluidized-bed at 500 °C under fast or slow heating conditions.

Where $K_D = K_A D_{AB} K_{Xs} C_0$ is equivalent to the overall average mass transfer coefficient of the sticky agent through the total biomass particles that interacted directly with the sand bed material at the reaction conditions investigated.

Equation (9.7) indicates that when plotting the differential particle size as a function of the overall differential char recovery, this should yield a slope which is equal to K_D/K_M so that the average overall mass transfer coefficient of the sticky agent can

now be estimated over the total reaction time (61.5 minutes for slow and 21.5 minutes for fast pyrolysis).

Indeed, as shown in Figure 9.4, the differential particle size correlates linearly with the differential char recovery. This in turn indicates that S_L is controlled by the mass transfer of the “sticky agent” to interact with sand to form bed agglomerates, S_L decreases with increasing D_P at $D_P > 430 \mu\text{m}$ and the mass transfer coefficient becomes constant at particle diameters greater than the transition diameter due to the diffusion of the sticky agent through particle being limited. The derived overall average mass transfer coefficients of sticky agent are listed in Table 9.2.

Table 9.2 Values of the average overall mass transfer coefficient K_D during the pyrolysis of biomass with various sizes at 500 °C and 15 minutes holding under either slow or fast heating conditions

biomass	pyrolysis	slope (K_D/K_M)	K_M from Table 9.1	average mass transfer coefficient moles $\text{m}^{-2} \text{hr}^{-1}$
leaf	slow ^a	1.9E+00	6.4E-03	1.2E-02
leaf	fast ^b	9.5E+00	8.9E-04	2.4E-02
bark	slow ^a	4.2E-01	2.3E-02	9.4E-03
bark	fast ^b	3.2E+00	3.8E-03	3.4E-02

^aslow pyrolysis at $10 \text{ }^\circ\text{C min}^{-1}$, ^bfast pyrolysis at $>200 \text{ K s}^{-1}$

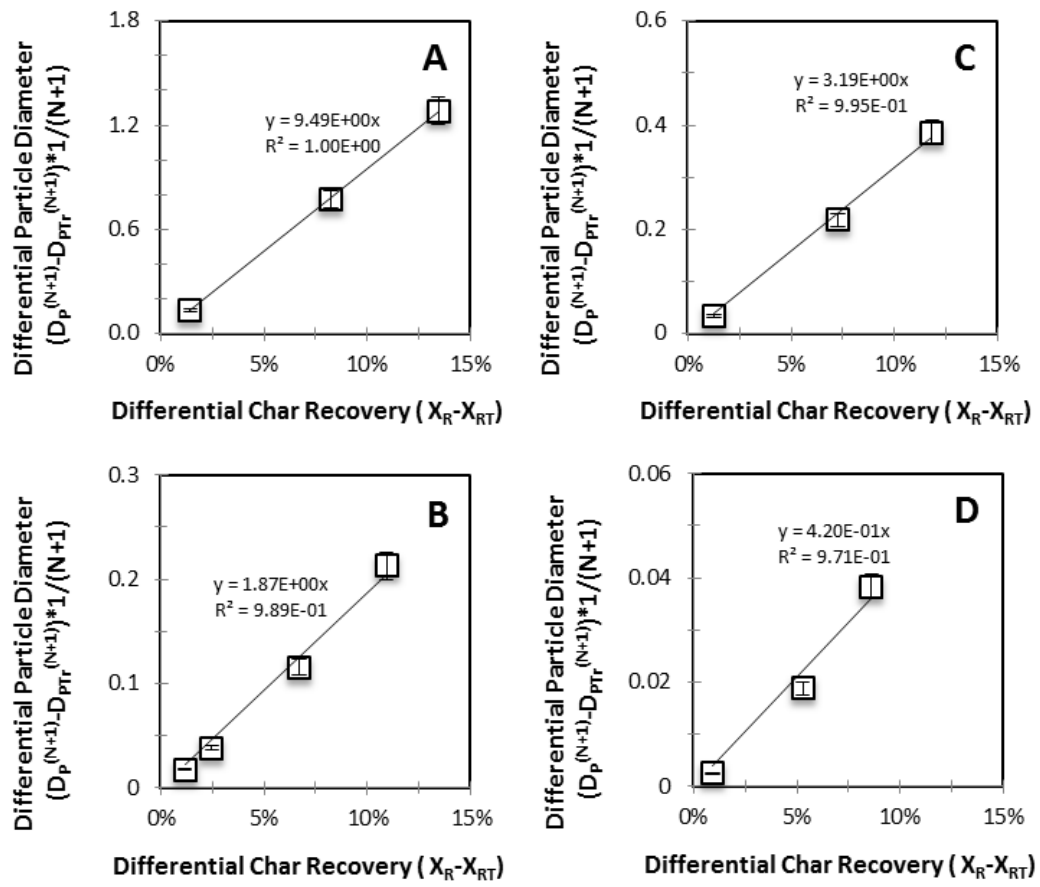


Figure 9.4 Differential particle size as a function of differential char recovery during the pyrolysis of leaf and bark with various sizes (430–3000 μm) at 500 °C. Panel A: fast pyrolysis of leaf; panel B: slow pyrolysis of leaf; panel C: fast pyrolysis of bark; panel D: slow pyrolysis of bark biomass.

It is interesting to see that the average diffusion transfer coefficient of the sticky agent produced under slow or fast pyrolysis of leaf or bark are actually similar in magnitude, with the fast pyrolysis being larger than that for the slow pyrolysis. This is consistent with the data in Figure 9.1 where the values of S_L under slow pyrolysis for both the bark and leaf biomass are similar in magnitude at particle diameters $>430 \mu\text{m}$. Under slow heating conditions, pyrolysis reaction is slow. The generation of sticky agent is slow (experiencing intensive secondary reactions) and less sensitive to the properties of the parent biomass, leading to the similar average mass transfer coefficients of the sticky agent for leaf or bark. Under fast heating

conditions, pyrolysis reactions proceed intensively and the generation of sticky agent is rapid so that the differences in parent biomass properties become important. This is evident in Figure 9.1 that the bark undergoing fast pyrolysis seems to interact more with the sand bed material as reflected by the higher sand loading values and the subsequent larger average mass transfer coefficient (3.4×10^{-2} moles m^{-2} hr^{-1}) than the leaf biomass under the same conditions having a lower average mass transfer coefficient (2.4×10^{-2} moles m^{-2} hr^{-1}). These results suggest that while the shapes of the curves are similar in Figure 9.1, the actual “sticky agent” formed from bark pyrolysis leads to more bed agglomeration (i.e., high S_L values) than that from leaf pyrolysis. This is most likely due to the differences in the chemistry of the parent biomass. Leaf and bark are known to have chemically-different extractible matter that plays an important role in bed agglomeration during biomass fast pyrolysis as shown in chapter 5 above.

9.4 Conclusions

Under the experimental conditions investigated in this study, the biomass particle size has a significant influence on bed agglomeration, hence the values of sand loading (S_L) that are diagnosis parameters developed for quantifying the interaction between pyrolysing biomass particles and sand particles to form bed agglomerates. Based on mass transfer theory, S_L correlates to biomass particle size D_P via $S_L = K_M D_P^N$, where the values of K_M and N can be determined experimentally. It was found that at $D_P \leq 430 \mu\text{m}$, S_L is controlled by the convective mass transfer of the sticky agent while at $D_P > 430 \mu\text{m}$, S_L is controlled by the intra-particle diffusion transfer of the sticky agent.

CHAPTER 10 CONCLUSIONS, IMPLICATIONS AND RECOMMENDATIONS FOR FUTURE TEST WORK

10.1 Conclusions from current test work

10.1.1 Agglomeration occurring in the pyrolyser

The results presented in chapter 4 clearly show that bed agglomeration does take place by the resulting particle size distributions obtained. The resulting agglomerates are an overall mix of char-char and char-sand bonding, which are connected by carbon-enriched necks. The overall yield of the bed agglomerates decreased with increasing pyrolysis temperature (300–700 °C).

Two main types of bed agglomerates have been identified. The first is due to solvent-soluble organic matter, which can be disassembled via solvent washing, while the second is due to solvent-insoluble organic matter. Not only is the overall yield of the agglomerates dependent on the pyrolysis temperature, but so is the distribution of the two types of agglomerations (solvent soluble and solvent insoluble) that are formed. Solvent-insoluble organic matter dominates at low pyrolysis temperatures (300–500 °C), while solvent-soluble organic matter dominates at higher pyrolysis temperatures (500–700 °C). Agglomeration is the result of sticky agents (solvent-soluble and solvent-insoluble), which are produced during biomass pyrolysis reactions.

10.1.2 Differences in bed agglomeration behaviour of biomass components wood, leaf and bark

Results predominately presented in chapter 5 show there are significant differences in bed agglomeration which is formed when processing wood, bark and leaf in a fluidized-bed reactor at 500 °C. The wood component of the biomass results in insignificant bed agglomeration formation, while that of the leaf and bark components result in significant amounts of bed agglomeration. When removing the ethanol-soluble extractive materials from both the leaf and bark biomass components, the resulting agglomeration was drastically reduced but not eliminated at the same process conditions. Directly reacting the ethanol-soluble extractive materials obtained from both the leaf or bark biomass components lead to substantial increases in the bed agglomeration formation. This indicates the ethanol-soluble extractive materials in the biomass have a significant influence on the overall bed agglomeration produced.

10.1.3 Determining whether the agglomeration is a random or a direct consequence of the pyrolysis process

With the definition and introduction of the new diagnostic parameter, sand loading (S_L), having the units $\text{g}_{\text{sand}}/\text{g}_{\text{biomass (db)}}$, in chapter 6, it is now possible to measure experimentally the overall interaction of the biomass undergoing pyrolysis with the sand bed material. The variable sand loading has been found to be a superior indication and measurement of the interaction of the biomass and sand bed material than that of the agglomeration yield (Y_{AP}). The interaction of the biomass with the sand bed material during the continuous feeding phase is in a negative order of 0.4 and during the holding phase of the reaction interacts in a zero-order reaction kinetic.

The parameter sand loading has shown that the bed agglomeration is not a random phenomenon, but is dependent on the biomass pyrolysis reactions occurring in the pyrolyser.

10.1.4 How process conditions in the pyrolyser affect the interaction of the fluidized-bed sand material and the biomass particles

With the introduction of the sand loading (S_L) variable, it is now possible to directly measure experimentally the interaction of the biomass and the sand bed material with the process reaction conditions. The reaction parameters examined during the experimental program were the amount of biomass fed into the reactor. This is actually reflected in the biomass to sand bed mass ratio (R) chapter 6; the fluidized-bed temperature (T) chapters 4, 7 and 8; the holding time (t_h) chapter 6; and the particle diameter (D_p) chapter 9.

10.1.4.1 Biomass to sand bed mass ratio

The results from chapter 6 indicate that as the biomass to sand ratio (R) is increased, there is actually a reduction in the sand loading value measured. This is indicated by the negative order of 0.5 obtained for the generic relationship between the sand loading and biomass feed to sand bed ratio ($S_L = KR^{-0.5}$) found for a constant reaction temperature and holding time ($t_h = 15$ minutes). At a biomass to sand bed ratio below 12 wt. %, the bed agglomeration is mainly driven by sand-char bonding, but as this ratio is increased above 12 wt. % the char-char bonding becomes more prevalent.

10.1.4.2 Holding time

The results in chapter 6 indicate there is a zero-order reaction kinetic relationship between the resulting sand loading (S_L) and the holding time (t_h). This relationship indicates that during the holding time there is no new sand or biomass interaction occurring but that the existing connections are starting to disseminate following a zero-order reaction kinetic and that the generation of the agglomerates, or increase in the sand loading, occurs only during the feeding phase of the reaction.

10.1.4.3 Reaction Temperature

When increasing the temperature (T) from 200 to 310 °C, the sand loading (S_L) increases dramatically (0.2 to 4 g_{sand}/g_{biomass (db)}). When there is a further increase in temperature from 350 to 700 °C, the sand loading decreases (4 to 0.23 g_{sand}/g_{biomass (db)}) as indicated by the results detailed in chapters 4, 7 and 8. The generic sand loading equation developed in chapter 6 ($S_L = KR^{-0.5}$) can be used for modelling the sand loading values at different fluidized-bed temperatures under the same biomass to sand bed ratio ($R = 0.095$) and holding time ($t_h = 15$ minutes). The K values calculated from the experimental data were found to obey the Arrhenius law for reaction kinetics as a function of reaction temperature. This once again shows that the interaction between the sand bed and the biomass feed material is not a random process but is dependent on the reaction conditions in the Pyrolyser. From the Arrhenius equation it was found that during the temperature increase from 200 to 310 °C the activation energy (E_a) required for the formation of the complexes to form the sand-char and char-char bonds which make up the agglomeration was endothermic and had a value of 27.6 kJ mole⁻¹. When the temperature was increased

further from 350 to 700 °C, the activation energy is exothermic and has a value of $-44.6 \text{ kJ mole}^{-1}$. In the range from 310 to 350 °C the activation energy has a turning point where it changes from endothermic to exothermic in nature. It was further found that when the ethanol extracts were reacted directly with the same overall change in activation energy, it changed from endothermic to exothermic, although the turning point temperature was much lower (250 to 280 °C). The actual activation energy to form the required complexes was $13.7 \text{ kJ mole}^{-1}$ and the sand loading reached a peak value of $8.24 \text{ g}_{\text{sand}}/\text{g}_{\text{biomass (db)}}$ at a temperature of 275 °C. What this result indicates is that the ethanol extracts interact within the biomass particle itself as indicated by the increase of the activation energy from $13.7 \text{ kJ mole}^{-1}$ (extract only) to $27.6 \text{ kJ mole}^{-1}$ for the raw biomass sample. This is further supported by the value of the exothermic activation energy for the sand loading of the extract at the higher temperature range (275 to 600 °C) being lower $-16.6 \text{ kJ mole}^{-1}$ than $-44.6 \text{ kJ mole}^{-1}$ for the untreated biomass sample.

10.1.4.4 Particle diameter

The effect of the biomass particle (D_P) has a large influence on the sand loading (S_L) values obtained for fast or slow pyrolysis as shown by the results outlined in chapter 9. The sand loading values correlate to the generic equation $S_L = K_M D_P^N$, which is based on mass transfer theory. The values of K_M and N are determined experimentally. When the particle diameter is $<430 \mu\text{m}$, the sand loading is controlled by the convective mass transfer of the sticky agent from the particle, but at particle diameters $>430 \mu\text{m}$, the sand loading is controlled by the intra-particle diffusion transfer of the sticky agent through the particle.

10.1.5 Effect of drying biomass

Bed agglomeration occurs during the drying of biomass in either air or argon atmosphere temperatures $<200\text{ }^{\circ}\text{C}$ as indicated by the results in chapter 8. The sand loading (S_L) values obtained for drying in an air or argon atmosphere are of similar value up to approximately $200\text{ }^{\circ}\text{C}$, after which the sand loading values for the biomass in the argon atmosphere is larger than that for the biomass in the air atmosphere. The generic sand loading equation ($S_L = KR^{0.5}$, from chapter 6 and 7) can be used to model the resulting sand loading in either the air or argon atmosphere. K is determined experimentally at different temperatures keeping the biomass feed to sand bed ratio ($R = 0.095$) and holding time ($t_h = 15$ minutes) constant and varying the fluidized-bed temperature (T). This result indicates that the process by which the sticky agent is produced and then interacts with the sand bed material is similar up to a temperature of $200\text{ }^{\circ}\text{C}$, regardless of atmosphere. At temperatures $>200\text{ }^{\circ}\text{C}$ the reactions producing the sticky agent differ and are dependent on the atmosphere in which the reactions are occurring as indicated by the different activation energies (E_a) calculated (28 kJ mole^{-1} for the argon atmosphere and 19 kJ mole^{-1} for the air atmosphere).

10.2 Practical implications of the current research

The overall finding from this research indicates that appreciable agglomeration occurs during either the fast or slow pyrolysis of both bark or leaf biomass components in a fluidized-bed Pyrolyser. Very little agglomeration is formed during the fast or slow pyrolysis of the wood biomass component. Ethanol extracts from

the leaf and bark biomass components have a dramatic effect on the degree to which agglomeration occurs. Even when this extract is removed from the biomass components, an appreciable amount of agglomeration still occurs. What this result indicates is that the biomass material must still be separated into the various biomass components wood, leaf and bark and cannot be treated as a single mixture in the Pyrolyser as agglomeration will occur. This also indicates that the extracts contained within the leaf and bark material must be removed to decrease the agglomeration occurring during pyrolysis.

The power of the sand loading (S_L) variable has been shown as it pertains to the reaction conditions in the Pyrolyser, in that the sand loading can be correlated to the temperature (T), biomass feed to sand bed mass ratio (R) and holding time (t_h) over a wide range of temperatures (120–700 °C).

The agglomeration is formed by the direct interaction of “sticky agents” that are either directly or indirectly produced by the pyrolysis reaction conditions occurring in the Pyrolyser and is reflected in the sand loading measurement. This result indicates that the agglomeration or the sand and biomass interaction is not a random occurrence but is totally dependent on the pyrolysis reaction conditions occurring in the Pyrolyser.

Low temperature drying in either an air or inert (argon) atmosphere produces agglomeration even at temperatures as low as 120 °C and as such it cannot be ignored when using a fluidized-bed dryer to increase the calorific value of the biomass.

10.3 Recommendations and future work

Agglomeration yield (Y_{AP}), although a useful tool when used to determine if agglomeration is occurring, is not a good tool for measuring the actual direct interaction of the biomass and the fluidized-bed material as it pertains to reaction conditions. It is recommended that sand loading (S_L) should be used from now on to measure and model the direct interaction of the biomass and fluidized sand bed material.

The experimentation performed in this thesis is but a brief introduction for the sand loading variable and its use to describe the interaction of the biomass and fluidized-bed material. Further experimentation should be conducted to accurately determine the points of inflection for the activation energy (E_a) and the reasons why this occurs should be determined.

An overall reaction equation that correlates the particle diameter (D_P), fluidized-bed temperature (T), feed to sand bed mass ratio (R) and holding time (t_h) to the sand loading (S_L) during pyrolysis should be developed with further and more detailed experimentation.

It would be of great value to determine if the sand loading (S_L) variable can be used to measure the interaction of the biomass and fluidized-bed material during combustion or gasification and can be ultimately correlated to the reaction conditions such as, particle diameter (D_P), temperature (T), feed to sand bed mass ratio (R) holding time (t_h) and AAEM concentration in the biomass.

REFERENCES

1. Mohan, D.; Pittman, C. U.; Steele, P. H., Pyrolysis of Wood/Biomass for Bio-oil: A Critical Review. *Energy & Fuels* **2006**, 20, (3), 848-889.
2. Elliott, D. C., Historical Developments in Hydroprocessing Bio-oils. *Energy & Fuels* **2007**, 21, (3), 1792-1815.
3. Elliott, D. C.; Hart, T. R., Catalytic Hydroprocessing of Chemical Models for Bio-oil. *Energy & Fuels* **2008**, 23, (2), 631-637.
4. Huang, J.; Long, W.; Agrawal, P. K.; Jones, C. W., Effects of Acidity on the Conversion of the Model Bio-oil Ketone Cyclopentanone on H-Y Zeolites. *The Journal of Physical Chemistry C* **2009**, 113, (38), 16702-16710.
5. Tang, Z.; Lu, Q.; Zhang, Y.; Zhu, X.; Guo, Q., One Step Bio-Oil Upgrading through Hydrotreatment, Esterification, and Cracking. *Industrial & Engineering Chemistry Research* **2009**, 48, (15), 6923-6929.
6. Christensen, E. D.; Chupka, G. M.; Luecke, J.; Smurthwaite, T.; Alleman, T. L.; Iisa, K.; Franz, J. A.; Elliott, D. C.; McCormick, R. L., Analysis of Oxygenated Compounds in Hydrotreated Biomass Fast Pyrolysis Oil Distillate Fractions. *Energy & Fuels* **2011**, 25, (11), 5462-5471.
7. French, R. J.; Stunkel, J.; Baldwin, R. M., Mild Hydrotreating of Bio-Oil: Effect of Reaction Severity and Fate of Oxygenated Species. *Energy & Fuels* **2011**, 25, (7), 3266-3274.
8. Sadhukhan, J.; Ng, K. S., Economic and European Union Environmental Sustainability Criteria Assessment of Bio-Oil-Based Biofuel Systems: Refinery Integration Cases. *Industrial & Engineering Chemistry Research* **2011**, 50, (11), 6794-6808.
9. Zheng, A.; Zhao, Z.; Chang, S.; Huang, Z.; He, F.; Li, H., Effect of Torrefaction Temperature on Product Distribution from Two-Stage Pyrolysis of Biomass. *Energy & Fuels* **2012**, 26, (5), 2968-2974.
10. Bartels, M.; Nijenhuis, J.; Lensselink, J.; Siedlecki, M.; de Jong, W.; Kapteijn, F.; van Ommen, J. R., Detecting and Counteracting Agglomeration in Fluidized-bed Biomass Combustion. *Energy & Fuels* **2008**, 23, (1), 157-169.
11. Baxter, L. L., Ash deposition during biomass and coal combustion: A mechanistic approach. *Biomass and Bioenergy* **1993**, 4, (2), 85-102.
12. Brus, E.; Öhman, M.; Nordin, A., Mechanisms of Bed Agglomeration during Fluidized-Bed Combustion of Biomass Fuels. *Energy & Fuels* **2005**, 19, (3), 825-832.
13. Chaivatamaset, P.; Sricharoon, P.; Tia, S.; Bilitewski, B., A prediction of defluidization time in biomass fired fluidized-bed combustion. *Applied Thermal Engineering* **2013**, 50, (1), 722-731.
14. Kuo, J.-H.; Lin, C.-L.; Wey, M.-Y., Effect of alkali concentrations and operating conditions on agglomeration/defluidization behavior during fluidized-bed air gasification. *Powder Technology* **2011**, 214, (3), 443-446.
15. Liliedahl, T.; Sjöström, K.; Engvall, K.; Rosén, C., Defluidisation of fluidized-beds during gasification of biomass. *Biomass and Bioenergy* **2011**, 35, Supplement 1, S63-S70.
16. Liu, R.; Jin, B.; Zhong, Z.; Zhao, J., Reduction of Bed Agglomeration in CFB Combustion Biomass with Aluminium-Contain Bed Material. *Process Safety and Environmental Protection* **2007**, 85, (5), 441-445.

17. Johansson, B., A broadened typology on energy and security. *Energy* **2013**, 53,199-205.
18. Below, A., Obstacles in energy security: An analysis of congressional and presidential framing in the United States. *Energy Policy* **2013**, 62, 860-868.
19. Chaudry M, E. P., Ramachandran K, Shakoor A, Skea J, Strbac G, , Building a resilient UK energy system,. *UK Energy Research Centre* **2009**.
20. Forum., W. E., The new energy security paradigm. **2006**.
21. Sovacool, B. K.; Mukherjee, I., Conceptualizing and measuring energy security: A synthesized approach. *Energy* **2011**, 36, (8), 5343-5355.
22. Mortimer, A. D. a. E., Strategic Insights 54 - Keeping the home fires burning: Australia's energy security. *Australian Strategic Policy Institute* **December 2011**.
23. Australian Government Department of Industry : Energy Security <http://www.innovation.gov.au/Energy/EnergySecurity/Pages/default.aspx>
24. Energy, O. o., Strategic Energy Initiative, Energy2031. **2011**.
25. Zhang, Z.; Jiang, H.; Liu, J. X.; Zhou, G. M.; Liu, S. R.; Zhang, X. Y., Assessment on water use efficiency under climate change and heterogeneous carbon dioxide in China terrestrial ecosystems. *Procedia Environmental Sciences* **2012**, 13, 2031-2044.
26. Rehan, R.; Nehdi, M., Carbon dioxide emissions and climate change: policy implications for the cement industry. *Environmental Science & Policy* **2005**, 8, (2), 105-114.
27. Letcher, T. M., Chapter 1 - Introduction with a Focus on Atmospheric Carbon Dioxide and Climate Change. In *Future Energy (Second Edition)*, Letcher, T. M., Ed. Elsevier: Boston, 2014; pp 3-16.
28. Reilly, J.; Paltsev, S.; Felzer, B.; Wang, X.; Kicklighter, D.; Melillo, J.; Prinn, R.; Sarofim, M.; Sokolov, A.; Wang, C., Global economic effects of changes in crops, pasture, and forests due to changing climate, carbon dioxide, and ozone. *Energy Policy* **2007**, 35, (11), 5370-5383.
29. Sundblad, E. L.; Biel, A.; Gärling, T., Intention to change activities that reduce carbon dioxide emissions related to worry about global climate change consequences. *Revue Européenne de Psychologie Appliquée/European Review of Applied Psychology* **2014**, 64, (1), 13-17.
30. Wamelink, G. W. W.; Wieggers, H. J. J.; Reinds, G. J.; Kros, J.; Mol-Dijkstra, J. P.; van Oijen, M.; de Vries, W., Modelling impacts of changes in carbon dioxide concentration, climate and nitrogen deposition on carbon sequestration by European forests and forest soils. *Forest Ecology and Management* **2009**, 258, (8), 1794-1805.
31. Shafiullah, G. M.; Amanullah, M. T. O.; Shawkat Ali, A. B. M.; Jarvis, D.; Wolfs, P., Prospects of renewable energy – a feasibility study in the Australian context. *Renewable Energy* **2012**, 39, (1), 183-197.
32. Sims, R. E. H., Renewable energy: a response to climate change. *Solar Energy* **2004**, 76, (1-3), 9-17.
33. Moriarty, P.; Honnery, D., What is the global potential for renewable energy? *Renewable and Sustainable Energy Reviews* **2012**, 16, (1), 244-252.
34. Trappey, A. J. C.; Trappey, C. V.; Lin, G. Y. P.; Chang, Y.-S., The analysis of renewable energy policies for the Taiwan Penghu island administrative region. *Renewable and Sustainable Energy Reviews* **2012**, 16, (1), 958-965.

35. Green, C.; Baksi, S.; Dilmaghani, M., Challenges to a climate stabilizing energy future. *Energy Policy* **2007**, 35, (1), 616-626.
36. Ramachandra, T. V.; Shwetmala, Decentralised carbon footprint analysis for opting climate change mitigation strategies in India. *Renewable and Sustainable Energy Reviews* **2012**, 16, (8), 5820-5833.
37. Hong, T.; Koo, C.; Kwak, T.; Park, H. S., An economic and environmental assessment for selecting the optimum new renewable energy system for educational facility. *Renewable and Sustainable Energy Reviews* **2014**, 29, `286-300.
38. de Alegría Mancisidor, I. M.; Díaz de Basurto Uruga, P.; Martínez de Alegría Mancisidor, I.; Ruiz de Arbuló López, P., European Union's renewable energy sources and energy efficiency policy review: The Spanish perspective. *Renewable and Sustainable Energy Reviews* **2009**, 13, (1), 100-114.
39. Anandarajah, G.; Strachan, N., Interactions and implications of renewable and climate change policy on UK energy scenarios. *Energy Policy* **2010**, 38, (11), 6724-6735.
40. George, R. J., Management of sandplain seeps in the wheatbelt of Western Australia. *Agricultural Water Management* **1991**, 19, (2), 85-104.
41. Australian Bureau of Statistics, W. A. I., Salinity and Land Management on Western Australian Farms **2003**, (Report No 1 3 6 7 . 5 • J U N E 2 0 0 3).
42. George, S. J.; Harper, R. J.; Hobbs, R. J.; Tibbett, M., A sustainable agricultural landscape for Australia: A review of interlacing carbon sequestration, biodiversity and salinity management in agroforestry systems. *Agriculture, Ecosystems & Environment* **2012**, 163, 28-36.
43. Bari, M.A.; Ruprecht, J.K., Water yield response to land use change in south-west Western Australia; Resource Science Division, Department of Environment: November 2003.
44. Smith, F. P., Who's planting what, where and why – and who's paying?: An analysis of farmland revegetation in the central wheatbelt of Western Australia. *Landscape and Urban Planning* **2008**, 86, (1), 66-78.
45. Pannell, D. J.; Ewing, M. A., Managing secondary dryland salinity: Options and challenges. *Agricultural Water Management* **2006**, 80, (1–3), 41-56.
46. Dunin, F. X., Integrating agroforestry and perennial pastures to mitigate water logging and secondary salinity. *Agricultural Water Management* **2002**, 53, (1–3), 259-270.
47. George, R. J.; Nulsen, R. A.; Ferdowsian, R.; Raper, G. P., Interactions between trees and groundwaters in recharge and discharge areas – A survey of Western Australian sites. *Agricultural Water Management* **1999**, 39, (2–3), 91-113.
48. Brooksbank, K.; Veneklaas, E. J.; White, D. A.; Carter, J. L., Water availability determines hydrological impact of tree belts in dryland cropping systems. *Agricultural Water Management* **2011**, 100, (1), 76-83.
49. Milthorpe, P. L.; Brooker, M. I. H.; Slee, A.; Nicol, H. I., Optimum planting densities for the production of eucalyptus oil from blue mallee (*Eucalyptus polybractea*) and oil mallee (*E. kochii*). *Industrial Crops and Products* **1998**, 8, (3), 219-227.
50. Milthorpe, P. L.; Hillan, J. M.; Nicol, H. I., The effect of time of harvest, fertilizer and irrigation on dry matter and oil production of blue mallee. *Industrial Crops and Products* **1994**, 3, (3), 165-173.

51. Wildy, D. T.; Bartle, J. R.; Pate, J. S.; Arthur, D. J., Sapling and coppice biomass production by alley-farmed 'oil mallee' Eucalyptus species in the Western Australian wheatbelt. *Australian Forestry* **2000**, 63, (2), 147-157.
52. Wildy, D. T.; Pate, J. S.; Bartle, J. R., Variations in composition and yield of leaf oils from alley-farmed oil mallees (Eucalyptus spp.) at a range of contrasting sites in the Western Australian wheatbelt. *Forest Ecology and Management* **2000**, 134, (1-3), 205-217.
53. Zhang, L.; Dawes, W. R.; Hatton, T. J.; Hume, I. H.; O'Connell, M. G.; Mitchell, D. C.; Milthorpe, P. L.; Yee, M., Estimating episodic recharge under different crop/pasture rotations in the Mallee region. Part 2. Recharge control by agronomic practices. *Agricultural Water Management* **1999**, 42, (2), 237-249.
54. Zhang, L.; Hume, I. H.; O'Connell, M. G.; Mitchell, D. C.; Milthorpe, P. L.; Yee, M.; Dawes, W. R.; Hatton, T. J., Estimating episodic recharge under different crop/pasture rotations in the Mallee region. Part 1. Experiments and model calibration. *Agricultural Water Management* **1999**, 42, (2), 219-235.
55. Barrier, J. W.; Bulls, M. M., Feedstock Availability of Biomass and Wastes. In *Emerging Technologies for Materials and Chemicals from Biomass*, American Chemical Society: 1992; Vol. 476, pp 410-421.
56. Bathgate, A.; Pannell, D. J., Economics of deep-rooted perennials in western Australia. *Agricultural Water Management* **2002**, 53, (1-3), 117-132.
57. Dale, G.; Dieters, M., Economic returns from environmental problems: Breeding salt- and drought-tolerant eucalypts for salinity abatement and commercial forestry. *Ecological Engineering* **2007**, 31, (3), 175-182.
58. David, Z.; Deepak, R.; Gal, H., Economist's Perspective on Biofuels. In *Perspectives on Biofuels: Potential Benefits and Possible Pitfalls*, American Chemical Society: 2012; Vol. 1116, pp 155-169.
59. Ltd, E. P., Integrated Tree Processing of Mallee Eucalypts, A report for the RIRDC/Land & Water Australia/FWPRDC, Joint Venture Agroforestry Program. **November 2001**, RIRDC Publication No 01/160 , RIRDC Project No OIL-3A.
60. Ledig F, T., Silvicultural Systems for the Energy Efficient Production of Fuel Biomass. In *Biomass as a Nonfossil Fuel Source*, AMERICAN CHEMICAL SOCIETY: 1981; Vol. 144, pp 447-461.
61. Wu, H.; Fu, Q.; Giles, R.; Bartle, J., Production of Mallee Biomass in Western Australia: Energy Balance Analysis†. *Energy & Fuels* **2007**, 22, (1), 190-198.
62. He, M.; Mourant, D.; Gunawan, R.; Lievens, C.; Wang, X. S.; Ling, K.; Bartle, J.; Li, C.-Z., Yield and properties of bio-oil from the pyrolysis of mallee leaves in a fluidized-bed reactor. *Fuel* **2012**, 102, 506-513.
63. Mourant, D.; Lievens, C.; Gunawan, R.; Wang, Y.; Hu, X.; Wu, L.; Syed-Hassan, S. S. A.; Li, C.-Z., Effects of temperature on the yields and properties of bio-oil from the fast pyrolysis of mallee bark. *Fuel* **2013**, 108, 400-408.
64. Dutta, S.; Pal, S., Promises in direct conversion of cellulose and lignocellulosic biomass to chemicals and fuels: Combined solvent–nanocatalysis approach for biorefinary. *Biomass and Bioenergy*.
65. Smith, H. D., Structure of Cellulose. *Industrial & Engineering Chemistry* **1937**, 29, (9), 1081-1084.
66. Klemm, D.; Heublein, B.; Fink, H.-P.; Bohn, A., Cellulose: Fascinating Biopolymer and Sustainable Raw Material. *Angewandte Chemie International Edition* **2005**, 44, (22), 3358-3393.

67. Pettersen, R. C., The Chemical Composition of Wood. In Forest Service, F. P. L., Ed. American Chemical Society: 1984.
68. Pandey, K. K., A study of chemical structure of soft and hardwood and wood polymers by FTIR spectroscopy. *Journal of Applied Polymer Science* **1999**, 71, (12), 1969-1975.
69. Kačuráková, M.; Capek, P.; Sasinková, V.; Wellner, N.; Ebringerová, A., FT-IR study of plant cell wall model compounds: pectic polysaccharides and hemicelluloses. *Carbohydrate Polymers* **2000**, 43, (2), 195-203.
70. Harder, M. L. M. L. H., John D. ; Einspahr, Dean W. ; Swanson, John W., Bark and wood properties of pulpwood species as related to separation and segregation of chip/bark mixtures. Project 3212, report three: a progress report to members of Group Project 3212. In <http://hdl.handle.net/1853/1063>, Ed. Appleton, Wisconsin : Institute of Paper Chemistry, Georgia Institute of Technology: 1975; pp Institute of Paper Chemistry (Appleton,Wis.). Project 3212 ; report 3.
71. Guo, X.-j.; Wang, S.-r.; Wang, K.-g.; Liu, Q.; Luo, Z.-y., Influence of extractives on mechanism of biomass pyrolysis. *Journal of Fuel Chemistry and Technology* **2010**, 38, (1), 42-46.
72. He, W.; Hu, H., Prediction of hot-water-soluble extractive, pentosan and cellulose content of various wood species using FT-NIR spectroscopy. *Bioresource Technology* **2013**, 140, 299-305.
73. Melzer, M.; Blin, J.; Bensakhria, A.; Valette, J.; Broust, F., Pyrolysis of extractive rich agroindustrial residues. *Journal of Analytical and Applied Pyrolysis* **2013**, 104, 448-460.
74. Telmo, C.; Lousada, J., The explained variation by lignin and extractive contents on higher heating value of wood. *Biomass and Bioenergy* **2011**, 35, (5), 1663-1667.
75. C. H. Bamford, J. C. a. D. H. M., The combustion of wood. Part I. *Mathematical Proceedings of the Cambridge Philosophical Society* **1946**, 42, (2), 166-182.
76. Gani, A.; Morishita, K.; Nishikawa, K.; Naruse, I., Characteristics of Co-combustion of Low-Rank Coal with Biomass. *Energy & Fuels* **2005**, 19, (4), 1652-1659.
77. Grammelis, P.; Kakaras, E., Biomass Combustion Modeling in Fluidized-beds. *Energy & Fuels* **2004**, 19, (1), 292-297.
78. Jones, J. M.; Pourkashanian, M.; Williams, A.; Hainsworth, D., A comprehensive biomass combustion model. *Renewable Energy* **2000**, 19, (1-2), 229-234.
79. Kalisz, S.; Pronobis, M.; Baxter, D., Co-firing of biomass waste-derived syngas in coal power boiler. *Energy* **2008**, 33, (12), 1770-1778.
80. Lu, H.; Robert, W.; Peirce, G.; Ripa, B.; Baxter, L. L., Comprehensive Study of Biomass Particle Combustion. *Energy & Fuels* **2008**, 22, (4), 2826-2839.
81. Robinson, A. L.; Rhodes, J. S.; Keith, D. W., Assessment of Potential Carbon Dioxide Reductions Due to Biomass-Coal Cofiring in the United States. *Environmental Science & Technology* **2003**, 37, (22), 5081-5089.
82. Daood, S. S.; Javed, M. T.; Gibbs, B. M.; Nimmo, W., NOx control in coal combustion by combining biomass co-firing, oxygen enrichment and SNCR. *Fuel* **2013**, 105, 283-292.

83. Mullinger, P.; Jenkins, B., Chapter 2 - The Combustion Process. In *Industrial and Process Furnaces (Second Edition)*, Mullinger, P.; Jenkins, B., Eds. Butterworth-Heinemann: Oxford, 2013; pp 31-65.
84. Williams, A.; Pourkashanian, M.; Jones, J. M., Combustion of pulverised coal and biomass. *Progress in Energy and Combustion Science* **2001**, *27*, (6), 587-610.
85. Chmielniak, T.; Sciazko, M., Co-gasification of biomass and coal for methanol synthesis. *Applied Energy* **2003**, *74*, (3-4), 393-403.
86. Elder, T.; Groom, L. H., Pilot-scale gasification of woody biomass. *Biomass and Bioenergy* **2011**, *35*, (8), 3522-3528.
87. Rapagná, S.; Provendier, H.; Petit, C.; Kiennemann, A.; Foscolo, P. U., Development of catalysts suitable for hydrogen or syn-gas production from biomass gasification. *Biomass and Bioenergy* **2002**, *22*, (5), 377-388.
88. Wang, L.; Weller, C. L.; Jones, D. D.; Hanna, M. A., Contemporary issues in thermal gasification of biomass and its application to electricity and fuel production. *Biomass and Bioenergy* **2008**, *32*, (7), 573-581.
89. Barisano, D.; Canneto, G.; Nanna, F.; Villone, A.; Alvino, E.; Carnevale, M.; Pinto, G., Production of Gaseous Carriers Via Biomass Gasification for Energy Purposes. *Energy Procedia* **2014**, *45*, 2-11.
90. Bocci, E.; Sisinni, M.; Moneti, M.; Vecchione, L.; Di Carlo, A.; Villarini, M., State of Art of Small Scale Biomass Gasification Power Systems: A Review of the Different Typologies. *Energy Procedia* **2014**, *45*, 247-256.
91. Chaiwatanodom, P.; Vivapanarakij, S.; Assabumrungrat, S., Thermodynamic analysis of biomass gasification with CO₂ recycle for synthesis gas production. *Applied Energy* **2014**, *114*, 10-17.
92. Galindo, A. L.; Lora, E. S.; Andrade, R. V.; Giraldo, S. Y.; Jaén, R. L.; Cobas, V. M., Biomass gasification in a downdraft gasifier with a two-stage air supply: Effect of operating conditions on gas quality. *Biomass and Bioenergy* **2014**, *61*, 236-244.
93. Ghassemi, H.; Shahsavan-Markadeh, R., Effects of various operational parameters on biomass gasification process; a modified equilibrium model. *Energy Conversion and Management* **2014**, *79*, 18-24.
94. Hejazi, B.; Grace, J. R.; Bi, X.; Mahecha-Botero, A., Steam gasification of biomass coupled with lime-based CO₂ capture in a dual fluidized-bed reactor: A modeling study. *Fuel* **2014**, *117*, Part B, 1256-1266.
95. Kiendl, I.; Klemm, M.; Clemens, A.; Herrman, A., Dilute gas methanation of synthesis gas from biomass gasification. *Fuel* **2014**, *123*, 211-217.
96. Loha, C.; Chattopadhyay, H.; Chatterjee, P. K., Three dimensional kinetic modeling of fluidized-bed biomass gasification. *Chemical Engineering Science* **2014**, *109*, 53-64.
97. Miao, Q.; Zhu, J.; Barghi, S.; Wu, C.; Yin, X.; Zhou, Z., Model validation of a CFB biomass gasification model. *Renewable Energy* **2014**, *63*, 317-323.
98. Parthasarathy, P.; Narayanan, K. S., Hydrogen production from steam gasification of biomass: Influence of process parameters on hydrogen yield – A review. *Renewable Energy* **2014**, *66*, 570-579.
99. Xu, C.; Hu, S.; Xiang, J.; Zhang, L.; Sun, L.; Shuai, C.; Chen, Q.; He, L.; Edreis, E. M. A., Interaction and kinetic analysis for coal and biomass co-gasification by TG-FTIR. *Bioresour. Technol.* **2014**, *154*, 313-321.

100. McIlveen-Wright, D. R.; Huang, Y.; Rezvani, S.; Wang, Y., A technical and environmental analysis of co-combustion of coal and biomass in fluidized-bed technologies. *Fuel* **2007**, 86, (14), 2032-2042.
101. van den Broek, R.; Faaij, A.; van Wijk, A., Biomass combustion for power generation. *Biomass and Bioenergy* **1996**, 11, (4), 271-281.
102. Dai, J.; Cui, H.; Grace, J. R., Biomass feeding for thermochemical reactors. *Progress in Energy and Combustion Science* **2012**, 38, (5), 716-736.
103. Koornneef, J.; Junginger, M.; Faaij, A., Development of fluidized-bed combustion—An overview of trends, performance and cost. *Progress in Energy and Combustion Science* **2007**, 33, (1), 19-55.
104. Werther, J.; Saenger, M.; Hartge, E. U.; Ogada, T.; Siagi, Z., Combustion of agricultural residues. *Progress in Energy and Combustion Science* **2000**, 26, (1), 1-27.
105. Chirone, R.; Miccio, F.; Scala, F., Mechanism and prediction of bed agglomeration during fluidized-bed combustion of a biomass fuel: Effect of the reactor scale. *Chemical Engineering Journal* **2006**, 123, (3), 71-80.
106. De Geyter, S.; Öhman, M.; Boström, D.; Eriksson, M.; Nordin, A., Effects of Non-Quartz Minerals in Natural Bed Sand on Agglomeration Characteristics during Fluidized-bed Combustion of Biomass Fuels. *Energy & Fuels* **2007**, 21, (5), 2663-2668.
107. Öhman, M.; Pommer, L.; Nordin, A., Bed Agglomeration Characteristics and Mechanisms during Gasification and Combustion of Biomass Fuels. *Energy & Fuels* **2005**, 19, (4), 1742-1748.
108. Olofsson, G.; Ye, Z.; Bjerle, I.; Andersson, A., Bed Agglomeration Problems in Fluidized-Bed Biomass Combustion. *Industrial & Engineering Chemistry Research* **2002**, 41, (12), 2888-2894.
109. Scala, F.; Chirone, R., Characterization and Early Detection of Bed Agglomeration during the Fluidized-bed Combustion of Olive Husk. *Energy & Fuels* **2005**, 20, (1), 120-132.
110. Skrifvars, B. J.; Öhman, M.; Nordin, A.; Hupa, M., Predicting Bed Agglomeration Tendencies for Biomass Fuels Fired in FBC Boilers: A Comparison of Three Different Prediction Methods. *Energy & Fuels* **1999**, 13, (2), 359-363.
111. Wang, L.; Hustad, J. E.; Skreiberg, Ø.; Skjevraak, G.; Grønli, M., A Critical Review on Additives to Reduce Ash Related Operation Problems in Biomass Combustion Applications. *Energy Procedia* **2012**, 20, 20-29.
112. Scala, F.; Chirone, R.; Salatino, P., The influence of fine char particles burnout on bed agglomeration during the fluidized-bed combustion of a biomass fuel. *Fuel Processing Technology* **2003**, 84, (1-3), 229-241.
113. Fryda, L. E.; Panopoulos, K. D.; Kakaras, E., Agglomeration in fluidized-bed gasification of biomass. *Powder Technology* **2008**, 181, (3), 307-320.
114. Mac an Bhaird, S. T.; Walsh, E.; Hemmingway, P.; Maglinao, A. L.; Capareda, S. C.; McDonnell, K. P., Analysis of bed agglomeration during gasification of wheat straw in a bubbling fluidized-bed gasifier using mullite as bed material. *Powder Technology*.
115. Siegel, J. H., High-temperature de fluidization. *Powder Technology* **1984**, 38, (1), 13-22.
116. Yu, C.; Qin, J.; Nie, H.; Fang, M.; Luo, Z., Experimental research on agglomeration in straw-fired fluidized-beds. *Applied Energy* **2011**, 88, (12), 4534-4543.

117. Nijenhuis, J.; Korbee, R.; Lensselink, J.; Kiel, J. H. A.; van Ommen, J. R., A method for agglomeration detection and control in full-scale biomass fired fluidized-beds. *Chemical Engineering Science* **2007**, 62, (1–2), 644–654.
118. Haykiri-Acma, H.; Yaman, S.; Kucukbayrak, S., Effect of biomass on temperatures of sintering and initial deformation of lignite ash. *Fuel* **2010**, 89, (10), 3063–3068.
119. Kuo, J.-H.; Lin, C.-L.; Wey, M.-Y., Effect of agglomeration/defluidization on hydrogen generation during fluidized-bed air gasification of modified biomass. *International Journal of Hydrogen Energy* **2012**, 37, (2), 1409–1417.
120. Zandi, M.; Martinez-Pacheco, M.; Fray, T. A. T., Biomass for iron ore sintering. *Minerals Engineering* **2010**, 23, (14), 1139–1145.
121. Garba, M. U.; Ingham, D. B.; Ma, L.; Degereji, M. U.; Pourkashanian, M.; Williams, A., Modelling of deposit formation and sintering for the co-combustion of coal with biomass. *Fuel* **2013**, 113, 863–872.
122. Abd-Elhady, M. S.; Clevers, S. H.; Adriaans, T. N. G.; Rindt, C. C. M.; Wijers, J. G.; van Steenhoven, A. A., Influence of sintering on the growth rate of particulate fouling layers. *International Journal of Heat and Mass Transfer* **2007**, 50, (1–2), 196–207.
123. Piotrowska, P.; Zevenhoven, M.; Hupa, M.; Giuntoli, J.; de Jong, W., Residues from the production of biofuels for transportation: Characterization and ash sintering tendency. *Fuel Processing Technology* **2013**, 105, 37–45.
124. Teixeira, P.; Lopes, H.; Gulyurtlu, I.; Lapa, N.; Abelha, P., Evaluation of slagging and fouling tendency during biomass co-firing with coal in a fluidized-bed. *Biomass and Bioenergy* **2012**, 39, 192–203.
125. Llorente, M. J. F.; Laplaza, J. M. M.; Cuadrado, R. E.; García, J. E. C., Ash behaviour of lignocellulosic biomass in bubbling fluidized-bed combustion. *Fuel* **2006**, 85, (9), 1157–1165.
126. Fernández Llorente, M. J.; Escalada Cuadrado, R.; Murillo Laplaza, J. M.; Carrasco García, J. E., Combustion in bubbling fluidized-bed with bed material of limestone to reduce the biomass ash agglomeration and sintering. *Fuel* **2006**, 85, (14–15), 2081–2092.
127. Kuo, J.-H.; Lin, C.-L.; Wey, M.-Y., Effect of particle agglomeration on heavy metals adsorption by Al- and Ca-based sorbents during fluidized-bed incineration. *Fuel Processing Technology* **2011**, 92, (10), 2089–2098.
128. Chaouki, J.; Chavarie, C.; Klvana, D.; Pajonk, G., Effect of interparticle forces on the hydrodynamic behaviour of fluidized aerogels. *Powder Technology* **1985**, 43, (2), 117–125.
129. He, Y., A criterion for particle agglomeration by collision. *Powder Technology* **1999**, 103, (2), 189–193.
130. Zhou, T.; Li, H., Effects of adding different size particles on fluidization of cohesive particles. *Powder Technology* **1999**, 102, (3), 215–220.
131. Öhman, M.; Nordin, A.; Skrifvars, B.-J.; Backman, R.; Hupa, M., Bed Agglomeration Characteristics during Fluidized-bed Combustion of Biomass Fuels. *Energy & Fuels* **2000**, 14, (1), 169–178.
132. Zhou, T.; Li, H., Force balance modelling for agglomerating fluidization of cohesive particles. *Powder Technology* **2000**, 111, (1–2), 60–65.
133. Wang, J.; Shi, Q.; Huang, Z.; Gu, Y.; Musango, L.; Yang, Y., Experimental Investigation of Particle Size Effect on Agglomeration Behaviors in Gas–Solid

- Fluidized-beds. *Industrial & Engineering Chemistry Research* **2015**, 54, (48), 12177-12186.
134. Khadilkar, A. B.; Rozelle, P. L.; Pisupati, S. V., Review of Particle Physics and Chemistry in Fluidized-beds for Development of Comprehensive Ash Agglomeration Prediction Models. *Energy & Fuels* **2016**, 30, (5), 3714-3734.
135. Andrea Jordan, C.; Akay, G., Speciation and distribution of alkali, alkali earth metals and major ash forming elements during gasification of fuel cane bagasse. *Fuel* **2012**, 91, (1), 253-263.
136. Ma, J.; Liu, D.; Chen, Z.; Chen, X., Agglomeration characteristics during fluidized-bed combustion of salty wastewater. *Powder Technology* **2014**, 253, 537-547.
137. Lin, W.; Dam-Johansen, K.; Frandsen, F., Agglomeration in bio-fuel fired fluidized-bed combustors. *Chemical Engineering Journal* **2003**, 96, (1-3), 171-185.
138. Zevenhoven-Onderwater, M.; Backman, R.; Skrifvars, B. J.; Hupa, M.; Liliendahl, T.; Rosén, C.; Sjöström, K.; Engvall, K.; Hallgren, A., The ash chemistry in fluidized-bed gasification of biomass fuels. Part II: Ash behaviour prediction versus bench scale agglomeration tests. *Fuel* **2001**, 80, (10), 1503-1512.
139. Ergudenler, A.; Ghaly, A. E., Agglomeration of silica sand in a fluidized-bed gasifier operating on wheat straw. *Biomass and Bioenergy* **1993**, 4, (2), 135-147.
140. Zevenhoven-Onderwater, M.; Backman, R.; Skrifvars, B.-J.; Hupa, M., The ash chemistry in fluidized-bed gasification of biomass fuels. Part I: predicting the chemistry of melting ashes and ash-bed material interaction. *Fuel* **2001**, 80, (10), 1489-1502.
141. Vassilev, S. V.; Baxter, D.; Vassileva, C. G., An overview of the behaviour of biomass during combustion: Part I. Phase-mineral transformations of organic and inorganic matter. *Fuel* **2013**, 112, 391-449.
142. Nuutinen, L. H.; Tiainen, M. S.; Virtanen, M. E.; Enestam, S. H.; Laitinen, R. S., Coating Layers on Bed Particles during Biomass Fuel Combustion in Fluidized-Bed Boilers. *Energy & Fuels* **2003**, 18, (1), 127-139.
143. B.G. Langston, F. M. S. J., Self agglomerating fluidized-bed reduction. *Journal of Metals* **1960**, 12, (1960), 312.
144. Bridgwater, A. V.; Meier, D.; Radlein, D., An overview of fast pyrolysis of biomass. *Organic Geochemistry* **1999**, 30, (12), 1479-1493.
145. Luo, Z.; Wang, S.; Cen, K., A model of wood flash pyrolysis in fluidized-bed reactor. *Renewable Energy* **2005**, 30, (3), 377-392.
146. Blasi, C. D., Modelling the fast pyrolysis of cellulosic particles in fluid-bed reactors. *Chemical Engineering Science* **2000**, 55, (24), 5999-6013.
147. Branca, C.; Di Blasi, C.; Russo, C., Devolatilization in the temperature range 300-600K of liquids derived from wood pyrolysis and gasification. *Fuel* **2005**, 84, (1), 37-45.
148. Kersten, S. R. A.; Wang, X.; Prins, W.; van Swaaij, W. P. M., Biomass Pyrolysis in a Fluidized-bed Reactor. Part 1: Literature Review and Model Simulations. *Industrial & Engineering Chemistry Research* **2005**, 44, (23), 8773-8785.
149. Foscolo, P. U., Decomposition of Wood Particles in Fluidized-beds. *Industrial & Engineering Chemistry Research* **2004**, 44, (14), 5079-5089.
150. Wagenaar, B. M.; Prins, W.; van Swaaij, W. P. M., Flash pyrolysis kinetics of pine wood. *Fuel Processing Technology* **1993**, 36, (1-3), 291-298.

151. Thurner, F.; Mann, U., Kinetic investigation of wood pyrolysis. *Industrial & Engineering Chemistry Process Design and Development* **1981**, 20, (3), 482-488.
152. Pyle, D. L.; Zaror, C. A., Heat transfer and kinetics in the low temperature pyrolysis of solids. *Chemical Engineering Science* **1984**, 39, (1), 147-158.
153. Di Blasi, C.; Branca, C., Kinetics of Primary Product Formation from Wood Pyrolysis. *Industrial & Engineering Chemistry Research* **2001**, 40, (23), 5547-5556.
154. Bridgwater, A. V., Renewable fuels and chemicals by thermal processing of biomass. *Chemical Engineering Journal* **2003**, 91, (2-3), 87-102.
155. Di Blasi, C., Kinetic and Heat Transfer Control in the Slow and Flash Pyrolysis of Solids. *Industrial & Engineering Chemistry Research* **1996**, 35, (1), 37-46.
156. Salehi, E.; Abedi, J.; Harding, T., Bio-oil from Sawdust: Pyrolysis of Sawdust in a Fixed-Bed System. *Energy & Fuels* **2009**, 23, (7), 3767-3772.
157. Balat, M.; Balat, M.; Kırtay, E.; Balat, H., Main routes for the thermo-conversion of biomass into fuels and chemicals. Part I: Pyrolysis systems. *Energy Conversion and Management* **2009**, 50, (12), 3147-3157.
158. Bridgwater, A. V., Review of fast pyrolysis of biomass and product upgrading. *Biomass and Bioenergy* **2012**, 38, 68-94.
159. Chiaramonti, D.; Oasmaa, A.; Solantausta, Y., Power generation using fast pyrolysis liquids from biomass. *Renewable and Sustainable Energy Reviews* **2007**, 11, (6), 1056-1086.
160. Sadeghinezhad, E.; Kazi, S. N.; Sadeghinejad, F.; Badarudin, A.; Mehrali, M.; Sadri, R.; Reza Safaei, M., A comprehensive literature review of bio-fuel performance in internal combustion engine and relevant costs involvement. *Renewable and Sustainable Energy Reviews* **2014**, 30, 29-44.
161. Bridgwater, A. V.; Cottam, M. L., Opportunities for biomass pyrolysis liquids production and upgrading. *Energy & Fuels* **1992**, 6, (2), 113-120.
162. Jacob, A. M.; Igor, V. B., The Potential of Biomass in the Production of Clean Transportation Fuels and Base Chemicals. In *Production and Purification of Ultraclean Transportation Fuels*, American Chemical Society: 2011; Vol. 1088, pp 65-77.
163. Lappas, A. A.; Dimitropoulos, V. S.; Antonakou, E. V.; Voutetakis, S. S.; Vasalos, I. A., Design, Construction, and Operation of a Transported Fluid Bed Process Development Unit for Biomass Fast Pyrolysis: Effect of Pyrolysis Temperature. *Industrial & Engineering Chemistry Research* **2008**, 47, (3), 742-747.
164. Maschio, G.; Koufopoulos, C.; Lucchesi, A., Pyrolysis, a promising route for biomass utilization. *Bioresource Technology* **1992**, 42, (3), 219-231.
165. Trinh, T. N.; Jensen, P. A.; Sárossy, Z.; Dam-Johansen, K.; Knudsen, N. O.; Sørensen, H. R.; Egsgaard, H., Fast Pyrolysis of Lignin Using a Pyrolysis Centrifuge Reactor. *Energy & Fuels* **2013**, 27, (7), 3802-3810.
166. Zhang, L.; Xu, C.; Champagne, P., Overview of recent advances in thermo-chemical conversion of biomass. *Energy Conversion and Management* **2010**, 51, (5), 969-982.
167. Commercializing biomass conversion. *Environmental Science & Technology* **1983**, 17, (1), 24A-31A.
168. Bailie, R.; Richmond C, A., Economics Associated with Waste or Biomass Pyrolysis Systems. In *Solid Wastes and Residues*, American Chemical Society: 1978; Vol. 76, pp 21-43.

169. de Diego, L. F.; García-Labiano, F.; Abad, A.; Gayán, P.; Adánez, J., Modeling of the Devolatilization of Nonspherical Wet Pine Wood Particles in Fluidized-beds. *Industrial & Engineering Chemistry Research* **2002**, 41, (15), 3642-3650.
170. Brus, E.; Öhman, M.; Nordin, A.; Boström, D.; Hedman, H.; Eklund, A., Bed Agglomeration Characteristics of Biomass Fuels Using Blast-Furnace Slag as Bed Material. *Energy & Fuels* **2004**, 18, (4), 1187-1193.
171. Di Blasi, C., Heat, momentum and mass transport through a shrinking biomass particle exposed to thermal radiation. *Chemical Engineering Science* **1996**, 51, (7), 1121-1132.
172. Font, R.; Marcilla, A.; Verdu, E.; Devesa, J., Kinetics of the pyrolysis of almond shells and almond shells impregnated with cobalt dichloride in a fluidized-bed reactor and in a pyroprobe 100. *Industrial & Engineering Chemistry Research* **1990**, 29, (9), 1846-1855.
173. Di Blasi, C., Modeling chemical and physical processes of wood and biomass pyrolysis. *Progress in Energy and Combustion Science* **2008**, 34, (1), 47-90.
174. Miller, R. S.; Bellan, J., A Generalized Biomass Pyrolysis Model Based on Superimposed Cellulose, Hemicellulose and Lignin Kinetics. *Combustion Science and Technology* **1997**, 126, (1-6), 97-137.
175. Orfão, J. J. M.; Antunes, F. J. A.; Figueiredo, J. L., Pyrolysis kinetics of lignocellulosic materials—three independent reactions model. *Fuel* **1999**, 78, (3), 349-358.
176. Antal Jr, M. J., Mathematical modelling of biomass pyrolysis phenomena: Introduction. *Fuel* **1985**, 64, (11), 1483-1486.
177. Chan, W.-C. R.; Kelbon, M.; Krieger, B. B., Modelling and experimental verification of physical and chemical processes during pyrolysis of a large biomass particle. *Fuel* **1985**, 64, (11), 1505-1513.
178. Varhegyi, G.; Antal, M. J.; Szekeely, T.; Szabo, P., Kinetics of the thermal decomposition of cellulose, hemicellulose, and sugarcane bagasse. *Energy & Fuels* **1989**, 3, (3), 329-335.
179. Saastamoinen, J. J., Simplified model for calculation of devolatilization in fluidized-beds. *Fuel* **2006**, 85, (17-18), 2388-2395.
180. Di Blasi, C., Analysis of Convection and Secondary Reaction Effects Within Porous Solid Fuels Undergoing Pyrolysis. *Combustion Science and Technology* **1993**, 90, (5-6), 315-340.
181. Koufopoulos, C. A.; Papayannakos, N.; Maschio, G.; Lucchesi, A., Modelling of the pyrolysis of biomass particles. Studies on kinetics, thermal and heat transfer effects. *The Canadian Journal of Chemical Engineering* **1991**, 69, (4), 907-915.
182. Bilbao, R.; Millera, A.; Murillo, M. B., Temperature profiles and weight loss in the thermal decomposition of large spherical wood particles. *Industrial & Engineering Chemistry Research* **1993**, 32, (9), 1811-1817.
183. Hu, J.; Wang, Y.; Cao, C.; Elliott, D. C.; Stevens, D. J.; White, J. F., Conversion of biomass-derived syngas to alcohols and C2 oxygenates using supported Rh catalysts in a microchannel reactor. *Catalysis Today* **2007**, 120, (1), 90-95.
184. Griffith, R. B.; Jeffrey, R. N., Determining Chlorophyll, Carotene, and Xanthophyll in Plants. *Industrial & Engineering Chemistry Analytical Edition* **1944**, 16, (7), 438-440.

185. Petering, H. G.; Wolman, W.; Hibbard, R. P., Determination of chlorophyll and carotene in plant tissue. *Industrial & Engineering Chemistry Analytical Edition* **1940**, 12, (3), 148-151.
186. Alappat, B. J.; Deon, S.; Pre, P.; Delebarre, A.; Viazzo, S., Oil-Polluted Sands in a Fluidized-bed. *Industrial & Engineering Chemistry Research* **2005**, 44, (5), 1585-1591.
187. Ergun, S.; Orning, A. A., Fluid Flow through Randomly Packed Columns and Fluidized-beds. *Industrial & Engineering Chemistry* **1949**, 41, (6), 1179-1184.
188. Thorpe, R. B.; Davidson, J. F.; Pollitt, M.; Smith, J., Maldistribution in Fluidized-beds. *Industrial & Engineering Chemistry Research* **2002**, 41, (23), 5878-5889.
189. Li, C.-Z.; Bartle, K. D.; Kandiyoti, R., Vacuum pyrolysis of maceral concentrates in a wire-mesh reactor. *Fuel* **1993**, 72, 1459-1468.
190. International, A., ASTM E870-82(2013), Standard Test Methods for Analysis of Wood Fuels., In West Conshohocken, PA, 2013.
191. Kershaw, J. R.; Sathe, C.; Hayashi, J.-i.; Li, C.-Z.; Chiba, T., Fluorescence Spectroscopic Analysis of Tars from the Pyrolysis of a Victorian Brown Coal in a Wire-Mesh Reactor. *Energy & Fuels* **2000**, 14, (2), 476-482.
192. Yip, K.; Tian, F.; Hayashi, J.-i.; Wu, H., Effect of Alkali and Alkaline Earth Metallic Species on Biochar Reactivity and Syngas Compositions during Steam Gasification†. *Energy & Fuels* **2009**, 24, (1), 173-181.
193. Ergudenler, A.; Ghaly, E., Agglomeration of silica sand in a fluidized bed gasifier operating on wheat straw. *Biomass and Bioenergy* **1993**, 4, 135-147.
194. Baxter, L. L., Ash deposition during biomass and coal combustion a mechanistic approach. *Biomass and Bioenergy* **1993**, 4, 85-102.
195. Boström, D.; Skoglund, N.; Grimm, A.; Boman, C.; Öhman, M.; Broström, M.; Backman, R., Ash Transformation Chemistry during Combustion of Biomass. *Energy & Fuels* **2012**, 26, (1), 85-93.
196. Hupa, M., Ash-Related Issues in Fluidized-Bed Combustion of Biomasses: Recent Research Highlights. *Energy & Fuels* **2012**, 26, (1), 4-14.
197. Boutin, O.; Ferrer, M.; Lédé, J., Radiant flash pyrolysis of cellulose—Evidence for the formation of short life time intermediate liquid species. *Journal of Analytical and Applied Pyrolysis* **1998**, 47, (1), 13-31.
198. Cetin, E.; Moghtaderi, B.; Gupta, R.; Wall, T. F., Influence of pyrolysis conditions on the structure and gasification reactivity of biomass chars. *Fuel* **2004**, 83, (16), 2139-2150.
199. Mohan, D.; Pittman, C. U.; Steele, P. H., Pyrolysis of Wood/Biomass for Bio-oil: A Critical Review. *Energy Fuels* **2006**, 20, (3), 848-889.
200. Garcia-Perez, M.; Wang, X. S.; Shen, J.; Rhodes, M. J.; Tian, F.; Lee, W.-J.; Wu, H.; Li, C.-Z., Fast Pyrolysis of Oil Mallee Woody Biomass: Effect of Temperature on the Yield and Quality of Pyrolysis Products. *Industrial & Engineering Chemistry Research* **2008**, 47, (6), 1846-1854.
201. Wang, Y.; Li, X.; Mourant, D.; Gunawan, R.; Zhang, S.; Li, C.-Z., Formation of Aromatic Structures during the Pyrolysis of Bio-oil. *Energy & Fuels* **2011**, 26, (1), 241-247.
202. Ben Jemâa, J. M.; Haouel, S.; Bouaziz, M.; Khouja, M. L., Seasonal variations in chemical composition and fumigant activity of five Eucalyptus essential oils against three moth pests of stored dates in Tunisia. *Journal of Stored Products Research* **2012**, 48, 61-67.

203. Clará, R. A.; Marigliano, A. C. G. m.; Sólamo, H. N., Density, Viscosity, and Refractive Index in the Range (283.15 to 353.15) K and Vapor Pressure of α -Pinene, d-Limonene, (\pm)-Linalool, and Citral Over the Pressure Range 1.0 kPa Atmospheric Pressure. *Journal of Chemical & Engineering Data* **2009**, 54, (3), 1087-1090.
204. Elaissi, A.; Salah, K. H.; Mabrouk, S.; Larbi, K. M.; Chemli, R.; Harzallah-Skhiri, F., Antibacterial activity and chemical composition of 20 Eucalyptus species' essential oils. *Food Chemistry* **2011**, 129, (4), 1427-1434.
205. Gilles, M.; Zhao, J.; An, M.; Agboola, S., Chemical composition and antimicrobial properties of essential oils of three Australian Eucalyptus species. *Food Chemistry* **2010**, 119, (2), 731-737.
206. Maciel, M. V.; Morais, S. M.; Bevilaqua, C. M. L.; Silva, R. A.; Barros, R. S.; Sousa, R. N.; Sousa, L. C.; Brito, E. S.; Souza-Neto, M. A., Chemical composition of Eucalyptus spp. essential oils and their insecticidal effects on *Lutzomyia longipalpis*. *Veterinary Parasitology* **2010**, 167, (1), 1-7.
207. Santos, S. A. O.; Villaverde, J. J.; Freire, C. S. R.; Domingues, M. R. M.; Neto, C. P.; Silvestre, A. J. D., Phenolic composition and antioxidant activity of Eucalyptus grandis, E. urograndis (E. grandis; E. urophylla) and E. maidenii bark extracts. *Industrial Crops and Products* **2012**, 39, 120-127.
208. Domingues, R. M. A.; de Melo, M. M. R.; Neto, C. P.; Silvestre, A. J. D.; Silva, C. M., Measurement and modeling of supercritical fluid extraction curves of Eucalyptus globulus bark: Influence of the operating conditions upon yields and extract composition. *The Journal of Supercritical Fluids* **2012**, 72, 176-185.
209. Aho, A.; DeMartini, N.; Pranovich, A.; Krogell, J.; Kumar, N.; Eränen, K.; Holmbom, B.; Salmi, T.; Hupa, M.; Murzin, D. Y., Pyrolysis of pine and gasification of pine chars – Influence of organically bound metals. *Bioresource Technology* **2013**, 128, 22-29.
210. Miranda, I.; Gominho, J.; Mirra, I.; Pereira, H., Fractioning and chemical characterization of barks of *Betula pendula* and *Eucalyptus globulus*. *Industrial Crops and Products* **2013**, 41, 299-305.
211. Vassilev, S. V.; Baxter, D.; Andersen, L. K.; Vassileva, C. G.; Morgan, T. J., An overview of the organic and inorganic phase composition of biomass. *Fuel* **2012**, 94, 1-33.
212. Abdullah, H.; Mediaswanti, K. A.; Wu, H., Biochar as a Fuel: 2. Significant Differences in Fuel Quality and Ash Properties of Biochars from Various Biomass Components of Mallee Trees. *Energy & Fuels* **2010**, 24, (3), 1972-1979.
213. Mulligan, C. J.; Strezov, L.; Strezov, V., Thermal Decomposition of Wheat Straw and Mallee Residue Under Pyrolysis Conditions†. *Energy & Fuels* **2009**, 24, (1), 46-52.
214. Burrows, N. D., Flame residence times and rates of weight loss of eucalypt forest fuel particles. *International Journal of Wildland Fire* **2001**, 10, (2), 137-143.
215. Mullette, K.; Bamber, R. K., Studies of the Lignotubers of *Eucalyptus gummifera* (Gaertn. & Hochr.). III. Inheritance and Chemical Composition. *Australian Journal of Botany* **1978**, 26, (1), 23-28.
216. Scarff, F. R.; Westoby, M., Leaf litter flammability in some semi-arid Australian woodlands. *Functional Ecology* **2006**, 20, (5), 745-752.
217. Goto, M.; Smith, J. M.; McCoy, B. J., Kinetics and mass transfer for supercritical fluid extraction of wood. *Industrial & Engineering Chemistry Research* **1990**, 29, (2), 282-289.


218. Jand, N.; Foscolo, P. U., Decomposition of Wood Particles in Fluidized-beds. *Industrial & Engineering Chemistry Research* **2005**, 44, (14), 5079-5089.
219. Narayan, R.; Antal, M. J., Thermal Lag, Fusion, and the Compensation Effect during Biomass Pyrolysis. *Industrial & Engineering Chemistry Research* **1996**, 35, (5), 1711-1721.
220. Burton, A.; Wu, H., Mechanistic Investigation into Bed Agglomeration during Biomass Fast Pyrolysis in a Fluidized-Bed Reactor. *Energy & Fuels* **2012**, 26, (11), 6979-6987.
221. Espenson, J. H., *Chemical Kinetics and Reaction Mechanisms 2nd edition*. McGraw Hill, 1995.: New York, NY 1995.
222. Burton, A.; Wu, H., Differences in Bed Agglomeration Behavior during the Fast Pyrolysis of Mallee Bark, Leaf, and Wood in a Fluidized-Bed Reactor at 500 °C. *Energy Fuels* **2015**, DOI: 10.1021/acs.energyfuels.5b00651.
223. Chang, W.-h., A New Method of Determining the Order of Reaction and the Reaction Constant from Kinetics Data. *The Journal of Physical Chemistry* **1957**, 61, (6), 819-820.
224. Zimmerman, H. K., Method for determining order of a reaction. *Journal of Chemical Education* **1963**, 40, (7), 356.
225. Burton, A.; Wu, H., Quantification of Interactions between Sand and Pyrolyzing Biomass Particles in Fluidized-Bed under Fast Pyrolysis Conditions Pertinent to Bio-Oil Production. *Industrial & Engineering Chemistry Research* **2015**.
226. Gaston, K. R.; Jarvis, M. W.; Pepiot, P.; Smith, K. M.; Frederick, W. J.; Nimlos, M. R., Biomass Pyrolysis and Gasification of Varying Particle Sizes in a Fluidized-Bed Reactor. *Energy & Fuels* **2011**, 25, (8), 3747-3757.
227. Gebgeegziabher, T.; Oyedun, A. O.; Zhang, Y.; Hui, C. W., Effective Optimization Model for Biomass Drying. In *Computer Aided Chemical Engineering*, Andrzej, K.; Ilkka, T., Eds. Elsevier: 2013; Vol. Volume 32, pp 97-102.
228. Gebreegziabher, T.; Oyedun, A. O.; Hui, C. W., Optimum biomass drying for combustion – A modeling approach. *Energy* **2013**, 53, 67-73.
229. Gómez-de la Cruz, F. J.; Casanova-Peláez, P. J.; Palomar-Carnicero, J. M.; Cruz-Peragón, F., Drying kinetics of olive stone: A valuable source of biomass obtained in the olive oil extraction. *Energy* **2014**, 75, 146-152.
230. Jia, D.; Cathary, O.; Peng, J.; Bi, X.; Lim, C. J.; Sokhansanj, S.; Liu, Y.; Wang, R.; Tsutsumi, A., Fluidization and drying of biomass particles in a vibrating fluidized-bed with pulsed gas flow. *Fuel Processing Technology*.
231. Klavina, K.; Cinis, A.; Zandeckis, A., Experimental Study on the Effects of Air Velocity, Temperature and Depth on Low-temperature Bed Drying of Forest Biomass Residue. *Energy Procedia* **2015**, 72, 42-48.
232. Liu, Y.; Kansha, Y.; Ishizuka, M.; Fu, Q.; Tsutsumi, A., Experimental and simulation investigations on self-heat recuperative fluidized-bed dryer for biomass drying with superheated steam. *Fuel Processing Technology* **2015**, 136, 79-86.
233. Liu, Y.; Peng, J.; Kansha, Y.; Ishizuka, M.; Tsutsumi, A.; Jia, D.; Bi, X. T.; Lim, C. J.; Sokhansanj, S., Novel fluidized-bed dryer for biomass drying. *Fuel Processing Technology* **2014**, 122, 170-175.
234. Burton, A.; Wu, H., Differences in Bed Agglomeration Behaviour during the Fast Pyrolysis of Mallee bark, Leaf and Wood in a Fluidized-bed Reactor at 500 °C. *Energy & Fuels* **2015**.
235. D.Ebbing, *General Chemistry*. 1 ed.; Houghton Mifflin Company: Boston, 1984; p 970.

236. James R. Welty, C. E. W., Robert E. Wilson *Fundamentals of Momentum, Heat and Mass Transfer* Third ed.; John Wiley and Sons New York, 1984.

Every reasonable effort has been made to acknowledge the owners of copyright material. I would be pleased to hear from any copyright owner who has been omitted or incorrectly acknowledged.

APPENDICES

Rightslink permission for : Burton, A, Wu, H, Mechanistic Investigation into Bed Agglomeration during Biomass Fast Pyrolysis in a Fluidized-Bed Reactor. *Energy Fuels* **2012**, 26, 6979-6987.




Copyright Clearance Center

RightsLink[®]


Home

Create Account

Help



Live Chat



ACS Publications
Most Trusted. Most Cited. Most Rec.

Title: Mechanistic Investigation into Bed Agglomeration during Biomass Fast Pyrolysis in a Fluidized-Bed Reactor

Author: Alan Burton, Hongwei Wu

Publication: Energy & Fuels

Publisher: American Chemical Society

Date: Nov 1, 2012

Copyright © 2012, American Chemical Society

LOGIN

If you're a [copyright.com](#) user, you can login to RightsLink using your [copyright.com](#) credentials. Already a [RightsLink](#) user or want to [learn more?](#)

PERMISSION/LICENSE IS GRANTED FOR YOUR ORDER AT NO CHARGE

This type of permission/license, instead of the standard Terms & Conditions, is sent to you because no fee is being charged for your order. Please note the following:


- Permission is granted for your request in both print and electronic formats, and translations.
- If figures and/or tables were requested, they may be adapted or used in part.
- Please print this page for your records and send a copy of it to your publisher/graduate school.
- Appropriate credit for the requested material should be given as follows: "Reprinted (adapted) with permission from (COMPLETE REFERENCE CITATION). Copyright (YEAR) American Chemical Society." Insert appropriate information in place of the capitalized words.
- One-time permission is granted only for the use specified in your request. No additional uses are granted (such as derivative works or other editions). For any other uses, please submit a new request.

BACK

CLOSE WINDOW

Copyright © 2016 [Copyright Clearance Center, Inc.](#) All Rights Reserved. [Privacy statement](#). [Terms and Conditions](#). Comments? We would like to hear from you. E-mail us at customer@copyright.com

Rightslink permission for: Burton, A.; Wu, H., Quantification of Interactions between Sand and Pyrolyzing Biomass Particles in Fluidized-Bed under Fast Pyrolysis Conditions Pertinent to Bio-Oil Production. *Ind Eng Chem Res* **2015**, *54*, 7990-7997.




Copyright Clearance Center


Most Trusted. Most Cited. Most Respected.

RightsLink®

[Home](#)
[Create Account](#)
[Help](#)



Live Chat



ACS Publications

Most Trusted. Most Cited. Most Respected.

Title: Quantification of Interactions between Sand and Pyrolyzing Biomass Particles in Fluidized-Bed under Fast Pyrolysis Conditions Pertinent to Bio-Oil Production

Author: Alan Burton, Hongwei Wu

Publication: Industrial & Engineering Chemistry Research

Publisher: American Chemical Society

Date: Aug 1, 2015

Copyright © 2015, American Chemical Society

LOGIN

If you're a [copyright.com](#) user, you can login to RightsLink using your [copyright.com](#) credentials. Already a [RightsLink](#) user or want to [learn more?](#)

PERMISSION/LICENSE IS GRANTED FOR YOUR ORDER AT NO CHARGE


This type of permission/license, instead of the standard Terms & Conditions, is sent to you because no fee is being charged for your order. Please note the following:

- Permission is granted for your request in both print and electronic formats, and translations.
- If figures and/or tables were requested, they may be adapted or used in part.
- Please print this page for your records and send a copy of it to your publisher/graduate school.
- Appropriate credit for the requested material should be given as follows: "Reprinted (adapted) with permission from (COMPLETE REFERENCE CITATION). Copyright (YEAR) American Chemical Society." Insert appropriate information in place of the capitalized words.
- One-time permission is granted only for the use specified in your request. No additional uses are granted (such as derivative works or other editions). For any other uses, please submit a new request.

[BACK](#)
[CLOSE WINDOW](#)


Copyright © 2016 [Copyright Clearance Center, Inc.](#) All Rights Reserved. [Privacy statement](#). [Terms and Conditions](#). Comments? We would like to hear from you. E-mail us at customer-care@copyright.com


Rightslink permission for: Burton, A, Wu, H, Differences in Bed Agglomeration Behavior during the Fast Pyrolysis of Mallee Bark, Leaf, and Wood in a Fluidized-Bed Reactor at 500 °C. *Energy Fuels* **2015**, 29, 3753-3759. Rightslink Permission



Copyright Clearance Center

RightsLink®

[Home](#)
[Create Account](#)
[Help](#)




ACS Publications
Most Trusted. Most Cited. Most Read.

Title: Differences in Bed Agglomeration Behavior during the Fast Pyrolysis of Mallee Bark, Leaf, and Wood in a Fluidized-Bed Reactor at 500 °C

Author: Alan Burton, Hongwei Wu

Publication: Energy & Fuels

Publisher: American Chemical Society

Date: Jun 1, 2015

Copyright © 2015, American Chemical Society

[LOGIN](#)

If you're a [copyright.com](#) user, you can login to RightsLink using your [copyright.com](#) credentials. Already a [RightsLink](#) user or want to [learn more?](#)

PERMISSION/LICENSE IS GRANTED FOR YOUR ORDER AT NO CHARGE


This type of permission/license, instead of the standard Terms & Conditions, is sent to you because no fee is being charged for your order. Please note the following:

- Permission is granted for your request in both print and electronic formats, and translations.
- If figures and/or tables were requested, they may be adapted or used in part.
- Please print this page for your records and send a copy of it to your publisher/graduate school.
- Appropriate credit for the requested material should be given as follows: "Reprinted (adapted) with permission from (COMPLETE REFERENCE CITATION). Copyright (YEAR) American Chemical Society." Insert appropriate information in place of the capitalized words.
- One-time permission is granted only for the use specified in your request. No additional uses are granted (such as derivative works or other editions). For any other uses, please submit a new request.


[BACK](#)
[CLOSE WINDOW](#)

Copyright © 2016 [Copyright Clearance Center, Inc.](#) All Rights Reserved. [Privacy statement.](#) [Terms and Conditions.](#) Comments? We would like to hear from you. E-mail us at customercare@copyright.com

[4] Burton, A.; Wu, H., Bed Agglomeration during the Drying of Mallee Leaf in Fluidized-bed. *Ind Eng Chem Res*, **2016**, *55*, 1796–1800, Rightslink Permission



RightsLink®

[Home](#)
[Create Account](#)
[Help](#)


ACS Publications Most Trusted. Most Cited. Most Read.

Title: Bed Agglomeration during the Drying of Mallee Leaf in Fluidized Bed

Author: Alan Burton, Hongwei Wu

Publication: Industrial & Engineering Chemistry Research

Publisher: American Chemical Society

Date: Feb 1, 2016

Copyright © 2016, American Chemical Society

LOGIN

If you're a [copyright.com](#) user, you can login to RightsLink using your [copyright.com](#) credentials. Already a RightsLink user or want to [learn more?](#)

PERMISSION/LICENSE IS GRANTED FOR YOUR ORDER AT NO CHARGE

This type of permission/license, instead of the standard Terms & Conditions, is sent to you because no fee is being charged for your order. Please note the following:

- Permission is granted for your request in both print and electronic formats, and translations.
- If figures and/or tables were requested, they may be adapted or used in part.
- Please print this page for your records and send a copy of it to your publisher/graduate school.
- Appropriate credit for the requested material should be given as follows: "Reprinted (adapted) with permission from (COMPLETE REFERENCE CITATION). Copyright (YEAR) American Chemical Society." Insert appropriate information in place of the capitalized words.
- One-time permission is granted only for the use specified in your request. No additional uses are granted (such as derivative works or other editions). For any other uses, please submit a new request.

BACK

CLOSE WINDOW

Copyright © 2016 [Copyright Clearance Center, Inc.](#) All Rights Reserved. [Privacy statement.](#) [Terms and Conditions.](#)
Comments? We would like to hear from you. E-mail us at customer-care@copyright.com

[5] Burton, A.; Wu, H., Diagnosis of bed agglomeration in fluidized-bed under conditions for biomass pyrolysis at a wide range of temperatures. *Fuel*, **2016**, 179, 103–107

RightsLink Printable License

4/05/2016, 10:05 PM

**ELSEVIER LICENSE
TERMS AND CONDITIONS**

May 04, 2016

This is a License Agreement between Alan Burton ("You") and Elsevier ("Elsevier") provided by Copyright Clearance Center ("CCC"). The license consists of your order details, the terms and conditions provided by Elsevier, and the payment terms and conditions.

All payments must be made in full to CCC. For payment instructions, please see information listed at the bottom of this form.

Supplier	Elsevier Limited The Boulevard, Langford Lane Kidlington, Oxford, OX5 1GB, UK
Registered Company Number	1982084
Customer name	Alan Burton
Customer address	51 Montreal street Fremantle, 6162
License number	3861950614743
License date	May 04, 2016
Licensed content publisher	Elsevier
Licensed content publication	Fuel
Licensed content title	Diagnosis of bed agglomeration during biomass pyrolysis in fluidized-bed at a wide range of temperatures
Licensed content author	Alan Burton, Hongwei Wu
Licensed content date	1 September 2016
Licensed content volume number	179
Licensed content issue number	n/a
Number of pages	5
Start Page	103
End Page	107
Type of Use	reuse in a thesis/dissertation
Portion	full article
Format	both print and electronic
Are you the author of this Elsevier article?	Yes
Will you be translating?	No
Title of your thesis/dissertation	Bed Agglomeration During Biomass Fast Pyrolysis in a Fluidised Bed Reactor
Expected completion date	Jun 2016

<https://s100.copyright.com/App/PrintableLicenseFrame.jsp?publish...8-201e-40f4-9ede-486ba91193c0%20%20&targetPage=printablelicense>

Page 1 of 6